

**SYNTHESIS AND CHARACTERIZATION OF  
CATHODE CATALYSTS FOR  
USE IN DIRECT METHANOL FUEL CELLS**

**By**

**Marvin Piet**



A thesis submitted in fulfilment of the requirements for the degree of  
Magister Scientiae in the Department of Chemistry, University of the  
Western Cape.

**Supervisor:** Prof I.R Green

**Co supervisor:** Dr Lindiwe Khotseng

November 2010

## **DECLARATION**

I declare that SYNTHESIS AND CHARACTERIZATION OF CATHODE CATALYSTS FOR USE IN DIRECT METHANOL FUEL CELLS is my own work, that it has not been submitted for any degree or examination in any other university, and that all the sources I have used or quoted have been indicated and acknowledged by complete references.

Full name..... Date.....

Signed.....



## Acknowledgments

First and foremost I would like to thank God almighty for providing me with his mercy and grace to awake each day in order to complete the proposed work. If it were not for this the envisaged work could not be completed.

I would also like to extend my sincere appreciation to my supervisor **Prof I.R. Green**, if not for his enormous wealth of experience in chemistry and supervision the work would not be accomplished in the desired time period. His foresight and insight in the field greatly attributed into the chemist I developed into from when I started the proposed work. I would also like to thank **Dr. L. Khotseng**

I would also like to thank **Dr. H. Abbo** and **Dr. S. Titinchi** for assisting in the synthetic aspect of the work and instilling a good work ethic and lab practise in me, which are qualities I am grateful for and I am forever indebted to them. I would also like to thank **Dr. M. Williams** for his moral support and strong theoretical backround.

I would also like to thank my family, Elizabeth, Bonniegirl and Nerina Piet for their patience, moral and spiritual support and allowing me to pursue my dream in life.

I would also like to thank NRF and SAIAMC for financial assistance during the course of the proposed work.

The staff at SAIAMC for technical and theoretical support with relation to the work.

I would like to extend a warm-hearted thank you to my peer's at SAIAMC (**Bulelwa, Asanda, Lynwill**), in times of need I could always count on them for assistance.

**Adrian Josephs** (Electron Microscopy Unit, Department of Physics, University of the Western Cape)

**Remy Bucher**, X-Ray diffraction experiments (Materials Research Group, iThemba Labs)

I would also like to thank **Prof E. Iwuoha** for allowing us to use the UV-Vis spectrometer of the sensor lab.



## **ABSTRACT**

In this work a modified polyol method was developed to synthesize in-house catalysts. The method was modified for maximum delivery of product and proved to be quick and efficient as well as cost effective. The series of IH catalysts were characterized using techniques such as UV-vis and FT-IR spectroscopy, TEM, XRD, ICP and CV.

The polyol method developed effectively reduced and deposited Pt nanoparticles onto different carbon supports. Functionalization of some of the supports was also successfully carried out through acid oxidative treatment which introduced carboxylic acid and hydroxyl groups onto the surface of the supporting material, which was supported by FT-IR which demonstrated that there was a relative increase in absorbance of functionalities viz., carboxylic acid ( $1270\text{ cm}^{-1}$ ) and hydroxyl groups on the surface of the acid treated MWCNT's-F compared to the untreated MWCNT's. Addition of a sedimentation promoter proved to increase the amount of metal deposition on the support thereby improving the loading dramatically.

It was also found that addition of a specific amount of water in the polyol method allowed one to control the particle growth during the deposition phase on the various carbon supports investigated namely; XC-72 carbon, MWCNT's and MWCNT's-F. The in-house catalysts synthesized namely; Pt/C-IH, Pt/MWCNT's-IH and Pt/MWCNT's-F-IH all displayed narrow particle size distributions with average mean particle sizes of 2-5 nm, 2-6 nm and 3-6 nm respectively which was in good agreement with particle size measurements obtained from XRD using the Scherrer formula. All measured CV's obtained for the series of IH catalysts prepared by this protocol were comparable with the commercial catalyst. The IH catalysts displayed the characteristic XRD peaks associated with Pt on carbon supports in acidic media.

The ORR measurements for Pt/MWCNT's-F-IH (functionalised) proved to be slightly superior ( $0.058 \text{ A/cm}^2$ ) compared to that of the commercial catalyst ( $0.047 \text{ A/cm}^2$ ) at a potential of 0.3V. This was attributed to the fact that the addition of water effectively controlled particle growth and deposition onto the support, and the fact that MWCNT's-F offered a larger surface area and with the functionalized surface offering anchorage sites for Pt nanoparticles through carboxylic and hydroxyl functional groups.

Further attempts to modify the developed polyol method using NaOAc as an electrostatic stabilizer to control the growth of Pt nanoparticles were made. It was found that although the stabilizer employed effectively stabilized Pt nanoparticles supported on XC-72 carbon, in our hands we were not able to produce the same results in the case of Pt supported on the MWCNT's. TEM images revealed that Pt/C-NaOAc displayed narrow particle size distribution with a mean particle size of 2-5 nm whereas particle agglomeration was observed for Pt/MWCNT's-NaOAc and Pt/MWCNT's-F-NaOAc with a broader particle size distribution and average mean particle sizes of 2-7 and 2-8 nm in diameter respectively. The CV's obtained for these modified IH catalysts were in the main comparable to that of the commercial catalyst. However ORR activities of the IH Pt/C-NaOAc catalysts when carefully compared to the commercial catalyst revealed that it was indeed slightly superior ( $0.064 \text{ A/cm}^2$ ). This is mainly attributed to the narrow particle size and even distribution of particles on the carbon support and resembled the best particle required to provide maximum activity in the ORR as a consequence of the facial kinetics involved.

## Table of contents

Declaration.....	ii
Acknowledgements.....	iii
Abstract.....	v
Table of Contents.....	vii
List of Figures.....	xi
List of Tables.....	xiv
List of schemes.....	xiv
Abbreviations.....	xv

### Chapter 1: Introduction

1.1.Introduction.....	1
1.2. Fuel cell.....	2
1.3. Different kinds of fuel cells.....	4
1.3.1. SOFC.....	4
1.3.2. PEMFC.....	5
1.3.3. MCFC.....	6
1.3.4. PAFC.....	7
1.3.5. AFC.....	8
1.3.6. RFC.....	9
1.3.7. ZAFC.....	10
1.3.8. DMFC.....	11
1.3.8.1. Advantages of a DMFC.....	12
1.3.8.2. Disadvantages of a DMFC.....	13
1.4. Rationale of research.....	14
1.5. Thesis outline.....	16

## Chapter 2: Literature review

2.1. Literature review/Theoretical framework .....	17
2.2. Catalyst.....	17
2.3. Chemical action.....	17
2.4. Catalyst used in fuel cells.....	19
2.5. Supports for catalysts.....	20
2.5.1. Requirements of a good support.....	20
2.5.2. Supports used for catalysts.....	21
2.6. Oxygen reduction reaction.....	22
2.7. Platinum as a catalysts for DMFC's.....	24
2.8. Different synthetic routes for the synthesis of catalysts for fuel cells.....	25
2.8.1. Sulfite complex route.....	25
2.8.2. Bönneiman method.....	25
2.8.3. Impregnation method.....	26
2.8.4. Adams fusion method.....	26
2.8.5. Microemulsion method.....	27
2.8.6. Ion exchange method.....	28
2.8.7. Vapour phase method.....	28
2.8.8. Sol gel method.....	29
2.8.9. Polyol method.....	30
2.8.9.1. Literature concerning the polyol method.....	32
2.8.9.2. Dispersion and loading.....	32
2.8.9.3. Supports.....	35
2.8.9.4. Stabilizers.....	37
2.8.9.5. Steric stabilization.....	38



2.8.9.5. Electrostatic stabilization.....	39
---	----

### **Chapter 3: Materials and methods**

3.1. Materials and methods.....	42
3.1.1. Chemicals.....	42
3.1.2. Initial synthetic protocol employed .....	43
3.1.3. Functionalizing MWCNT's.....	43
3.1.4. Modified synthetic protocol (Change in pH).....	44
3.1.5. Modified synthetic protocol (Addition of H <sub>2</sub> O).....	44
3.1.6. Modified synthetic protocol (Addition of sodium acetate as a stabilizer).....	45
3.2. Physiochemical characterization.....	46
3.2.1. Transmission Electron Microscope (TEM).....	46
3.2.2. X-Ray Diffraction (XRD).....	47
3.2.3. (UV-vis) Visible spectroscopy.....	48
3.2.4. Infrared (IR) spectroscopy.....	49
3.3. Electrochemical characterization.....	50
3.3.1. Cyclic Voltammetry.....	50
3.3.2. Electrochemical cell design.....	51

### **Chapter 4: Results and discussion**

4.1. General.....	54
4.2. Reaction temperature.....	54
4.3. Reaction time.....	55
4.4. The effect of water on particle size and distribution using the polyol method for the synthesis of IH catalysts.....	65
4.4.1. Physiochemical characterization.....	65
4.4.2. Electrochemical characterization.....	70

**Chapter 5: RESULTS AND DISCUSSION**

5.1. Modified polyol method using sodium acetate as a stabilizer.....73  
5.1.1. Physiochemical characterization.....74  
5.1.2. Electrochemical characterization.....80

**Chapter 6: CONCLUSION AND RECOMMENDATIONS**

6.1. Conclusions.....83  
6.2. Recommendations for future work.....86

**Chapter 7: BIBLIOGRAPHY**

7.1. Bibliography.....87



## List of figures

<b>Figure 1.1:</b> Schematic diagram of the operating principle of a fuel cell.....	3
<b>Figure 1.2:</b> Diagram of a solid oxide fuel cell (SOFC).....	4
<b>Figure 1.3:</b> Diagram of a Proton Exchange Membrane Fuel Cell (PEMFC).....	5
<b>Figure 1.4:</b> Diagram of a Molten Carbonate Fuel Cell (MCFC).....	6
<b>Figure 1.5:</b> Diagram of a Phosphoric Acid Fuel Cell (PAFC).....	7
<b>Figure 1.6:</b> Diagram of an Alkaline Fuel Cell (AFC).....	8
<b>Figure 1.7:</b> Diagram of a RFC.....	9
<b>Figure 1.8:</b> Diagram of a ZAFC.....	10
<b>Figure 1.9:</b> Diagram of a Direct Methanol Fuel Cell (DMFC).....	11
<b>Figure 2.1:</b> Diagram displaying the activation energy pathways with and without a catalyst.....	18
<b>Figure 2.2:</b> Diagram displaying steric stabilization of metal colloid particles.....	38
<b>Figure 2.3:</b> Diagram displaying electrostatic stabilization of metal colloid particles.....	39
<b>Figure 3.1:</b> Image of the cell which was specifically designed for electrochemical measurements of the IH electrodes.....	52
<b>Figure 4.1:</b> UV-vis spectrum of $\text{H}_2\text{PtCl}_6$ in EG ( $7.23 \times 10^{-3}\text{M}$ ) quench at various time intervals during the reaction.....	55
<b>Figure 4.2:</b> Cyclic Voltammogram (CV) of the commercial catalyst (40wt %) from Johnson Matthey using the IH electrochemical cell, 0.5M $\text{H}_2\text{SO}_4$ de-aerated for 30 minutes, scan rate = $20\text{mvs}^{-1}$ .....	57
<b>Figure 4.3:</b> TEM image of the commercial catalyst Pt/C 40wt% (Johnson Matthey Company).....	58

<b>Figure 4.4:</b> Histogram displaying the particle size distribution of the commercial Pt/C 40 wt% catalyst.....	58
<b>Figure 4.5:</b> TEM image of IH Pt/C initial catalysts .....	59
<b>Figure 4.6:</b> Histogram showing the particle size distributions of the initial IH catalysts using the polyol method.....	60
<b>Figure 4.7:</b> TEM image of IH Pt/C initial catalysts obtained after the addition of a sediment promoter increasing the metal loading dramatically.....	61
<b>Figure 4.8:</b> Histogram showing the particle size distributions of the initial IH catalysts using the modified polyol method.....	61
<b>Figure 4.9:</b> IR spectrum of MWCNT's and F-MWCNT's magnified in the regions between 2000-1000cm <sup>-1</sup> .....	64
<b>Figure 4.10:</b> TEM images of IH catalysts synthesized using the modified polyol method, (a) Pt/C-IH, (b) Pt/MWCNT's-IH and (c) Pt/MWCNT's-F-IH.....	65
<b>Figure 4.11:</b> Histograms showing the particle size distributions obtained from random particles of IH catalysts synthesized using the modified polyol method, (a) Pt/C-IH.....	66
<b>Figure 4.12:</b> Histogram of the particle size distribution obtained from the TEM analysis from random particles of IH catalyst (Pt/MWCNT's-IH) synthesized using the modified polyol method.....	66
<b>Figure 4.13:</b> Histogram of the particle size distribution obtained from the TEM analysis from random particles of IH catalyst (Pt/MWCNT's-F-IH) synthesized using the modified polyol method.....	67
<b>Figure 4.14:</b> XRD pattern of commercial catalyst and IH catalysts prepared by modified polyol method.....	68

<b>Figure 4.15:</b> CV of commercial and IH catalysts prepared by the modified polyol method using H <sub>2</sub> O and without the use of a stabilizer in 0.5M H <sub>2</sub> SO <sub>4</sub> at a scan rate of 20 mv s <sup>-1</sup> .....	70
<b>Figure 4.16:</b> ORR of the commercial and IH catalysts prepared by the modified polyol method using H <sub>2</sub> O without the use of a stabilizer in O <sub>2</sub> saturated 0.5M H <sub>2</sub> SO <sub>4</sub> at a scan rate of 20 mv s <sup>-1</sup> .....	71
<b>Figure 5.1:</b> TEM images of IH catalysts synthesized using the sodium acetate modified polyol method, (a) Pt/C-IH, (b) Pt/MWCNT's-IH and (c) Pt/MWCNT's-F-IH.....	74
<b>Figure 5.2:</b> Histogram of the particle size distribution obtained from the TEM analysis from random particles of IH catalyst (Pt/C-NaOAc-IH) synthesized using the modified polyol method.....	75
<b>Figure 5.3:</b> Histogram of the particle size distribution obtained from the TEM analysis from random particles of IH catalyst (Pt/MWCNT's-NaOAc-IH) synthesized using the modified polyol method.....	76
<b>Figure 5.4:</b> Histogram of the particle size distribution obtained from the TEM analysis from random particles of IH catalyst (Pt/MWCNT's-F-NaOAc-IH) synthesized using the modified polyol method.....	76
<b>Figure 5.5:</b> XRD patterns of commercial and IH catalysts prepared by NaOAc as a stabilizer.....	78
<b>Figure 5.6:</b> CV of commercial and IH catalysts prepared by the modified polyol method using NaOAc as a stabilizer in 0.5M H <sub>2</sub> SO <sub>4</sub> at a scan rate of 20 mv s <sup>-1</sup> .....	80
<b>Figure 5.7:</b> ORR of the commercial and IH catalysts prepared by the modified polyol method using NaOAc as a stabilizer in a O <sub>2</sub> saturated 0.5M H <sub>2</sub> SO <sub>4</sub> at a scan rate of 20 mv s <sup>-1</sup> .....	81

## List of tables

<b>Table 2.1:</b> Properties of platinum.....	24
<b>Table 3.1:</b> Chemicals used for synthesis.....	42
<b>Table 3.2:</b> FT-IR instrument setup.....	49
<b>Table 4.1:</b> Summary of results obtained form TEM and XRD of the commercial and IH catalyts .....	69
<b>Table 4.2:</b> ORR current at 0.3 V.....	72
<b>Table 5.1:</b> Summary of results obtained form TEM and XRD of the commercial and IH catalyts synthesized using NaOAc as a stabilizer.....	79
<b>Table 5.2:</b> ORR current densities at 0.3 V.....	82



## List of schemes

<b>Scheme 2.1:</b> ORR mechanism.....	22
<b>Scheme 2.2:</b> Schematic diagram of a typical reaction using the polyol method.....	30
<b>Scheme 2.3:</b> Chemical reaction for the polyol method.....	31

## Abbreviations

<b>AFC</b>	Alkaline Fuel Cell
<b>CH<sub>3</sub>OH</b>	Methanol
<b>CO<sub>2</sub></b>	Carbon dioxide
<b>CNT's</b>	Carbon nanotubes
<b>CV</b>	Cyclic Voltammetry
<b>DMFC</b>	Direct Methanol Fuel Cell
<b>DWCNT's</b>	Double- walled carbon nanotubes
<b>EG</b>	Ethylene Glycol
<b>FC</b>	Fuel cell
<b>GNF's</b>	Graphite nanofibres
<b>H<sub>2</sub></b>	Hydrogen gas
<b>HCl</b>	Hydrochloric acid
<b>H<sub>2</sub>O</b>	Water
<b>H<sub>2</sub>PtCl<sub>6</sub></b>	Chloroplatinic acid
<b>H<sub>2</sub>SO<sub>4</sub></b>	Sulphuric acid
<b>IH</b>	In-house
<b>MCFC</b>	Molten carbonate fuel cell
<b>MEA</b>	Membrane electrode assembly
<b>MWCNT's</b>	Multi walled carbon nanotubes
<b>N<sub>2</sub></b>	Nitrogen gas
<b>NaCl</b>	Sodium chloride
<b>NaOAc</b>	Sodium acetate
<b>NaHSO<sub>3</sub></b>	Sodium sulphate
<b>NaOH</b>	Sodium hydroxide
<b>O<sub>2</sub></b>	Oxygen
<b>ORR</b>	Oxygen reduction reaction
<b>PAFC</b>	Phosphoric acid fuel cell
<b>PEMFC</b>	Proton exchange membrane fuel cell
<b>RDE</b>	Rotating disk electrode
<b>RFC</b>	Regenerative fuel cell
<b>SOFC</b>	Solid oxide fuel cell
<b>TEM</b>	Transmission electron microscope

**XRD**

X-ray diffraction

**ZAFC**

Zinc air fuel cell



UNIVERSITY *of the*  
WESTERN CAPE



**CHAPTER 1****1.1 INTRODUCTION**

In the day and age we as human beings are living in, there is an increasing demand on the amount of energy needed to ensure that daily activities are accomplished in the most efficient manner as possible.

In light of the predicted energy reserves and the expected lifetime of subterranean fossil fuel reservoirs, alternative sources of energy have to be considered. If one were to look at the statistics, approximately 27% of the world's energy is generated from the single primary source viz., coal [1]. This is a brownish to black sedimentary rock found in rock strata called coal beds. Coal is mainly made of carbon with varying amounts of trace elements such as sulphur, hydrogen, nitrogen and oxygen. The world's coal consumption is expected to increase from 5.3 billion tons in 2001 to 7.5 billion tons in 2025 [2], [3]. In light of this it can be envisaged that due to this increased demand the reserves will be depleted much sooner than predicted and present a crisis unless alternative sources of coal are found.

It is thus abundantly clear that alternative methods of providing energy requirements have to be investigated. These other avenues have not only to be more efficient than the existing systems, but their environmental impacts should be as minimal as possible. It is a fact that the existing infrastructures used to generate electricity emit a considerable amount of noxious gases into the atmosphere which leads to what is known as the Green House Effect, which is causing an alarming rise in temperature on the earth's surface. The rise in temperature has an additional cause viz., the depletion of the ozone layer which acts as a barrier to light wavelengths from the sun harmful and detrimental to our existence on earth. It is thus imperative that we search for alternative sources of energy to meet our daily needs with minimal impact on the

environment to ensure that the rest of our civilization's existence on this planet is as pleasant as possible.

This has resulted in a whole new body of research involving searching for new means and ways of generating electricity in a much more efficient and environmentally friendly way. From these efforts arose the Alternative Energy concept [4], which entails the use of renewable sources of energy e.g. the sun, wind, hydro etc in order to generate the power needed to sustain our daily requirements as well as the standard of living.

### **1.2 Fuel cell: An alternative energy source**

The first fuel cell was discovered and built in 1889 by a Welsh scientist named Sir William Grove. He was a physical chemist who discovered that when immersing two ends of platinum electrodes in sulphuric acid and each of the other ends were placed in two separate containers containing oxygen and hydrogen, a constant current flow would result. This led him to combine a few of these cells and he found that by connecting them he in fact invented what he called a gas battery. The research continued in an erratic manner for the next 75 years until the US space program in the 1960's breathed new life into this field by using these fuel cells as power sources in the shuttle's space flights. Subsequently many breakthroughs in fuel cell technologies have seen the light of day, and there have been major improvements when comparing the current status to the "gas battery" discovered by Sir William Grove.

A fuel cell is essentially a device that converts chemical energy into electrical energy.

Electrochemical devices generate electricity without combustion of the fuel and oxidizer, as opposed to the many traditional methods of electricity generation. In reality a fuel cell may be depicted as given in Fig 1.

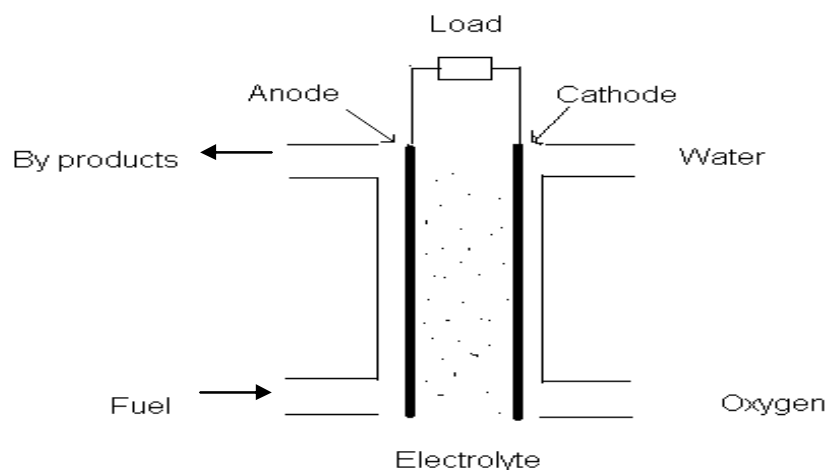


**Figure 1.1: Schematic diagram of the operating principle of a fuel cell:**



The diagram above (figure 1.1) illustrates the general operating principle of a fuel cell. On the anode side of the cell fuel enters and reaches the surface of one of the electrodes which are normally made up of highly conductive and porous carbon (Vulcan X26) onto which singular or in most cases binary catalysts are finely dispersed. Platinum metal is currently the most prominent metal in commercial use. At this stage an electrochemical reaction takes place, either oxidation or reduction depending on the type of fuel cell which then results in the gain or loss of electrons. The electrons are then passed through an external load and is measured as current. The by-products of these types of fuel cells are mainly water and a minimal amount of the Green House gases, viz., CO<sub>2</sub>. The beauty of these fuel cells is the fact they may serve a variety of purposes, from use in pocket and hand held devices to automobiles.

### 1.3 Different kinds of fuel cells

To date a number of fuel cells have been manufactured and commercialized. Examples include: the Solid Oxide Fuel Cell (**SOFC**), Proton Exchange Membrane Fuel Cell (**PEMFC**), Molten Carbonate Fuel Cell (**MCFC**), Phosphoric Acid Fuel Cell (**PAFC**), Alkaline Fuel Cell (**AFC**), Regenerative Fuel Cell (**RFC**), Zinc Air Fuel Cell (**ZAFC**) and last but not least the Direct Methanol Fuel Cell (**DMFC**). The different kinds of fuel cells are classified by their electrolyte used in their construction.

#### 1.3.1 SOFC:

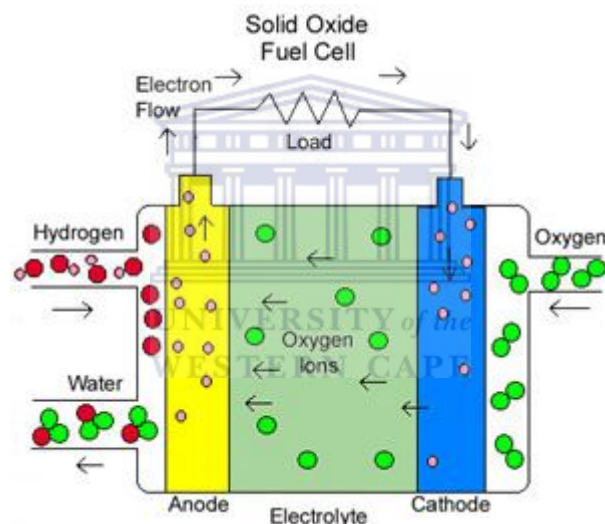


**Figure 1.2:** Diagram of a solid oxide fuel cell (SOFC)

The Solid Oxide Fuel Cell (SOFC) (Figure 1.2) consists of a solid oxide which acts as the electrolyte material. Unlike the conventional fuel cells, the SOFC generates a current by conducting negative oxygen ions from the cathode end of the cell to the anode where oxidation of oxygen ions occurs. The SOFC has an efficiency of approximately 50-60% in converting the fuel into electricity. Since a SOFC operates at high temperatures non-precious metals are normally employed instead of the conventional more expensive platinum due to the lack of poisonous substances that

reduce the activity and lifetime of the catalysts used under the relatively mild operating conditions. However the SOFC has a disadvantage in that it requires a slow startup time and the heat generated during power generation requires the correct thermal protection for the operational personal. Another disadvantage the SOFC possesses is the fact the because the materials used in the SOFC are exposed to fairly stringent conditions, durability may become a crucial factor in the efficiency of the SOFC [5]

### 1.3.2 PEMFC

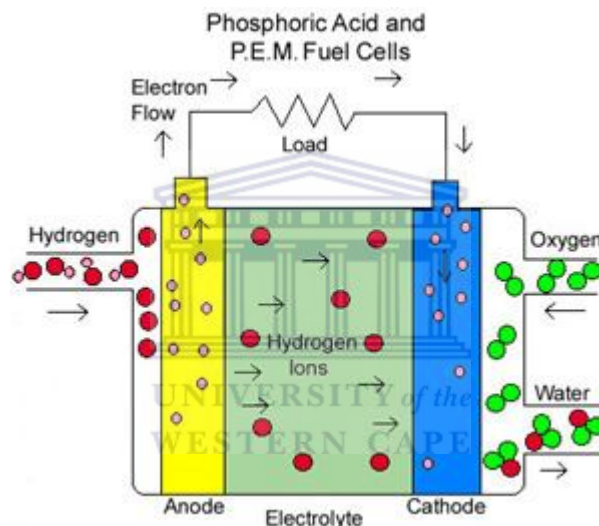


**Figure 1.3:** Diagram of a Proton Exchange Membrane Fuel Cell (PEMFC)

The Proton Exchange Membrane Fuel Cell (PEMFC) ( figure 1.3), also known as the polymer electrolyte membrane uses hydrogen gas as the primary fuel source which is either fed directly into the cell or is reformed from methanol or other bio fuel sources. The fuel is then catalytically split into protons and electrons at the anode. The protons pass through the selective permeable membrane while the electrons are passed through an external circuit representing the current. On arrival, after passing through the membrane the protons at the cathode end become reduced in the presence of oxygen to form water.

The PEMFC usually operates at low temperatures (100 °C). However, recent developments have made it possible for these kinds of fuel cells to operate at higher temperatures (200 °C). The advantages the PEMFC exhibits in comparison to the other fuel cells is that they have a good power to weight ratio, they are quiet and they operate at moderate temperature which prolongs the lifetime of the components used by the fuel cell. The advantages these kinds of fuel cells possess make them ideal for automotive use, viz., light motor vehicles, scooters and other small applications. This is due to their quick start up time and the fact that the total power output is reached in virtually a few minutes.

The disadvantage though, is that the precious metals used as catalysts are expensive and the cost of scaling up would be much higher as compared it to the existing systems in use [6].

### 1.3.3 MCFC

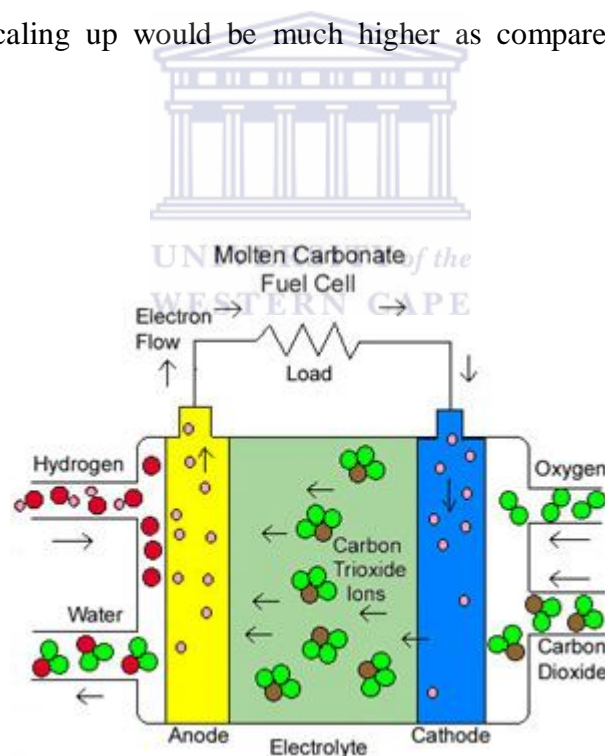


**Figure 1.4:** Diagram of a Molten Carbonate Fuel Cell (MCFC)

The Molten Carbonate Fuel Cell (MCFC) (figure 1.4) utilizes high melting temperature salts viz., sodium or magnesium carbonates as an electrolyte. These kinds of fuel cells normally operate at high temperatures, and as a result these kinds of fuel

cells do not use expensive catalysts and are not subjected to carbon monoxide poisoning and the heat generated may be recycled and used to generate more electricity. The efficiency of these cells range from 60 to 80%, and the operating temperature is about 650 °C. The high operating temperatures of the MCFC allows it to use natural gases directly and thus does not need any reforming. Thus the beauty of these kinds of fuel cells is that, due to their high operating temperatures they reform the natural gases internally and this contributes to a reduction in their operational cost. In light of the high temperature the MCFC operates under, the major problem researchers are facing now is in durability. The high operating temperatures gives rise to corrosive problems and short lifespan of parts due to excessive heat formation over prolonged periods of time, which would in turn lead to an overall decrease in terms of the fuel cells efficiency [7].

#### 1.3.4 PAFC

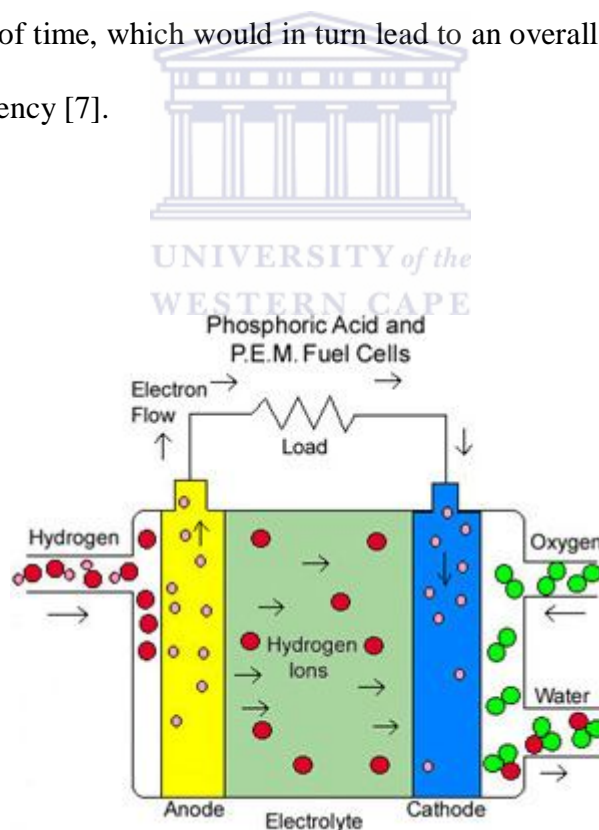


**Figure1.5:** Diagram of a Phosphoric Acid Fuel Cell

The Phosphoric Acid Fuel Cell (PAFC) (figure 1.5) uses phosphoric acid as an electrolyte. These kinds of fuel cells are used under high temperature applications.

The efficiency ranges from 40 to 80%, and the operating temperature ranges between 150 to 200 °C. The beauty of PAFCs is the fact that they can tolerate carbon monoxide impurities in any gaseous feedstock and this reduces the limitations of the fuels one can use.

These kinds of fuel cells are mainly used in stationary applications due to their weight to volume ratio. In considering their efficiency, these cells are not that efficient when one only considers the production of electricity. However when these cells are used in cogeneration systems their efficiency increases almost two fold. The major disadvantage of these kinds of fuel cells is much like the others viz., their cost. The PAFC makes use of precious metals as both anode and cathode catalysts which could prove costly if one thinks of production and commercial use [8].

### 1.3.5 AFC

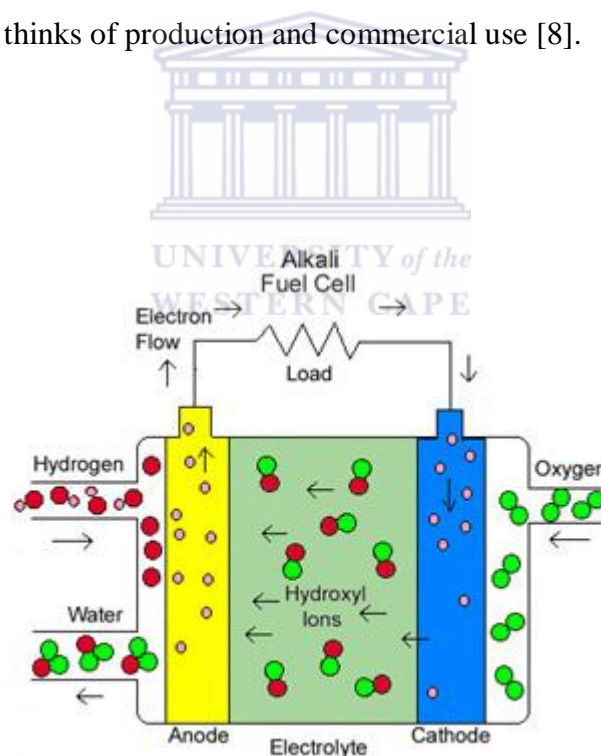


**Figure 1.6:** Diagram of an Alkaline Fuel Cell (AFC)

In an Alkaline Fuel Cell (AFC) (figure 1.6) the electrolyte consists of an alkaline solution, normally potassium hydroxide. The reactant gases used in these kinds of cells are normally pure compressed hydrogen and oxygen. These cells have an efficiency of 70% and operating temperatures of 120 °C to 200 °C [9].



### 1.3.6 Regenerative fuel cells (RFC's)

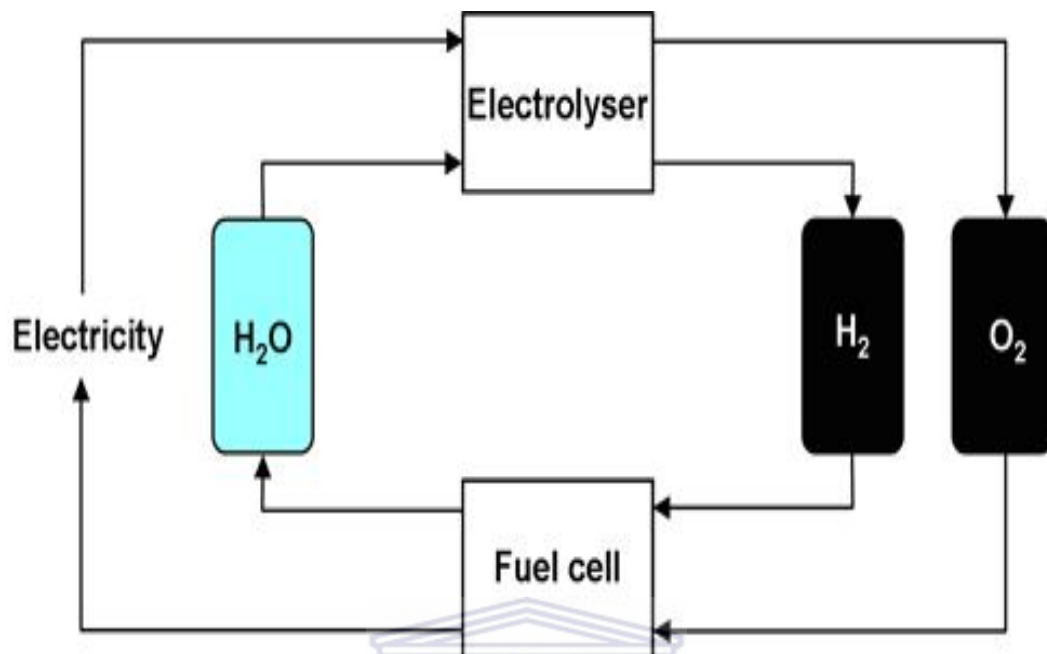


**Figure 1.7:** Diagram of an RFC (RFC diagrammed sourced from CMR PROTECH [10])

A fuel cell generates electricity from the chemical energy of its reactants whereas an electrolyser generates hydrogen and oxygen from water using electricity. A Regenerative Fuel Cell (RFC) makes use of regenerative sources in order to generate electricity. RFC's are bifunctional which means they RFC can operate in both electrolysis and fuel cell mode. In electrolysis mode the RFC makes use of electricity and water to produce hydrogen and oxygen. In fuel cell mode the RFC takes in hydrogen and oxygen/air to produce electricity and water. RFC's have a wide variety of applications including energy storage devices linked to renewable energy sources, in the automobile industry. They are also being considered for use in NASA missions [11], [12], [13].

## 1.3.7 Zinc-Air Fuel cell (ZAFC)

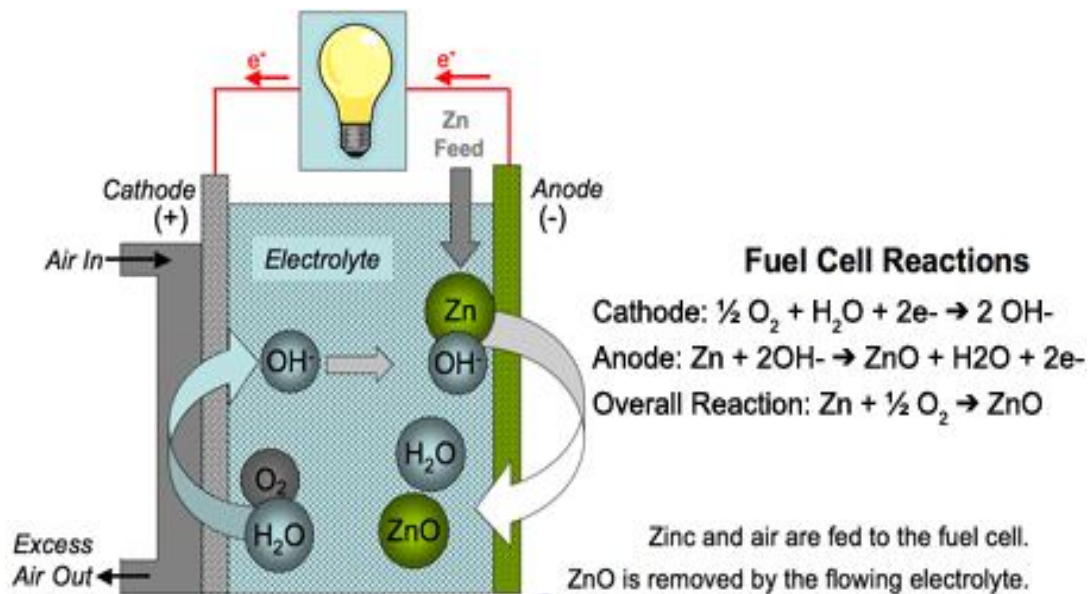
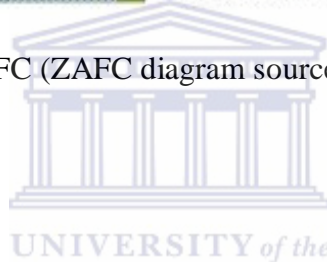


**Figure 1.8:** Diagram of a ZAFC (ZAFC diagram sourced from zincenergystorage.org [14].



A ZAFC consists of a zinc anode and an alkaline electrolyte separating the anode from the cathode. The ZAFC generates its current through a reaction between zinc pellets and atmospheric oxygen in an alkaline electrolyte. At the cathode end of the ZAFC, oxygen is electrochemically reduced to hydroxide ions by reacting with water on the gas permeable electrode. Zinc undergoes oxidation via the hydroxide ions and the discharged electrons pass through an external load which generates the current. ZAFC theoretically should generate 1.64 V but in practical terms this has not yet been achieved. ZAFC's are environmentally friendly and its components are recyclable [15].

## 1.3.8 Direct Methanol Fuel Cell (DMFC)

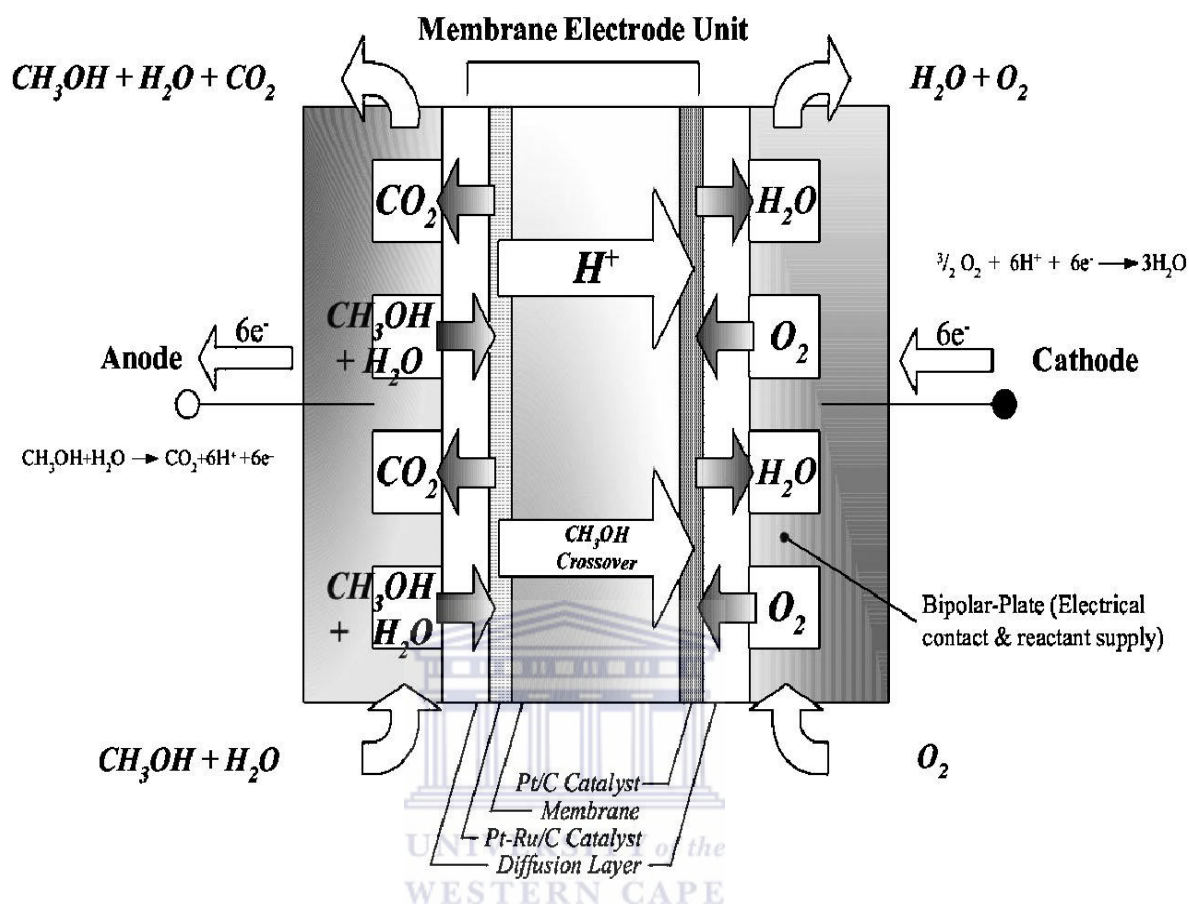
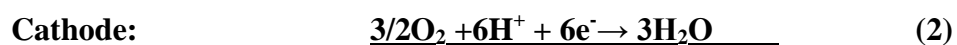
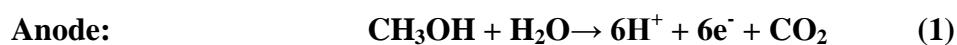


**Figure 1.9:** Diagram of a Direct Methanol Fuel Cell (DMFC)

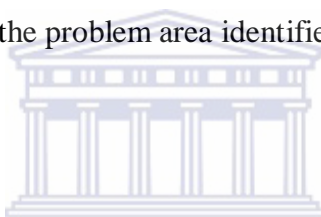
Direct Methanol Fuel Cells (DMFC's) (figure 1.7) represent one of the most promising advanced electrochemical systems for the production of electricity. If one looks at fuel cells from an environmental point of view, then fuel cells represent one of the most environmentally friendly technologies while not forgetting the other green technologies currently present.

The overall reaction of what happens in a DMFC is represented as follows:



At the anode end of the DMFC a mixture of methanol and water is fed into the cell and this is where the methanol/water mixture is oxidized with the release of 6 protons and 6 electrons with carbon dioxide as the by-product. The protons migrate through the selectively permeable membrane and the electrons travel through an external load to generate a current.

On the cathode end of the DMFC oxygen is reduced at the surface of the electrode to water via the 6 protons which permeated through the selectively permeable membrane to the cathode end of the DMFC. The byproduct of this reaction is water and this may be recycled and used again in the fuel cell, whether it be as part of the fuel or as a temperature regulator through cooling the whole system. This is where the oxygen reduction reaction occurs and the problem area identified for the proposed research.



#### 1.3.8.1 Advantages of a DMFC:

The main advantage of the DMFC technology in comparison to the conventional processes available today is that it does not make use of a combustion process since it utilizes electrochemical technologies. In relation to the conventional processes, fuel cells are also very energy efficient, fuel flexible and reliable. In essence the DMFC uses methanol as the primary fuel source. DMFC's are a subcategory of proton-exchange fuel cells where the methanol ( $\text{CH}_3\text{OH}$ ) fuel is not reformed, but fed directly to the fuel cell [16]. DMFC's operate at moderate temperatures and thus do not need complicated cooling systems to remove heat generated during the reactions that take place in the fuel cell. This also reduces the overall weight of the system and makes it much more affordable in portable systems. The fuel source may be extended to not only use methanol but include other sources such as natural gas, biomasses and

fermentation of agricultural products such as ethanol [17].

Storage of  $\text{CH}_3\text{OH}$  is much easier when compared to hydrogen as it does not need high pressures or low temperatures, since methanol is a liquid from  $-97.0\text{ }^\circ\text{C}$  to  $64.7\text{ }^\circ\text{C}$  ( $-142.6\text{ }^\circ\text{F}$  to  $148.5\text{ }^\circ\text{F}$ ). As a result of this, DMFC's are ideal for application in consumer goods such as cell phones, laptops, digital cameras and other small items.

### 1.3.8.2 Disadvantages of a DMFC

One of the problems associated with DMFC's is in their poor methanol electro-oxidation kinetics [18], [19]. Methanol membrane crossover gives rise to mixed potentials and results in an over potential of  $\sim 0.3\text{ V}$  at the cathode end even under open circuit conditions due to the highly irreversible oxygen reduction reaction, which results in a loss of  $\sim 0.2\text{ V}$ . Methanol membrane crossover that originates from methanol permeating through the selectively permeable membrane also cause short circuits at the cathode end resulting in a further loss of  $0.1\text{ V}$ . The thermodynamic efficiency of a DMFC is  $1.19\text{ V}$  but given the losses mentioned above the overall efficiency of the DMFC is 25% less than what is theoretically expected at the cathode end of the cell. This gives rise to the sluggish reaction kinetics at the cathode end of the DMFC and this is counterbalanced by requiring considerable amounts of catalysts to promote the oxygen reduction reaction which in turn increases the overall cost of the fuel cell unit.

### 1.4 Rationale of the research project

One of the major problems associated with the DMFC deals with the cathode end of the fuel cell where reduction of oxygen to water occurs as discussed above. The sluggish kinetics with which this reaction proceeds results in a considerable loss in the overall efficiency of the DMFC.

This has led to intensive research being undertaken in order to address the problems associated with the DMFC. Due to the fact that all the problems associated with the DMFC can be traced back to the catalysts used at the electrode surfaces, a considerable amount of time and effort has been expended in addressing this problem and finding lasting solutions. In light of this fact the development of the aims and goals with regard to the project were developed.

Aims and Objectives:

- To develop cathode catalysts for the DMFC for the oxygen reduction reaction (ORR).
- To synthesize and formulate metal catalysts in a carbon matrix initially
- To evaluate all their properties using analytical electrochemical techniques such as X-ray Diffraction Spectroscopy, Transmission Electron Microscopy, and Electrochemical Cyclic Voltammetry. The above mentioned techniques will assist in the assessment of the various metal catalysts synthesized, and will assist in our better understanding of the nature of these catalysts
- To promote the improvement in the activity and efficiency of the proposed catalysts. These techniques have been used extensively.



**The variables or modifications envisioned that could be employed in developing a new synthetic protocol are as follows:**

- Varying the temperature of reduction of the metal and relative concentrations of the components to determine how these parameters play their roles during the synthetic protocols which would be employed
- Introduction of electrostatic stabilizers into the synthetic protocol and observing the effect on the stability and efficacy of the synthesized catalysts.
- The effect of pH and water content in the reaction mixture would also be investigated
- The use of different conductive supports viz., carbon black and multi walled carbon nanotubes (MWCNT's).
- Internal sonication will also be employed to obtain uniform distribution of metal nanoparticles in solution.
- The use of another solvent other than ethylene glycol that may also act as both solvent and reducing agent during synthesis.
- The introduction of a secondary cheaper metal to assist in both the oxygen reduction reaction and the longevity of the synthesized catalysts' lifetimes.

## **1.5 Thesis outline**

### **Chapter 2: Literature review**

This chapter focuses briefly on the concepts related to catalysts and catalysis. Fundamental concepts relating catalysis to fuel cell are presented in this chapter. The various synthetic protocols for synthesizing catalysts are also presented in this chapter. The informed choice on which synthetic protocol to complete the proposed work could then be made. The chapter aims at providing a concise and informative guide to the literature consulted for the proposed work.

### **Chapter 3: Materials and methods**

This chapter briefly describes the materials and methods used in order to complete the proposed work. The materials and synthetic routes are explained in detail. The various physiochemical and electrochemical techniques used to characterize the in-house (IH) proposed catalysts are briefly explained in this chapter.

### **Chapter 4: Results and discussion**

This chapter focuses on the physiochemical and electrochemical characterization of commercial catalyst as well as the IH catalysts synthesized using the modified polyol method.

### **Chapter 5: Results and discussion**

The chapter focuses on the physiochemical and electrochemical characterization of IH catalysts synthesized using sodium acetate as a stabilizer in the modified polyol method.

### **Chapter 6: Conclusion and recommendations**

This chapter gives an overall conclusion of the work completed in the thesis and future recommendations for fuel cell catalyst synthesis



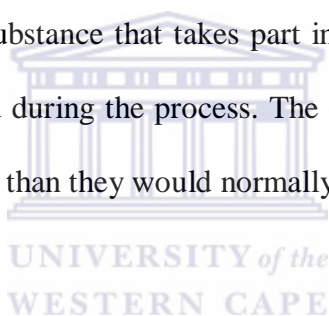
### **2.1 Literature review/Theoretical framework**

This chapter aims to familiarise the reader with the theory and literature consulted with regards to the proposed project. In light of this it is realised that not all the literature pertaining to the synthesis of catalysts has been extensively covered and thus only the relevant information in relation to the proposed project is presented.

In order for one to fully understand fuel cell catalysts in general one has to have a fundamental understanding of what catalysts are, able to do and what they are currently used for.

### **2.2 Catalyst**

A catalyst is an element or substance that takes part in a chemical reaction but does not get used up nor destroyed during the process. The catalyst facilitates reactions to proceed at much quicker rates than they would normally proceed.



### **2.3 Chemical action**

Catalysts provide an alternative pathway for a reaction to follow which uses less energy and gives the same products as the more energy intensive process would require. Molecules that would not have had the energy to react or have such low energies that it is likely that they would take a long time to do so, are able to react in the presence of a catalyst.

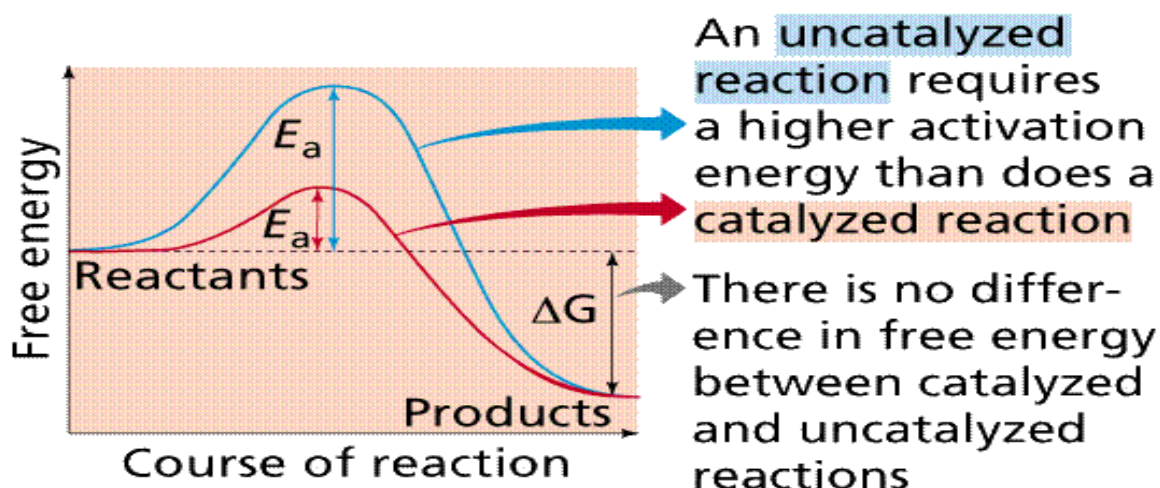


**Figure 2.1:** Diagram displaying the activation energy pathways with and without a catalyst

As seen from the above diagram an uncatalyzed reaction requires higher activation energy than that of a catalyzed reaction. The conclusion can thus be made about the importance of a catalyst during reactions. Catalytic reactions can be classed into two groups viz., homogenous and heterogeneous catalysis.

In homogeneous catalysis the catalyst and reactants are in the same phase. An example of this would be if all the reactants and the catalyst would be in a gaseous or liquid phase. In heterogeneous catalysis on the other hand, the catalyst and reactants are in two different phases. An example of this would be when the catalyst is in a solid phase and the reactants were in a liquid or gaseous phase. In industry heterogeneous catalysis is extensively used to produce a variety of commercially available products today. The major advantage for the latter process is because the catalyst can be separated from reactants/products and may be recycled and thus makes commercial sense on an industrial scale.

## 2.4 Catalysts used in fuel cells

The catalysts used in fuel cells may be classified as heterogeneous catalysts. This is due to the fact that the catalysts used for fuel cells are normally noble metals immobilized on a conductive support.

Catalysts used in fuel cells are classified according to specific reactions they would undergo in a fuel cell. In terms of a DMFC the catalyst would either be referred to as an anode or a cathode catalyst. An anode catalyst would usually be used in oxidizing fuels at the anode end of the cell and cathode catalysts would usually be used in reducing reactants at the cathode end in the fuel cell.

As mentioned in chapter 1, in a DMFC, methanol is used as a fuel source. This means that the anode catalyst used in the DMFC should be capable of oxidizing methanol and would have to meet certain requirements for this reaction.

The same goes for the cathode catalyst. At the cathode end of the DMFC the catalysts used must be able to reduce oxygen to water and in turn would have to meet certain requirements for this reaction [20], [21].

The same goes for the cathode catalyst. At the anode end of the DMFC the catalysts used must be able to reduce oxygen to water.

## 2.5 Supports for catalysts

The catalysts used at the electrode interfaces are either unsupported or supported on some or other conductive support to facilitate the electronic transfer and various other processes associated with reactions at the catalyst surfaces.

In the case of unsupported catalysts one has the joy of no interferences of the support on the activity of the catalysts. However, the disadvantage of these catalysts is that it generally requires one to use more of the catalyst than one would normally use.

Consequently supported catalysts are generally the ones in use due to both their practicality and influence on surface area [22].

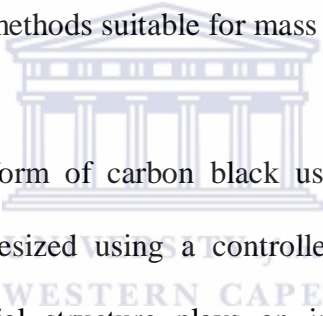
### 2.5.1 Requirements of a good support

A good support must adhere to the following requirements for it to be used for FC's;

- Provide a high electrical conductivity
- Allow reactant gases to get to the catalysts easily
- It should have adequate water handling capabilities at the cathode where water is generated.
- It should also have good corrosion resistance because the cathode end of the DMFC experiences strong oxidizing conditions

### 2.5.2 Supports used for electrocatalysts

The ideal supports generally used for nano sized catalysts in fuel cells are high surface area carbon blacks. Carbon blacks are virtually pure elemental carbon in the form of colloidal particles that are formed from the incomplete combustion or thermal decomposition of hydrocarbons under controlled conditions [23]. The characteristics of carbon blacks vary depending on the synthetic route followed to produce them. Furnace blacks are produced by blowing petroleum oil or coal oil as raw material into high-temperature gases to partially combust them. Acetylene blacks are produced by the thermal decomposition of acetylene gas. The Lampblack process involves the collection of soot from the fumes generated by burning oils or pine wood and this is regarded as one of the oldest methods suitable for mass production of carbon [24]



Vulcan XC72 is powdered form of carbon black used as a support for fuel cell catalysts and they are synthesized using a controlled vapour phase pyrolysis of hydrocarbons. Carbon material structure plays an important role in the catalyst dispersion, in its crystallographic characteristics, and consequently in its electrochemical properties as well as in the way the catalyst redistributes on the carbon support surface during cell operation [25], [26], [27], [28], [29].

In recent times alternative conductive supports other than carbon blacks have come to the fore. Carbon nanotubes have attracted much interest as an alternative support for fuel cell catalysts due to their unique properties.

Carbon nanotubes (CNT's) are made of hexagonally shaped structures of carbon arranged in such a manner as to form a tube from which it derives its name. CNT's are generally synthesized by carbon arc discharge, laser ablation of carbon and chemical vapour deposition methods which is generally using catalytic particles. The

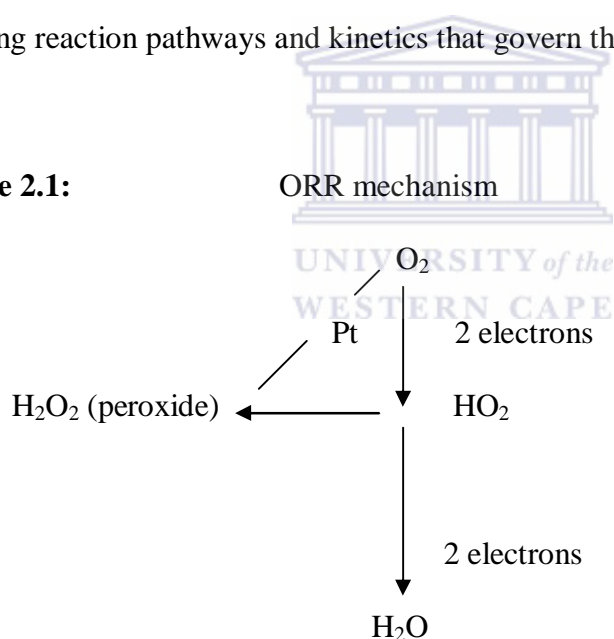
major reason why CNT's are attracting so much attention as supports for catalysts are not only because of their strength and electrical conductivity but due to the larger surface area available for the catalysts to be deposited onto.

Other avenues have also been explored in an aid to find the ideal support for cathode catalysts. This includes the study of carbon nanofibres [30], [31], [32], [33], graphitic mesoporous carbon [34] and carbon xerogels [35].

## 2.6 Oxygen reduction reaction (ORR)

The oxygen reduction reaction at the cathode end of the fuel cell is a complex reaction which is not quite fully understood and many research groups have put effort into proposing reaction pathways and kinetics that govern the reaction.

**Scheme 2.1:**



The ORR on platinum surfaces is explained by the above diagram (scheme 2.1). The reduction occurs via two parallel reactions, the first being the direct reduction of oxygen to water by a four electron transfer and the second via an intermediate two electron transfer process where hydrogen peroxide is generated [36]. Rotating ring disc electrode (RRDE) studies have also confirmed the fact that on a platinum surface

O<sub>2</sub> reduction occurs in a 4 electron transfer process from O<sub>2</sub> to H<sub>2</sub>O in both acidic and aqueous solutions if no impurities are present [37].

The most familiar ORR catalysts are based on noble metals due to their characteristic electrochemical properties, the most prominent of them being platinum. They have been investigated in their pure metal form, nanoparticles and as polycrystalline and single crystal faces [38].

Platinum is the most promising electrocatalyst for the ORR since it exhibits good activity and chemical stability under operating conditions. Studies have been undertaken to study the effect of loading, dispersion and surface structures would have on the ORR. It was observed that the electrocatalytic activity of Pt was 20 times lower on 1.5 nm crystallites than on crystalline platinum black [39]. On the other hand Bett et al. did not observe any changes in activity for supported platinum catalysts in the range of 3-40 nm [40]. Kinoshito contradicted the effect of particle size on electro catalytic activity in acidic media [41]. He discovered that maximum mass activity (current per gram of platinum) was evident at a particle size of 3-5nm. This was also attributed to the fact that a change in the fraction of surface atoms occurred on the (100) and (111) crystal faces of platinum particles and predicted that the specific mass activity would increase with an increase in particle size [42]. Other studies have also been done and all of them supported this latter fact viz, [43], [44], [45].

### 2.7 Platinum as a catalyst for DMFC's

Platinum is a chemical element that belongs to a group of metals known as noble metals and they are found in group 10 of the periodic table of elements. Platinum is dense, malleable, ductile and a most precious metal (Table 2.2). Platinum is also extremely conductive and corrosion resistant which makes it ideal for fuel cell applications.

<b>Name:</b>	Platinum
<b>Symbol:</b>	Pt
<b>Atomic weight:</b>	195.084 g/mol
<b>Standard state:</b>	Solid at 298K
<b>Group:</b>	10
<b>Group name:</b>	Precious metal or platinum group metal
<b>Color:</b>	Grayish white
<b>Classification:</b>	Metallic

**Table 2.1:** Properties of platinum supplied by <http://www.webelements.com/platinum>

Platinum which is normally used in the synthesis of catalysts for fuel cells comes in the form of chloroplatinic acid. This metal salt is formed when platinum is digested in a mixture of hydrochloric and nitric acid (1:3) respectively to form a salt. The metal salt is very stable if kept under a controlled environment. However, if not, it becomes hygroscopic and sensitive to water and light.



## **2.8 Different synthetic routes for the synthesis of catalysts for fuel cells:**

### **2.8.1 Sulfite complex route**

This method involves the synthesis of Pt sulfite complexes in an aqueous solution. The general starting metal precursor salts are  $\text{H}_2\text{PtCl}_6$  which is suspended in an aqueous solution containing  $\text{NaHSO}_3$ . This is then subjected to oxidative decomposition with hydrogen peroxide with simultaneous adsorption onto the support already suspended in solution. The catalysts are then filtered and further subjected to heat treatment and reduced under a flow of hydrogen gas, [46], [47]. The advantage of this method is that one is able to obtain monomodal platinum nanoparticles with a mean particle size value of 2.6 nm

### **2.8.2 Bönnerman method**

Bönnerman's method involves suspending  $\text{PtCl}_2$  in anhydrous tetrahydrofuran (THF) which is then treated with tetra-alkyl ammonium hydro-tri-organoborate, which results in a platinum metal colloid solution with a minimal evolution of hydrogen. This colloidal solution is evaporated to dryness under high vacuum, and the resultant waxy residue is mixed with ether. The colloid is then precipitated by addition of ethanol. The gray-black metal colloidal powder thus obtained has a particle size between 1 and 5 nm [48], [49]. This method is renowned for the preparation of bimetallic systems which require a narrow particle size distribution. However a disadvantage of this method is that it involves a number of complicated and expensive steps and takes a fair amount of time.

### 2.8.3 Impregnation method

The impregnation method is seen as one of the most common and simplest methods for the preparation of fuel cell catalysts. The method generally involves the impregnation of a metal salt solution onto a support after certain time intervals. The slurry is then heated to remove the solvent and the residue is subsequently reduced at elevated temperatures to decompose the salt and give rise to the desired catalyst. A variation of this method known as the incipient wet impregnation general reaction involves soaking a metal precursor ( $\text{PtCl}_6^{2-}$ ) into the pores of a support before the reduction step. The reduction step is usually carried out using borohydrides, hydrazine, formic acid or hydrogen gas depending on the desired result [50]. The major disadvantage of the impregnation method is that it is difficult to prepare a homogeneous catalyst with a narrow particle size distribution especially when chlorine containing metal precursors are used [51]. A number of researchers have used this method for the synthesis of mono and bimetallic catalysts systems for fuel cells [52], [53] and [54].

### 2.8.4 Adams fusion method

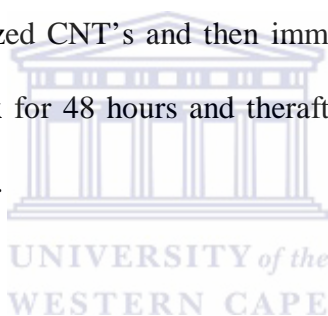
This method is generally used for the synthesis of unsupported metal catalysts for fuel cells and is based on the oxidation of metal precursors in a molten nitrate melt. The method generally involves heat treatment of metal salts in a solvent of choice and the resulting metal oxide evaporated to dryness and then collected. The method is ideal for synthesizing metal powders with small particle sizes. The disadvantage of this technique is that during the synthesis, impurities are generated in the form of a salt which can only be removed with a great amount of difficulty [55].

### 2.8.5 Microemulsion method

The microemulsion method may be defined as a method of dispersing immiscible liquid such that one of the liquids form nanosized droplets by shaking, stirring or homogenising the mixture. As the definition states, the method generally involves the use of two immiscible liquids, e.g. water and cyclohexane followed by the addition of a surfactant and reducing agents depending on the desired result. The chemical reaction occurs the small drop of the metal precursor liquid that is surrounded by a surfactant molecule. The microemulsion is dispersed in a continuous liquid phase which is immiscible in the metal precursor liquid containing phase. The sizes of the microemulsion droplet generally range from a few nanometers to hundreds of nanometers. The particle sizes are controlled through varying the amount of surfactant or the free energy differences arising from the immiscibility of the two liquid phases. Hu et. al. concluded that the main factors affecting particle growth are: sol preparation and phase transfer, removal of water, solvent, drying and calcination [56]. Barnickal and coworkers showed that just by varying the water to surfactant ratio one could control the particle sizes obtained [57]. The disadvantage of the microemulsion method is that it requires expensive surfactants and numerous washing steps which in terms of scaling up, it would not be that economical.

### 2.8.6 Ion exchange method

This method involves depositing platinum nanoparticles onto a support e.g. carbon (CNT's) without the aid of protective and reducing agents and metal precursor complexes which are not that easy to decompose. The technique makes use of a Pt cation complexes viz.,  $[\text{Pt}(\text{NH}_3)_4]^{2+}$  which is exchanged by hydrogen ions of the acid groups on the surface of the CNT's. Thus it may be envisaged that the dispersion of platinum nanoparticles would be dependant on the interaction between the cation and the acidic groups. If the ion-exchange process is complete the Pt cation complex then is reduced in a  $\text{H}_2$  atmosphere. Yin and coworkers used the method to fabricate an electrode composed of platinum nanoparticles supported on CNT's. The group electrochemically functionalized CNT's and then immersed the CNT's in a solution of a platinum cation complex for 48 hours and thereafter reduced the product with a flowing stream of  $\text{H}_2$  gas [58].



### 2.8.7 Vapour phase method

In the vapour phase method used for the synthesis of nanoparticles, conditions are created where the vapour phase mixture is thermodynamically unstable relative to the formation of the solid material to be prepared in the nanoparticulate form [59]. There are two kinds of gas phase reactions that are employed for the synthesis of nanoparticles; ie the two-step process which consists of the gas-phase adsorption of the precursor on the support followed by thermal treatments required to obtain the active catalyst and the other being a one-step process in which the precursor is simultaneously adsorbed and decomposed on the heated support.

### 2.8.8 Sol-gel method

The sol-gel method involves dissolving the desired metal precursor salts in solvents such as acetone at the desired concentrations (e.g. 0.00338 moles of each salt per 100 mL of acetone) at a temperature of 50 °C. A solution of 25% tetramethylammonium hydroxide  $[(\text{CH}_3)_4\text{NOH}]$ , also denoted as TMAH] in methanol is then added to the precursor salts in acetone solution to act as a high-molecular-weight hydrolyzing agent. The addition of the TMAH counteracts the undesired tendency of the metal precursors have to precipitate as separate phases during the subsequent evaporation of the solvent, thereby helping to yield a desired homogeneous amorphous gel. The solution is stirred and the solvent is evaporated until the solution becomes viscous, eventually transforming into a gel. The viscous gel is dried in air at elevated temperatures for a predetermined time. The dried gel is crushed into a fine powder to be used as catalysts in fuel cells [60].

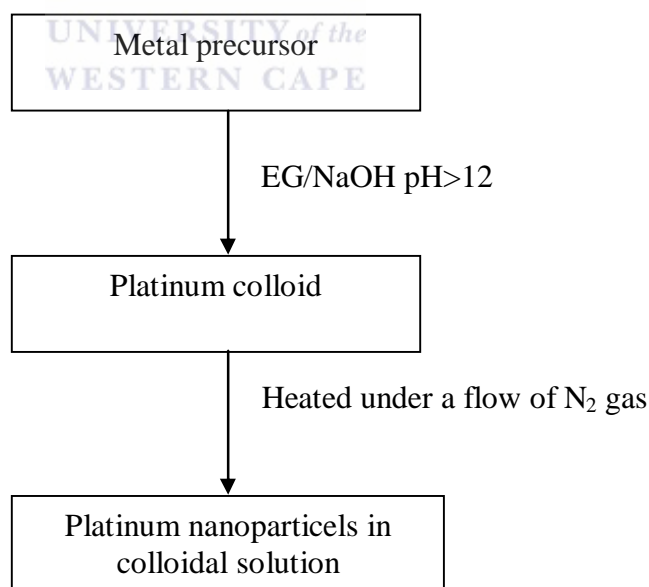
H. B. Suffrendini and co workers used the sol-gel method to synthesize Pt–RuO<sub>2</sub> deposits on a carbon black substrate and evaluated the catalysts activity towards methanol electrooxidation [61]. Hua studied the effect of metal precursor and calcination on the synthesized catalysts using the sol-gel method [62]. M.L. Calegario and co workers showed that the sol-gel method is an attractive way of synthesizing catalysts by incorporating different metal oxides on a substrate composed of platinum dispersed on carbon [63].

### 2.8.9 Polyol method

The polyol method belongs to a class of syntheses of catalysts; namely the colloidal methods. This approach to making is more generally known as a “bottom-up” method similarly to the synthetic methods mentioned in section 2.8. The colloidal method involves dissolving metal precursors, generally chloroplatinic acid in reducing agents in the presence of a wide variety of stabilizing agents.

The polyol method was developed by Fievet et al [64]. In this method a diol or polyalcohol (ethylene glycol {EG}, diethylglycol, buteneglycol) is used as both the solvent and reducing agent for the metal precursors [65]. Liu and co-workers reported though that when other glycols like propylene 1,2-glycol and butylene 1,4-glycol were used in the polyol method they could not form stable metal colloids [66].

#### Polyol method reaction mechanism



**Scheme 2.2:** Schematic diagram of a typical reaction using the polyol method.



The beauty of the polyol method is that the diol acts as both reducing agent and as a stabilizer, when compared to the other methods mentioned previously where reducing and stabilizing agents had to be added to control the nanoparticle growth.

### **2.8.9.1 Literature concerning the polyol method**

The polyol method has been extensively investigated by researchers to fully understand the reactions involved and the complexity that goes with it [71], [72]. In light of this many groups have focused their research on reducing the particle size and distribution of the nanoparticles onto the supports using this technique. The research focus areas concerning Pt on various supports are mainly;

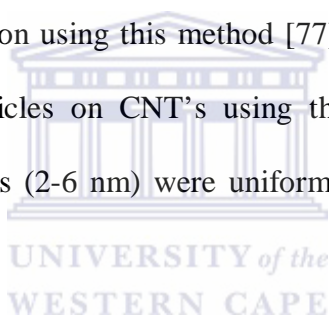
- ❖ Dispersion and loading
- ❖ Using steric or electrostatic stabilizers
- ❖ The use of various supports

### **2.8.9.2 Dispersion and loading**

Cushing et al found it difficult to obtain a homogeneous dispersion of platinum nanoparticles (2-5 nm) onto carbon supports [73], however highly dispersed Pt/C catalysts with high metal loading is known to be an efficient electrocatalyst for ORR DMFCs [69]. One of the major problems associated with loading nanoparticles onto a support is, as the loading increases so does the particle size. Legratiet et al reported that as the loading was increased from 10-60 wt% so too did the particle size show an increase from 2 to 8 nm respectively [74]. Thus in order to obtain the desired dispersion and loading onto a support the polyol method had to be modified. Many research groups have looked at means and ways of improving synthetic routes for catalysts [75]. The initial parameter that is often considered is temperature. Modifications in temperature influences the reaction by changing the stabilization of the nanoparticles of Pt formed and the nucleation rate of the reduced metallic atoms.



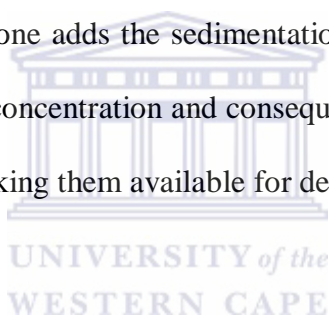
If the reactions are carried out at elevated temperature (80-160<sup>0</sup>C) EG may be more readily oxidized and the metal precursors more easily reduced. Other means of heating EG have also been investigated. Microwave irradiation of the colloid to reduce the metal precursor in solution has also been investigated. Microwave heating enables uniform heating, with considerable speed, energy efficiency and a certain degree of simplicity in terms of synthesis. Zhao and co workers synthesized Pt/C catalysts using the microwave assisted polyol method. The group focused on the effect that pH has on the particle size and distribution of Pt/C catalysts [76]. A pulse microwave assisted polyol method was also investigated and it was found that a very high loading of up to 50 wt% was achieved with very good dispersion and very narrow particle size distribution using this method [77]. Zhaolin Liu and co-workers deposited platinum nanoparticles on CNT's using the microwave assisted polyol method, and the nanoparticles (2-6 nm) were uniformly deposited onto the support [78].



The loading and dispersion of Pt nanoparticles onto supports was not only found to be dependant on temperature but was also found to be a function of pH. As mentioned above the mechanism by which the polyol method occurs and the concentration of the glycolate anion (which is a function of pH) plays an important role in Pt particle size and loading on carbon. Oh and co workers discovered that the loading of Pt onto the support decreased with increasing alkalinity of the solution. This was further supported by results obtained using Zeta potential measurements. A Zeta potential may be defined as the potential difference measured in a liquid, between the shear plane and the bulk of the liquid beyond the limits of the electrical double layer [79]. The magnitude of the Zeta potential gives an indication of the potential stability of

the colloidal solution. It was found that for the carbon supports the Zeta potential decreased to negative values with an increase in pH whereas the Zeta potentials remained constant at a negative charge after pH6. This therefore implied that poor adsorption forces between the metal colloids and the supports exist and would result in reduced metal loading. It was also observed that when conducting the reduction reactions under different atmosphere's (N<sub>2</sub>, O<sub>2</sub> etc.) one could effectively control the loading [80].

Typical “sedimentation promoters” would be acidic species, for example HCL, NaCl and H<sub>2</sub>SO<sub>4</sub>. The reason being, after complete reduction of the metal salt, the nanoparticles are suspended in solution by the glycolate anions which acts like a chelating type complexes. If one adds the sedimentation promoter, one is effectively reducing the glycolate anion concentration and consequently freeing the nanoparticles suspended in solution and making them available for deposition onto the support.



### 2.8.9.3 Supports

The supports used for catalysts have various conductive and structural properties associated with them. One of the most important properties associated with catalysts is its the surface area. The greater the surface area of the support the greater the area for the nanoparticles to deposit themselves onto. Generally Carbon Vulcan is used as conductive support for fuel cell catalysts [81], [82]. This is mainly due the structural and conductive properties of this carbon. Important in this regard however is that it provides an adequate surface area for nanoparticles to deposit themselves on. Research groups have observed that the activity and dispersion of nanoparticles onto a support can be related to the surface area which in turn leads to the search for supports other than just carbon blacks. The study of CNT's led to the use of CNT's as supports for fuel cell catalysts. Since then it has attracted much attention in fuel cell applications [83], [84]. An improved electrochemical performance of CNT based electrodes with respect to carbon blacks was also found to be due to the higher electrical conductivity ( $10^4 \text{ S cm}^{-1}$ ) of CNT's relative to that of carbon ( $4.0 \text{ S cm}^{-1}$ ) [85].

Many research groups have focused on synthesizing catalysts on different supports and studying their structural properties and electrochemical activity to the electro oxidation of methanol at the anode or the ORR at the cathode end of the DMFC.

Various novel carbon materials have been explored as supports to improve the electrocatalytic activity of catalysts for the ORR. This has included the study of tubule membranes prepared by template methods using chemical vapor deposition of carbon within the pores of alumina membranes. The tubules thus prepared had diameters of 200 nm [86]. Graphite nanofibres (GNFs) were also used as supports. Different kinds of GNFs were used and compared to that of Vulcan carbon (XC-72). The platinum supported on “platelet” and “ribbon” type GNFs that exposed mainly edge sites to the reactants exhibited activities comparable to that of the 25 wt % Pt/C. The study also found that Pt/GNFs were less susceptible to CO poisoning than Pt/C [87]. GNFs were also used as a support during the study of the effects of experimental parameters on the synthesis of Pt/CNF by polyol processing techniques. The study showed that although microwave heating accelerated the process it did not affect the particle size when compared to the conventional form of heating. The particle size could also be adjusted just by changing the water content [88]. Highly ordered nanoporous arrays of carbon were also viewed as novel supports for catalysts in fuel cells [89].

MWCNT's have remarkable structural and conductive properties when compared to carbon blacks but the main problem associated with MWCNT's is that they are relatively inert. The MWCNT's generally need to be modified and this is normally done by attaching functional groups onto their surface in order to deposit Pt particles on the surface [90]. Li et al. prepared Pt/MWCNT's (functionalised MWCNT's) using the polyol method. The method provided a high dispersion of spherical particles and a mean particle size of 2.6 nm. Homogeneous and controllable Pt nanoparticles were deposited onto MWCNT's using a modified polyol method. The reaction parameters such as pH and water content allowed for control of particle size and dispersion [91]. Double-walled CNTs (DWCNT's) have also been used as supports for Pt

nanoparticles for fuel cell applications. The DWCNT's were synthesized using CVD and were found to have a large specific surface area, good crystallization, and a netlike structure. Pt/DWCNT's exhibited better performance than the commercial catalysts under similar conditions and this was said to be due to the unique properties of the DWCNT's, which can facilitate electron transfer, water removal, and oxygen access to the catalyst active sites [92].

#### **2.8.9.4 Stabilizers**

The polyol method is a quick and efficient method for the synthesis of nanoparticles. However there are certain parameters that additionally aid and facilitate the desired end product. Factors influencing the end product, as mentioned before, are pH, water content, precursor concentration, amount of reducing agent and temperature among others. The aim of synthesizing nanoparticles to be used in fuel cells is to obtain homogeneous spherical particles with a narrow particle size distribution on carbon supports required for fuel cell applications. This led to stabilizing agents being used in the polyol method. The role of stabilizing agents is to prevent nanostructured colloidal metals from agglomerating. There is an enormous surface area to mass ratio, in a nanostructured material and this leads to excess surface free energy that is comparable to the lattice energy which leads to structural instabilities [93]. The general stabilization mechanisms of colloidal materials have been described in Derjaguin-Landau-Verwey-Overbeek (DLVO) theory [94].

The type of stabilization generally falls into two classes;

- ❖ Steric stabilization, and
- ❖ Electrostatic stabilization

### 2.8.9.5 Steric stabilization

This type of stabilization is achieved through the presence of sterically bulky organic molecules on the metal surfaces that act as protective shields.

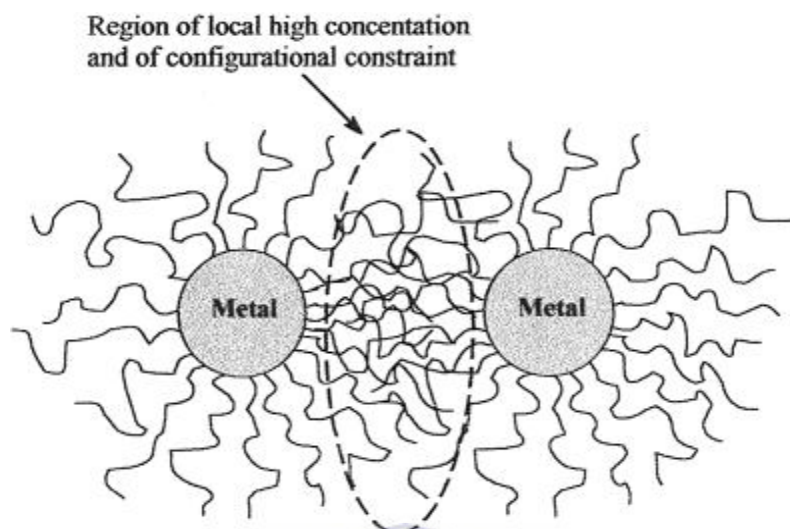


**Figure 2.2:** Diagram displaying steric stabilization of metal colloid particles [67].

As seen from the above diagram, in the interparticle space adsorbed molecules would be restricted in motion. This leads to a decrease in entropy and therefore an increase in free energy. Thus one can visualise how these molecules adsorb onto the surfaces of metals and provide a protective layer. The main class of protective groups that have been studied include polymers, block copolymers, P, N, S-donors, propylene carbonate, long chain alcohols and organometallics [95], [96]. Recent colloidal suspensions have been stabilized by polymers and oligomers such as polyvinyl alcohol (PVA), polyvinylpyrrolidinone (PVP), polyvinyl ether (PVE), or cyclodextrine [97],[98], [99], [100], [101], [102], [103], [104].

The problems associated with polymers like PVP is that these polymers tend to adsorb onto the metal surfaces. The presence of the molecule thus lowers the electrochemical activity of the synthesized catalysts. One way of removing the polymers is by subjecting the nanoparticles to excessive heat treatment that is required to remove the protective agents. Heat treatment removes the polymers but at the expense of particle sizes. Elevated heat treatments cause metal nanoparticles to agglomerate, thus increasing the particle size and lowering the electrochemical activity of catalysts.

#### 2.8.9.6 Electrostatic stabilization

This type of stabilization is caused by an electrical double layer formed by ions adsorbed at the particle surface and the corresponding counter ions causing a Coulombic repulsive force between particles. Ionic compounds such as halides, carboxylates, or polyoxoanions, dissolved in solution (generally aqueous) can generate the electrostatic stabilization (figure 2.3).

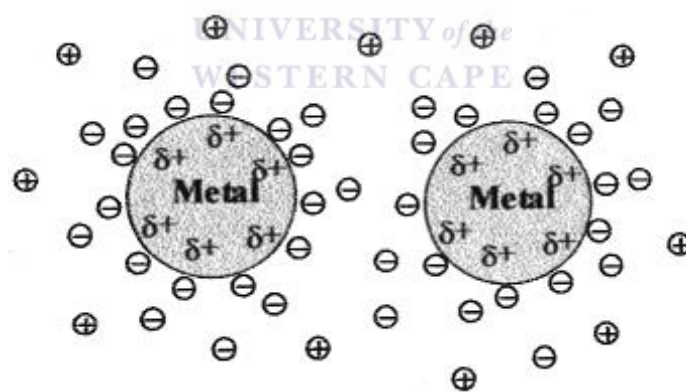


**Figure 2.3:** Diagram displaying electrostatic stabilization of metal colloid particles [67].

When the electric potential associated with the double layer is high enough the electrostatic repulsion will prevent particle to aggregation. Electrostatic stabilization in colloidal suspensions is sensitive to ionic strength and thermal motion, all factors which could disrupt the double layer region [105].

Pt/C nanocatalysts have been prepared by the reduction of chloroplatinic acid with sodium borohydride, with citric acid acting as an electrostatic stabilizer. It was found that well-dispersed Pt nanoparticles of around 3.82 nm in size were obtained when the citric acid/Pt ratio was maintained at 2:1 [106]. Platinum nanoparticles were also prepared using methanol and citrate. Platinum nanoparticles of 2–3 nm average size and ca.  $\pm 2$  nm distribution were successfully prepared by methanol reduction while using sodium citrate as the stabilizer [107]. Platinum nanoparticles were also synthesized using microwaves and stabilized with sodium acetate. It was found that the Pt nanoparticles were small and uniform in size, and highly dispersed on XC-72 carbon supports. The mean size of the Pt particles was 5.1, 4.3, 3.5 and 2.8 nm, respectively, correspondingly to the addition of 0, 0.1, 0.3 and 0.5 mL of 1.0 M sodium acetate solution in 50 mL of the synthesis solution [108]. Platinum on carbon electrocatalysts were also prepared using the polyol method. A solution of chloroplatinic acid in EG in the presence of XC-7 vulcan carbon and small amounts of sodium acetate was used to synthesize the catalysts. The catalysts obtained showed that the platinum nanoparticles were small and uniform in size and highly dispersed on XC-72 carbon supports when small amounts of sodium acetate solution was added to the synthesis solution [74]. The advantage of using electrostatic stabilizers instead of steric stabilizers is the fact that they are much easier to remove and removal of the stabilizer does not hamper the electrocatalytic activity of the catalyst whatsoever. The removal may require thorough rinsing of sample prior to drying which makes them ideal for stabilizing particle growth during synthesis.



In light of the above mentioned synthetic routes for the synthesis of fuel cell catalysts the polyol method was chosen as the method to be used for a quick, efficient and cost effect route for the synthesis of fuel cell catalysts.



**CHAPTER 3: MATERIALS AND METHODOLOGY****3.1 Materials and methodology**

The chapter provides a brief but informative description of the various chemicals and instrumentation used during the synthesis and characterization of the catalysts.

**3.1.1 Chemicals:**

The chemical used in this study are listed in table 3.1

<b>Chemicals</b>	<b>Company</b>
<b>H<sub>2</sub>PtCl<sub>6</sub></b>	Sigma Aldrich
<b>EG</b>	Sigma Aldrich
<b>NaOH</b>	KIMIX
<b>NaOAc</b>	KIMIX
<b>HCl</b>	KIMIX
<b>HNO<sub>3</sub></b>	KIMIX
<b>H<sub>2</sub>SO<sub>4</sub></b>	KIMIX
<b>Ultra pure water</b>	UWC

**Table 3.1:** Chemicals used for synthesis

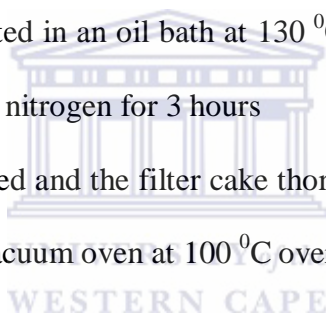
Commercial XC-72 carbon blacks were used were obtained form Cabot

Commerical MWCNT's were supplied by Carbon Nano-material Technology Co.,  
Ltd

### 3.1.2: Initial synthetic protocol employed

A typical reaction for the synthesis of catalysts involved the following;

- ❖ The generation of a solution made from 100 mg of chloroplatinic acid ( 0.24 mm) to obtain the desired loading(40 wt%) was placed in 30ml of ethylene glycol
- ❖ The solution was then sonicated for 30 minutes at 40% strength (intensity of the sonic pulse used) with a SONOPLUS probe sonicator to ensure uniform dispersion.
- ❖ The pH of the solution was then raised to  $\approx 12$  by addition of 1M NaOH solution and 70 mg of carbon black (Vulcan XC72) was added.
- ❖ The solution was heated in an oil bath at  $130^{\circ}\text{C}$  with magnetic stirring under an inert atmosphere of nitrogen for 3 hours
- ❖ The catalyst was filtered and the filter cake thoroughly washed with ultra pure water and dried in a vacuum oven at  $100^{\circ}\text{C}$  overnight.



### 3.1.3 Functionalization of MWCNT's

- ❖ MWCNT's (200 mg) were suspended in 4 M solutions of  $\text{H}_2\text{SO}_4$  and  $\text{HNO}_3$  in a 3:1 ratio respectively. The total volume of the solutions used was 50 ml.
- ❖ The mixture was then placed in an ultrasonic bath for 3 hours at  $25^{\circ}\text{C}$ .
- ❖ Thereafter the mixture was heated under reflux under nitrogen for 4 hours.
- ❖ The MWCNT's were filtered and washed thoroughly with ultrapure water until the pH of the filtrate was 7 to ensure that the sample was neutral.

### 3.1.4 Modified synthetic protocol (Change in pH):

- ❖ Chloroplatinic acid (100 mg) to obtain the desired loading(40 wt%) was placed in 30ml of ethylene glycol
- ❖ The solution was then sonicated for 30 minutes at 40% strength (intensity of the sonic pulse used) with a SONOPLUS probe sonicator to ensure uniform dispersion.
- ❖ The pH of the solution was then raised to  $\approx 12$  by addition of 1 M NaOH and 70 mg (Vulcan XC72 carbon or MWCNT's) was then added to the solution.
- ❖ The solution was heated in an oil bath at  $130\text{ }^{\circ}\text{C}$  with magnetic stirring under and inert atmosphere of nitrogen for 3 hours.
- ❖ Thereafter a few drops of HCl was added to the reaction mixture to lower the pH to  $\approx 4$ , as a sedimentation promoter and the solution was stirred overnight.
- ❖ The catalyst was filtered and the filter cake thoroughly washed with ultra pure water and dried in a vacuum oven at  $100\text{ }^{\circ}\text{C}$  overnight.

### 3.1.5 Modified synthetic protocol (Addition of H<sub>2</sub>O):

- ❖ Chloroplatinic acid (100 mg) in ultra pure water 15ml to obtain the desired loading(wt%) was placed in 30 ml of ethylene glycol
- ❖ The solution was then sonicated for 30 minutes at 40% strength (intensity of the sonic pulse used) with a SONOPLUS probe sonicator to ensure uniform dispersion.
- ❖ The pH of the solution was then raised to  $\approx 12$  as described earlier and 70 mg of Vulcan XC72 carbon (or MWCNT's) was then added.

- ❖ The solution was then heated in an oil bath at 130 °C with magnetic stirring under reflux in an inert atmosphere of nitrogen for 3 hours.
- ❖ Thereafter a few drops of HCl was added to the reaction mixture to lower the pH to  $\approx 4$ , as a sedimentation promoter and the solution was stirred overnight.
- ❖ The catalyst was filtered and the filter cake thoroughly washed with ultra pure water and dried in a vacuum oven at 100 °C overnight.

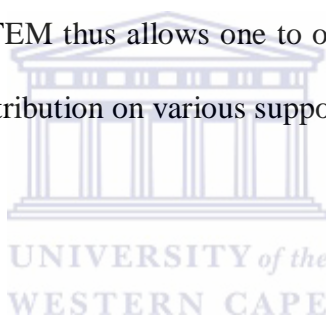
### 3.1.6 Modified synthetic protocol (addition of sodium acetate as a stabilizer):

- ❖ Chloroplatinic acid (74 mg) required to obtain the desired loading (40 wt%) was placed in 30ml of ethylene glycol
- ❖ The solution was then sonicated for 30 minutes at 40% strength (intensity of the sonic pulse used) with a SONOPLUS probe sonicator to ensure uniform dispersion.
- ❖ Sodium acetate (5 ml of 0.24 M) was then added to the mixture together with 40 mg of Vulcan XC72 carbon or MWCNT's.
- ❖ The solution was heated in an oil bath 130 °C with magnetic stirring under nitrogen for 3 hours.
- ❖ Thereafter a few drops of HCl was added to the reaction mixture (to lower the pH to  $\approx 4$ ) as a sedimentation promoter and the solution was stirred overnight.
- ❖ The catalyst was filtered and the filter cake thoroughly washed with ultra pure water and dried in a vacuum oven at 100 °C overnight

## **3.2 Physiochemical characterization:**

### **3.2.1 Transmission Electron Microscope (TEM)**

The transmission electron microscope (TEM) operates on the same basic principles as the light microscope but uses electrons instead of light. A TEM forms images by using transmitted electrons as a light source and this makes it much better than the conventional light microscope since it facilitates much better resolution. The TEM allows one to see objects to the order of a few angstroms ( $10^{-10}$  m) [109]. As a consequence one is able to extract key information with regards to morphology (size, shape and arrangement of particles which make up the sample), crystallography (arrangement of atoms) and compositional information viz., the elemental make up of the sample in question. The TEM thus allows one to observe, in the case of fuel cell catalysts, particle size and distribution on various supports.



#### **Sample preparation:**

A spatula tip of the sample is suspended in ethanol. The mixture is then sonicated for approximately 30 minutes to ensure efficient dispersion. A micro pipette is then used to extract some of the sample from the solution which is placed on a S147-4 holey carbon film or 400 mesh copper grids. The holey carbon film is then left to dry in air. The sample is then placed in the sample tray of the microscope for analysis.

#### **Instrument setup :**

HRTEM Technai G2 F20 X-Twin MAT 200 kV Field Emission Transmission Electron Microscope

**Gunlens used:** Gunlens 1

**Spot size:** 3

**C2 aperture:** 3

**Objective aperture:** 1

**Accelerating voltage:** 200 kV

### 3.2.2 X-Ray Diffraction (XRD)

The atomic planes of a crystal cause an incident beam of X-rays to interfere with one another as they leave the crystal. This phenomenon known as X-ray diffraction (XRD) is a versatile, non-destructive technique that reveals detailed information about the chemical composition and crystallographic structure of natural and manufactured materials. In addition, one can determine factors such as the orientation of single crystals, or measure the size and shape of crystalline regions [110]. XRD was used in this study to determine the crystallographic make-up of the synthesized catalysts. The crystallite sizes obtained from the results were all obtained through the angle position and on the full width at half maximum of the peaks. The metal crystallite sizes were calculated by the x-ray line broadening technique using the Debye-Scherrer equation [111].

$$D = 0.9\lambda / \beta \cos \theta$$

Where D = Particle size, 0.9 = shape factor,  $\lambda$  = x-ray wavelength,  $\beta$  = peak width at half peak height and  $\theta$  = angle of reflection

#### **Instrument setup:**

**Manufacturer:** BRUKER AXS (Germany), **Diffractometer:** D8 Advance

**Tube:** Cu-K $\alpha$  radiation ( $\lambda_{K\alpha_1}$ =1.5406Å)

**Detectors:** PSD Vantec-1, Gas detector with 1600 channels

#### **MEASUREMENTS:**

**Tube voltage:** 40 kV

**Tube current:** 40 mA

**Variable slits:** 0.28 mm

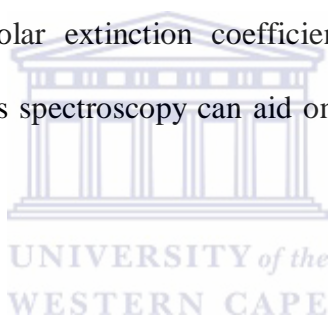
**2 $\theta$  Range:** 0-90 (angles in degrees)

**Increment  $\Delta 2\theta$ :** 0.048 deg

**Measurement time:** 1 sec

### 3.2.3 (UV-vis) Visible spectroscopy

UV-vis spectroscopy is the measurement of the wavelength and intensity of absorption of near-ultraviolet and visible light of a sample [112]. Unlike infrared spectroscopy (which looks at vibrational motions), ultraviolet-visible spectroscopy looks at electronic transitions. It allows one to determine the wavelength and maximum absorbance of compounds absorbing light of different wavelengths. From the absorbance information and using a relationship known as Beer's Law ( $A = \epsilon bc$ , where  $A$  = absorbance,  $\epsilon$  = molar extinction coefficient,  $b$  = path length, and  $c$  = concentration), one is able to determine either the concentration of a sample if the molar extinction coefficient is known, or the molar absorptivity, if the concentration is known (Wade 676-681). Molar extinction coefficients are specific to particular compounds; therefore UV-Vis spectroscopy can aid one in determining an unknown compound's identity.



#### Instrumentation

The UV-vis experiments were performed on a NICOLET EVOLUTION 100 purchased from the Thermo electron corporation

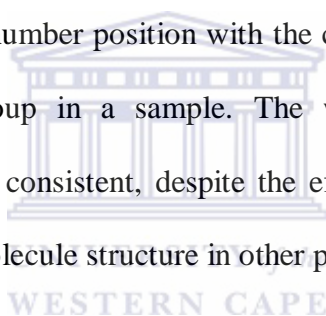
#### Sample preparation

The samples were quenched from the reaction at various intervals (0.5 h, 1 h, 1.5 h, 2 h, 2.5 h and 3 h). The samples were then diluted with the required amount of EG. The sample's recordings were taken as a function of reflux time and the data was corrected for EG background absorption. The scan was ran in the region of 200-110 nm



### 3.2.4 Infrared (IR) spectroscopy

IR spectroscopy is a technique based on the vibration of the atoms in molecule. An IR spectrum is obtained by passing radiation through a sample and determining what fraction of the incident radiation is absorbed at a particular energy. The energy at which any peak in an absorption spectrum appears corresponds to the frequency of a vibration of a part of a sample molecule [113]. Infrared spectroscopy detects the vibration characteristics of chemical functional groups in a sample. When an infrared light interacts with matter the chemical bonds will stretch, contract and bend. This implies that functional groups tend to adsorb infrared radiation in a specific wavenumber range regardless of the structure of the rest of the molecule. The correlation of the band wavenumber position with the chemical structure is then used to identify a functional group in a sample. The wavenumber positions where functional groups adsorb are consistent, despite the effect of temperature, pressure, sampling, or change in the molecule structure in other parts of the molecules.



#### Instrument setup

A Perkin Elmer Spectrum 100 series FT-IR Spectrometer with universal ATR (Attenuated total reflectance) sampling Accessory was used in this study

**Table 3.2:** FT-IR Instrument setup

<b>Scan range</b>	Start :4000 cm <sup>-1</sup> end: 380 cm <sup>-1</sup>
<b>Scan type</b>	Sample
<b>Number of scans</b>	8
<b>resolution</b>	400 cm <sup>-1</sup>

### 3.3 Electrochemical characterization

#### 3.3.1 Cyclic Voltammetry

Cyclic voltammetry is a potentiodynamic electrochemical technique used to study the electrocatalytic activity of species in acidic media. In a typical experiment the working electrode is ramped against time. Unlike linear sweep voltammetry where the experiment is run until a set potential, with cyclic voltammetry the working electrode's potential ramp is inverted. It enables the electrode potential to be rapidly scanned in search of redox couples [114]. If the couples are located it may be characterized from the potentials of peaks on the cyclic voltammogram and from changes caused by variation of the scan rate. When cyclic voltammetry reaches a set potential, the working electrode's potential ramp is inverted. This inversion can happen multiple times during a single experiment. The current at the working electrode is plotted versus the applied voltage to give the cyclic voltammogram [115]. In typical cyclic voltammetry a species is either oxidized or reduced by placing the solution in contact with an electrode surface, and then making that surface sufficiently positive or negative in voltage to force electron transfer. In most cases the electrode surface is started at a particular voltage with respect to a reference half-cell such as calomel or Ag/AgCl, and then the electrode voltage is changed to a higher or lower voltage at a linear rate, and finally, the voltage is changed back to the original value at the same linear rate. If the surface becomes sufficiently negative or positive, the solution species may gain electrons from the surface or transfer electrons to the surface. This results in a measurable current in the electrode circuitry.

A typical experiment consists of a three electrode system, a working electrode, a reference electrode (Ag/AgCl) and a platinum counter electrode.

### 3.3.2 Electrochemical cell design

An electrochemical cell was specially designed for the purpose of the proposed project study. The proposed cell was fabricated in such a way that it was suitable to do CV as well as ORR for the kind of electrodes that were prepared. The proposed cell had to accommodate purging by various gases, be completely sealed so that no external contaminants could enter the cell which would affect the results obtained and be temperature controlled if necessary. The electrodes in this instance was not the conventional glassy carbon (GC) electrode which are used in hydrodynamic studies using a rotating disk electrode system. The electrodes were fabricated on highly conductive carbon paper, similar to the carbon paper used in actual fuel cells in a membrane electrode assembly (MEA). The cell had to house the specially designed teflon working electrode in which the specially fabricated electrodes were placed for study. All the above factors had to be taken into account in designing the cell. This was accomplished through consultation with the supervisor and very esteemed post doctoral scientists in order to ensure a successful outcome.

The advantage of the in-house synthesized electrochemical cell is that compared to the RDE which supplies  $O_2$  to the electrode surface through rotation of the electrolyte, thus ensuring fresh reactants reach the surface of the electrode, the in-house cell electrode allows for the  $O_2$  to be directly fed to the surface of the electrode through its unique design. The teflon electrode has a specially inserted stainless steel tube that is positioned a few millimetres away from the specially fabricated electrode. This allows for “true” ORR results to be obtained due to the fact that it resembles conditions the actual catalysts would be exposed to in a fuel cell (see figure 3.2).

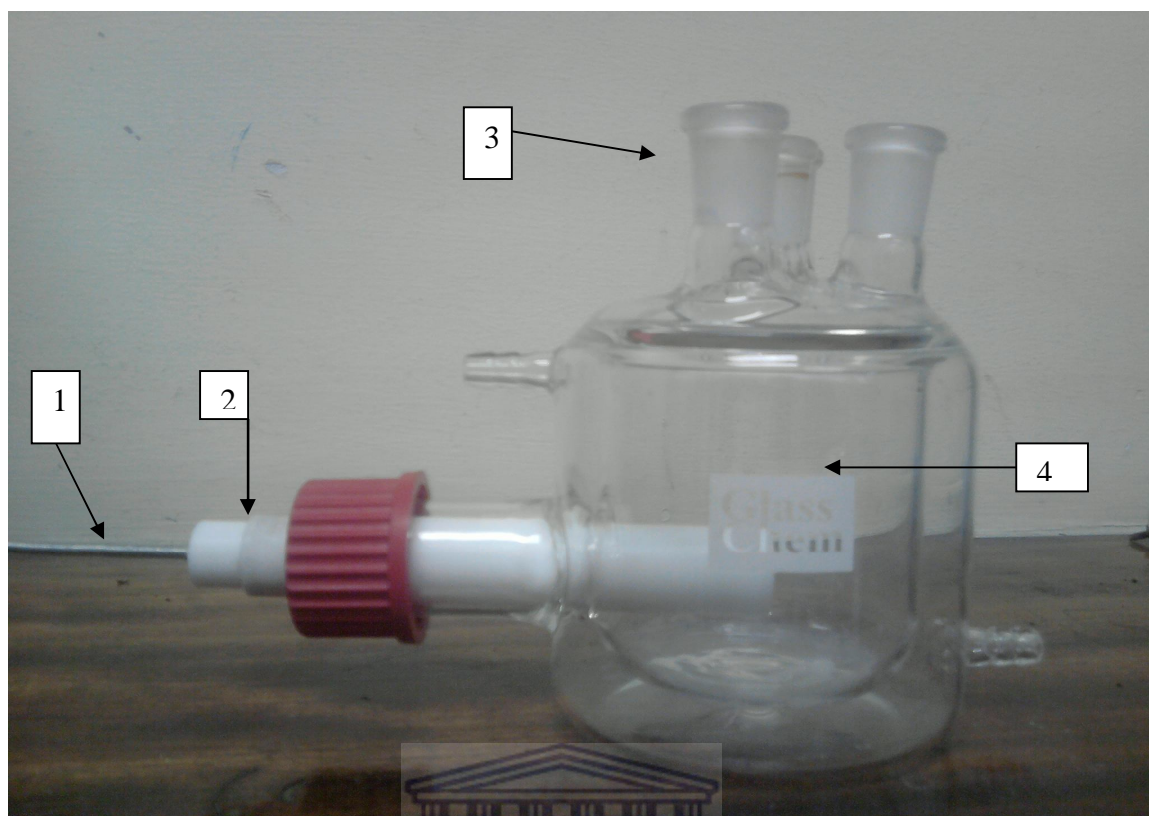


**Figure 3.2:** In-house cell which was specifically designed for electrochemical measurements of the IH electrodes, (1) Two small stainless steel tubes were inserted into the self fabricated Teflon electrode which houses the IH electrode. The one tube contains a platinum wire (0.5mm in diameter) which serves as a contact between the IH working electrode and the electrochemical instrument (Autolab connections). The other tube is used to transport gaseous reactants to the working electrodes surface, (2) IH Teflon housing representing the working electrode, (3) B14 glass fitting for the reference and counter electrodes and another fitting for which electrochemical studied may be required, (4) Enclosed vessel for the electrolyte solution so that an inert atmosphere may be maintained.

**The preparation of the working electrode preparation for the CV experiment:****Ink preparation****This entailed:**

25 mg of the catalyst was placed in a vial

The catalyst was then treated with 50 mg of water and 75 mg of nafion

The mixture was then externally sonicated for 30 minutes after which 5-10ml of isopropanol was added

The mixture was then externally sonicated for a further 1<sup>1</sup>/<sub>2</sub> hours.

**Electrode preparation**

The prepared ink was sprayed uniformly onto the carbon paper (6 mg) with a spray gun.

Nafion (100mg) in 10 ml of isopropanol was sonicated for 30 min and applied onto the electrode surface (carbon paper with the catalyst sprayed onto the surface) with a spray gun.

A 12 mm diameter circular electrode was then punched out with a round hole cutter from the carbon paper.

**Aparatus setup:**

**Potentiostat:** Eco chemie PGSTAT Autolab

**Working electrode:** In-house Pt/C

**Reference electrode:** Ag/AgCl

**Counter electrode:** Platinum gauze

**Scan rate:** 20 mv/s

**Potential range:** 1 to -0.2V

H<sub>2</sub>SO<sub>4</sub> (0.5 M) was purged with N<sub>2</sub> gas for 1 h prior to performing CV experiments and thereafter purged with high purity oxygen for 30 minutes to study the ORR

**Note:** The same scan rate and potential range was used when the ORR was studied



## CHAPTER 4: RESULTS AND DISCUSSION

### 4.1 General

Initial stages of the synthesis involved acquiring the optimal reaction conditions. This meant looking at reaction times and temperatures. In order to study the effect that one of these parameters would have on the nature of the products of the reaction the other parameter would have to be kept constant. The first parameter that was investigated was the effect temperature had on the synthesis of the catalysts. Once the reaction parameters were fully established a standardized method of preparing the in-house (IH) catalysts was developed. Additional variations of the standardized method was then undertaken.

### 4.2 Temperature

Temperature was chosen to be high enough to support the oxidation of EG which would in turn reduce the metal precursor. Temperature plays an important role in controlling the rate of the reaction as well influencing the reduction potential of the EG [116]. If the temperature is too high, the particle size would be too small due to more nuclei being formed in a shorter period of time [65]. The temperature chosen for the synthesis of the IH catalysts was chosen to be 130 °C, and was high enough to oxidize the EG [117], [118]. The aim in this instance was to use the minimal amount of energy required to drive the whole process.

### 4.3 Reaction time

To investigate the time taken for the reaction to run to completion an *in situ* technique had to be used. The most effective means of doing this was to use Ultraviolet visible (UV) spectroscopy. This technique allowed us to track the oxidation state of the metal precursors from its +4 to zero valent oxidation state. This was accomplished by quenching samples from the reaction mixture at various time intervals.

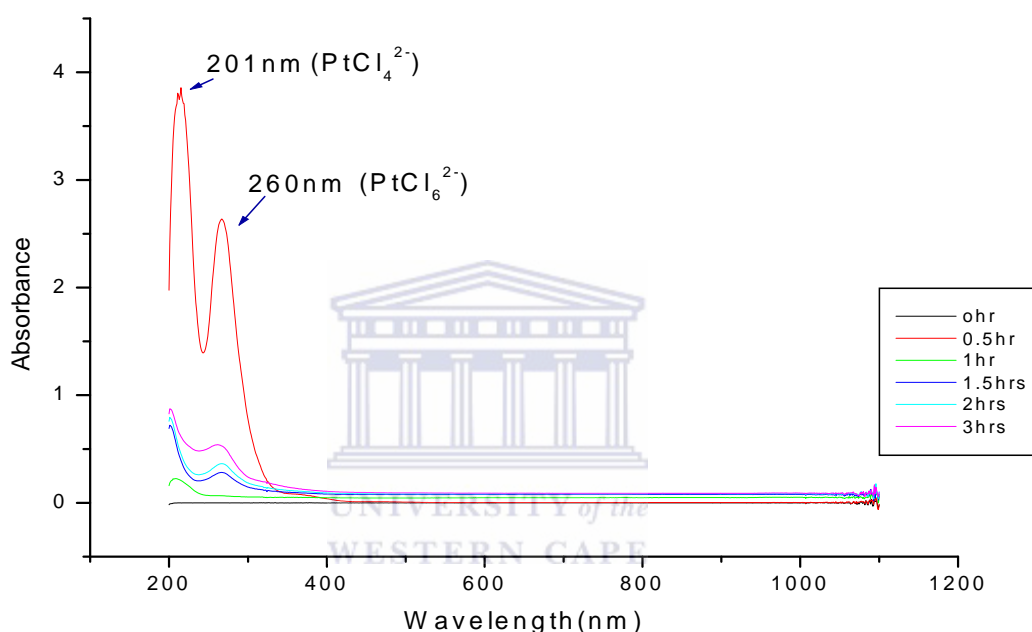


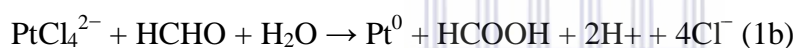
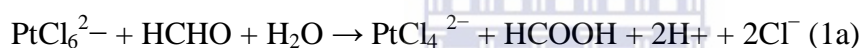
**Figure 4.1:** UV-vis spectrum of  $\text{H}_2\text{PtCl}_6$  in EG ( $7.23 \times 10^{-3}\text{M}$ ) quenched at various time intervals during the reaction.

Colloidal dispersions of metals exhibit absorption bands or broad regions of absorption in the UV–vis range. This is due to the excitation of plasma resonances or interband transitions and is a characteristic property of the metallic nature of the particles [119]. As seen in figure 4.1, initially no reaction occurred at  $t=0$  which was to be expected since no energy was put into the reaction mixture. After an induction period (0.5 h) peaks at 201 nm and 260 nm was observed and attributed to the presence of  $\text{Pt}^{2+}$  and  $\text{Pt}^{4+}$  respectively [65], [118]. The reduction of  $\text{PtCl}_4^{2-}$  occurred at a much quicker rate than  $\text{PtCl}_6^{2-}$  which was to be expected due to their relative



standard redox potentials, viz., 0.68 V for  $\text{PtCl}_6^{2-} / \text{PtCl}_4^{2-}$  and 0.755 V for  $\text{PtCl}_4^{2-} / \text{Pt}^0$  (vs the normal hydrogen electrode) [120]. The intensities of the absorbance peaks gradually decrease as the reaction time progresses. In fact after the first hour of the reaction the absorbance peak at around 201 nm had almost completely disappeared suggesting that the metal precursor is reduced. In fact at this time during synthesis the colour of the reaction mixture changed from yellow to dark brown confirming that the metal precursor had been reduced [121].

The typical absorptions of  $\text{Pt}^{2+}$  at 201 nm and Pt colloid at 215 nm seemed to coexist in the solution after the first hour of the reaction which would imply a two step reaction mechanism is involved where  $\text{PtCl}_4^{2-}$  would possibly serve as an intermediate;



This kind of mechanism was also observed by Zhou *et al.* who suggested the mechanism mentioned above [117].

In light of the information obtained from the UV-vis spectra with respect to the reduction of the metal precursor an informed decision could be deduced with respect to the reaction time. Most of the precursor was reduced within 1hr and 30min we could make a conclusion that to fully reduce the metal precursor, a period of 3 hr would be sufficient. This is in good agreement with reaction times found in literature which implied that UV-vis was an ideal *in situ* technique for determining the reaction time needed to completely reduce the metal precursor.

Once the experimental parameters were optimized, the synthesis of the IH catalysts could then be executed. To determine the viability of the IH catalysts, these had to be evaluated with respect to a standard procedure. In the case of the proposed work a commercial Pt/C 40 wt% catalysts supplied by Johnson Matthey Company was used for comparative purposes in terms of its electro activity and the ORR.

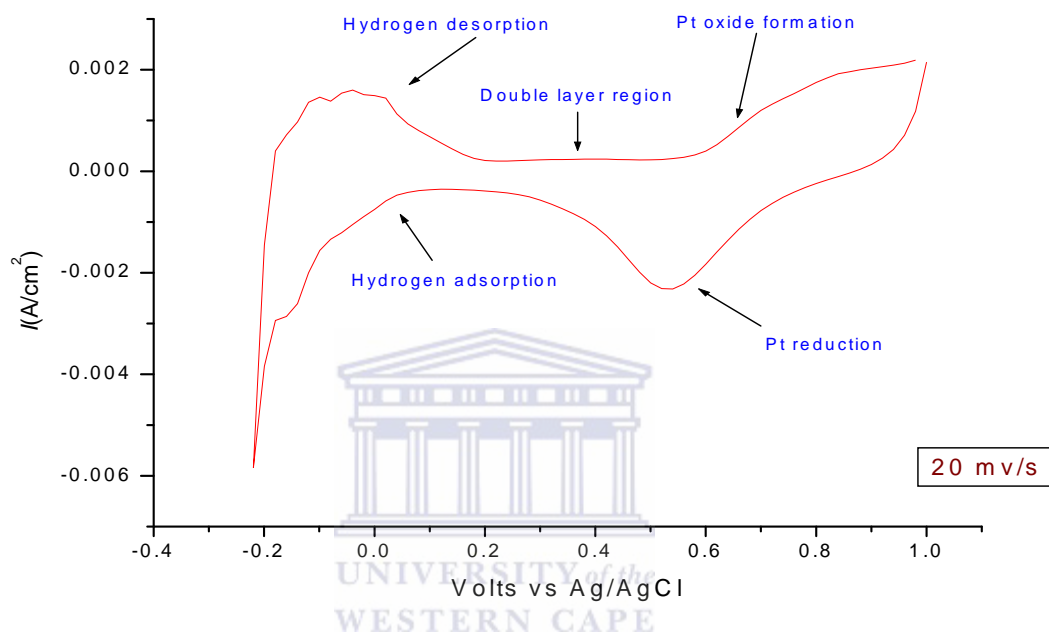
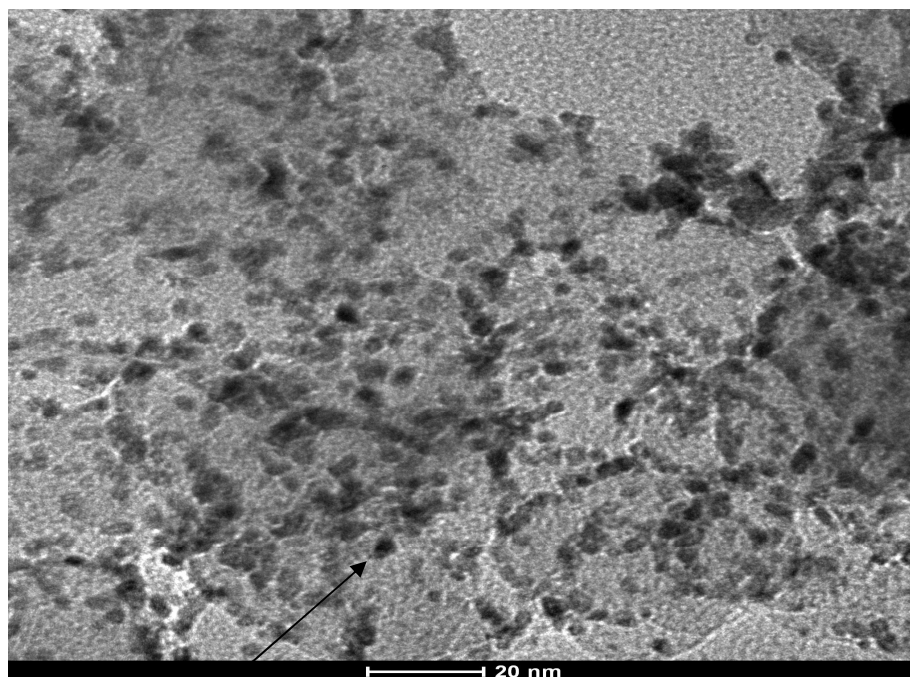


**Figure 4.2:** Cyclic voltammogram (CV) of the commercial catalyst (40wt %) from Johnson Matthey using the IH electrochemical cell, (0.5M H<sub>2</sub>SO<sub>4</sub> de-aerated for 30 minutes, scan rate = 20 mvs<sup>-1</sup>)

As seen in Fig 4.2 the CV obtained using the IH electrochemical cell displayed all the characteristic peaks associated with Pt/C catalysts. The peaks identified from the CV obtained are, viz., hydrogen desorption (-0.2-0.1V), where hydrogen is desorbed from platinum surface, the double layer region (0.15-0.56V), Pt oxide formation (0.6-1.2V) and platinum reduction in the regions of 0.9-0.5V. The peak at 0.1 to -0.2 may be attributed to hydrogen adsorption onto the Pt surface [122].



**Platinum nanoparticle**

**Figure 4.3:** TEM image of the commercial catalyst Pt/C 40 wt% (Johnson Matthey Company)

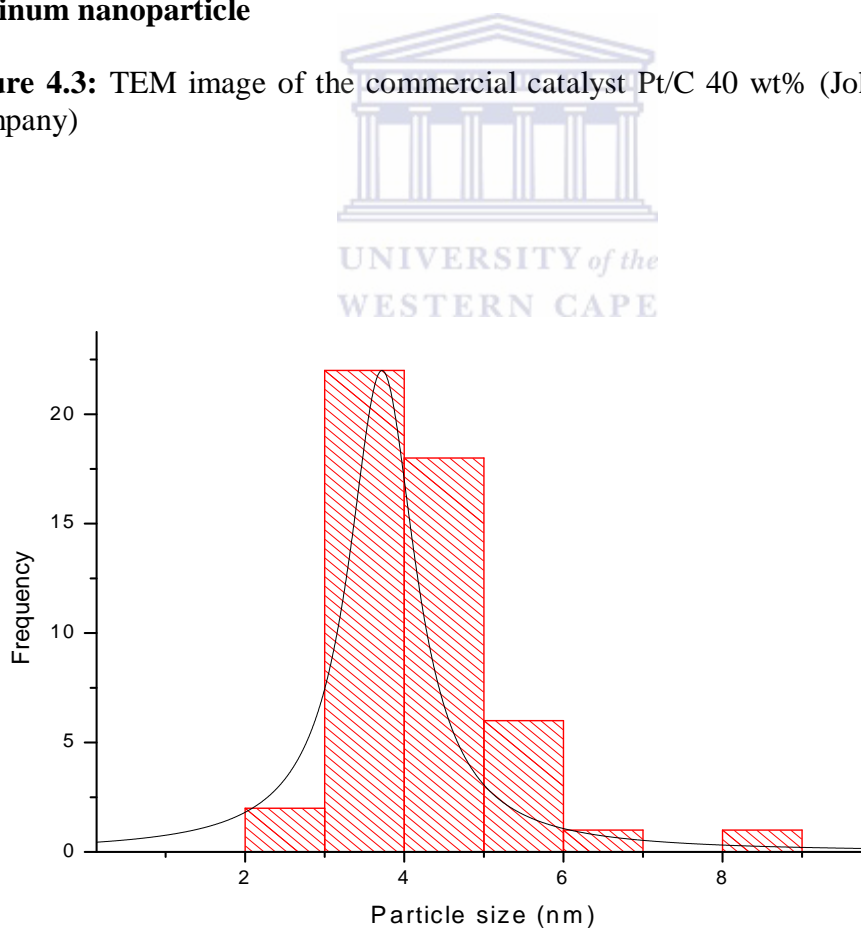


**Figure 4.4:** Histograms showing the particle size distributions of the commercial catalyst Pt/C 40 wt% (Johnson Matthey Company)

The TEM image obtained (figure 4.3) for the commercial catalysts displayed uniform and spherical particles of Pt. The Pt nanoparticles were well dispersed onto the support, thus fulfilling the required attributes of a fuel cell catalyst. The major problem associated with high loading of fuel cell catalysts is to achieve a high loading of nanoparticles. The TEM image obtained for the sample from the Johnson Matthey Company clearly illustrates that they managed to accomplish this. The histogram (figure 4.4) shows the narrow particle size distribution and average particle mean size of approximately 2-6 nm in diameter. The histogram (figure 4.4) shows the narrow particle size distribution of the commercial catalyst which thus makes it an ideal standard for comparative purposes with regards to the IH synthesized catalysts.

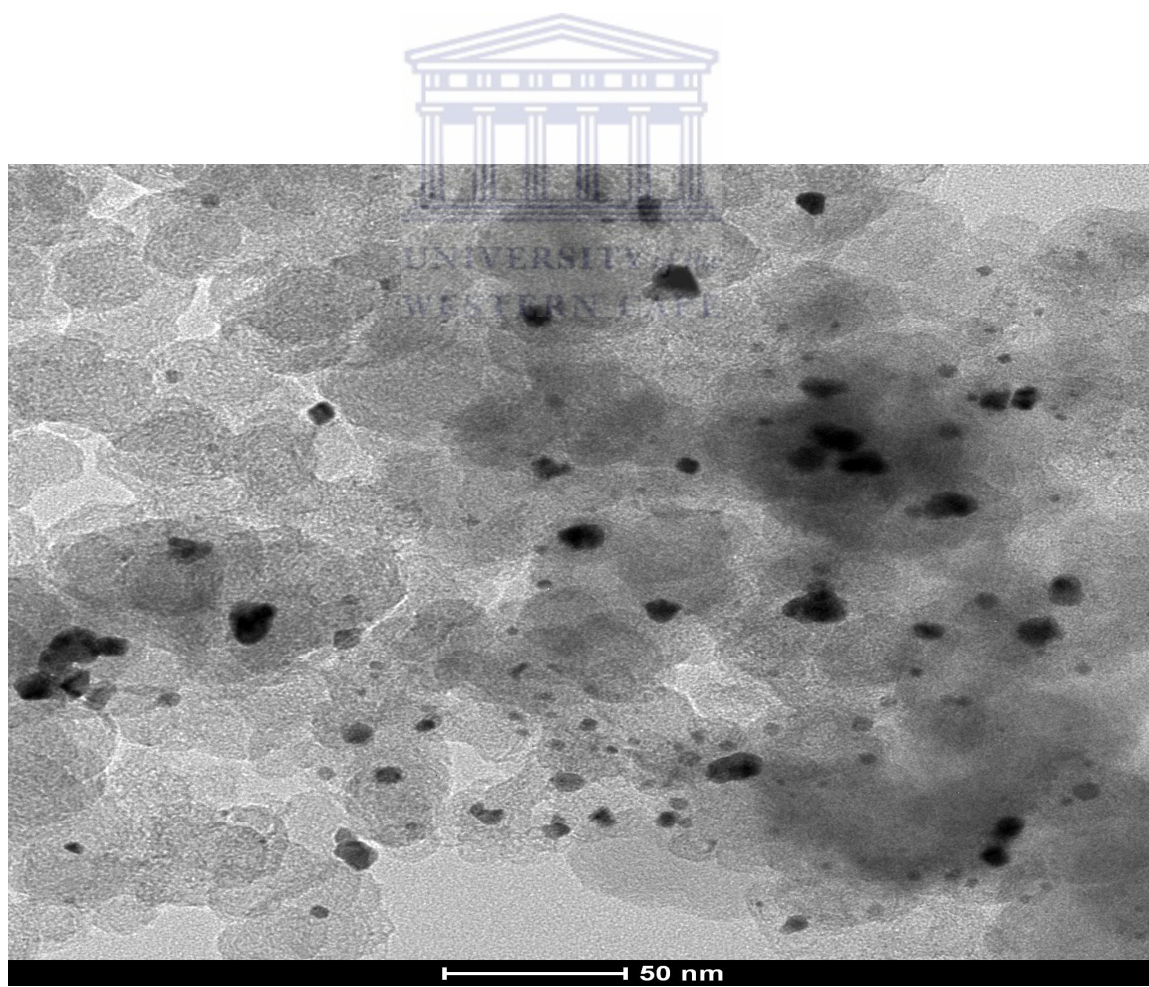


**Figure 4.5:** TEM image of IH Pt/C initial catalysts obtained.

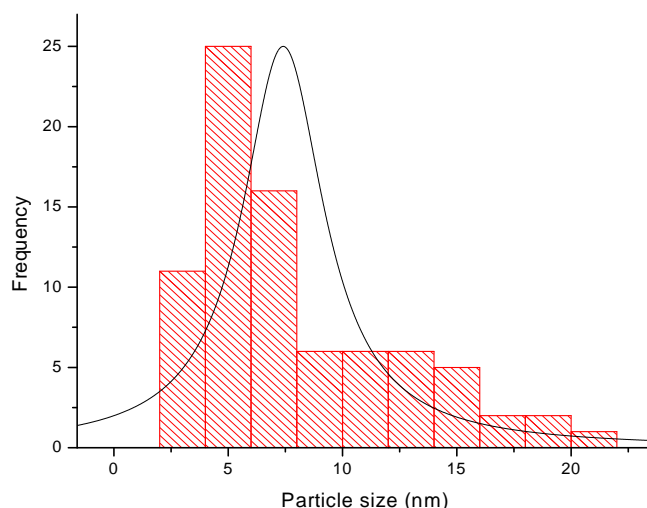


**Figure 4.6:** Histogram showing the particle size distributions of the initial IH catalysts using the polyol method.

Our initial synthetic protocol yielded Pt nanoparticles deposited on the carbon support as seen from Fig 4.5. The problem though was when comparing the IH catalyst's TEM image to that of the commercial catalyst; it was observed that Pt nanoparticle agglomeration occurred. The histogram (figure 4.6) showing the particle size distributions by measuring 100 random particles of the initial IH catalysts using the polyol method further concurred with the TEM image (figure 4.5) by the initial IH catalyst synthesized by the polyol method having a broad particle size distribution . This meant that the required metal loading was not accomplished and a fair comparison could thus not be made. This naturally implied that the synthetic protocol employed had to be altered in such a manner as to address the loading issue. The manner in which this was accomplished was with the aid of a sedimentation promoter. The fact that not all or most of the Pt used at the beginning of the reaction was deposited onto the support meant that some of the reduced metal was still suspended in solution. Therefore the sedimentation promoter was used to facilitate the deposition of the suspended nanoparticles onto the support.

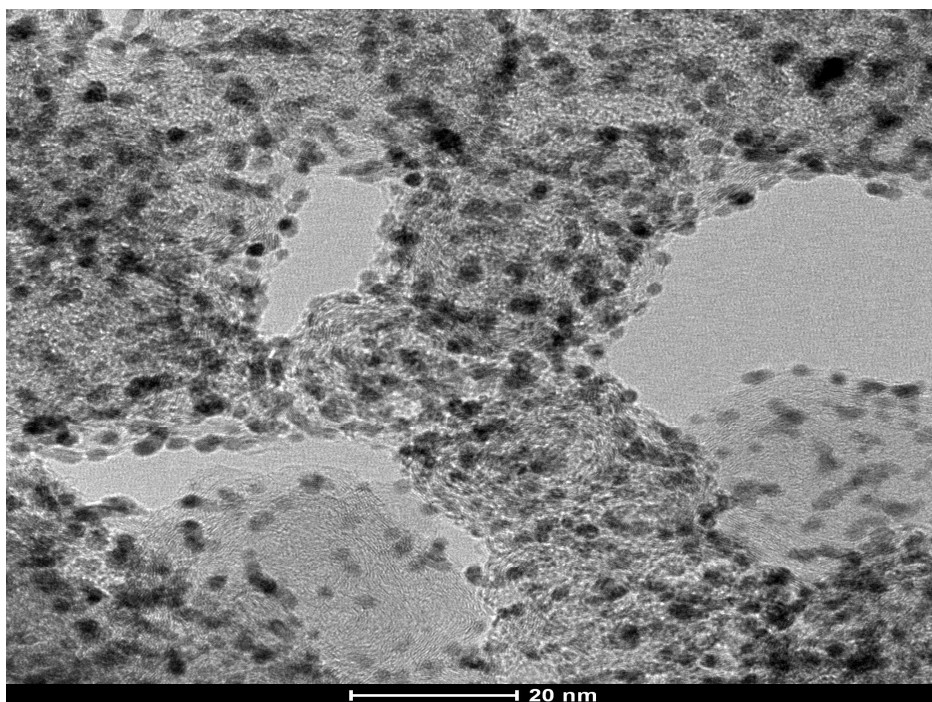


**Figure 4.7:** TEM image of IH Pt/C initial catalysts obtained after the addition of a sediment promoter.

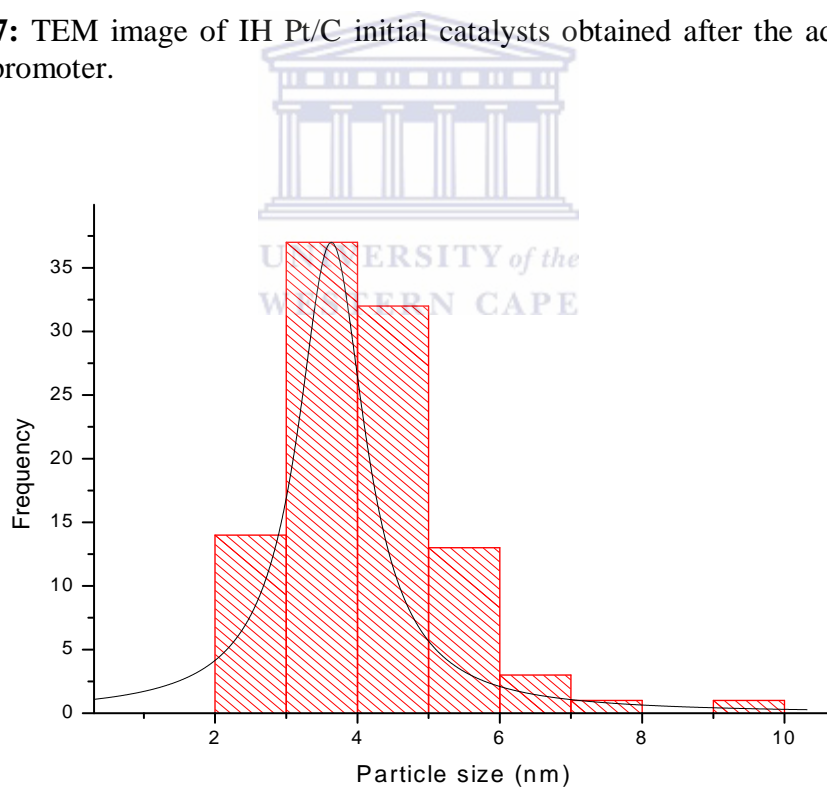


**Figure 4.8:** Histogram showing the particle size distributions of the initial IH catalysts using the modified polyol method.

Figure 4.7 showed that a considerable amount of platinum nanoparticles were deposited onto the support. This implied that using a sedimentation promoter during synthesis facilitated the deposition of the nanoparticles onto the support. This was confirmed by Hyung-Suk *et al.* who explained this phenomena using Zeta potential [79]. As the pH of the media became more alkaline, carbon tends to acquire a more negative charge. This would negate the deposition of Pt nanoparticles onto the support, seeing that the glycolate anions may be specifically adsorbed on the surfaces of Pt nanoparticles resulting in a negative charge. The stability of the colloid is dependant on attractive van der Waals and electrostatic repulsive forces between particles as they approach one another due to the Brownian motion they undergo [123].

This therefore implies that the adsorption of Pt onto the carbon support would be higher at a lower pH. Zeta potentials measurements were not conducted but simple pH measurements proved to be just as effective to determine whether a change in pH would influence metal loading. During synthesis the pH was found to be 9 after addition of the sedimentation promoter, which would result in more Pt being deposited onto the support. This phenomenon was evident in the Pt particles produced in the modified synthetic protocol used to make the IH catalysts (Figure 4.7). The histogram (figure 4.8) displayed that the modified polyol method gave rise to a narrow particle distribution and an average mean particle size of 2-6 nm.

The major aim of the proposed work was to develop a quick and efficient method to prepare Pt/C cathode catalysts for DMFC's. In doing so we embarked on a programme at covering all synthetic factors (reaction time, temperature etc.) influencing the outcome of the proposed catalysts.

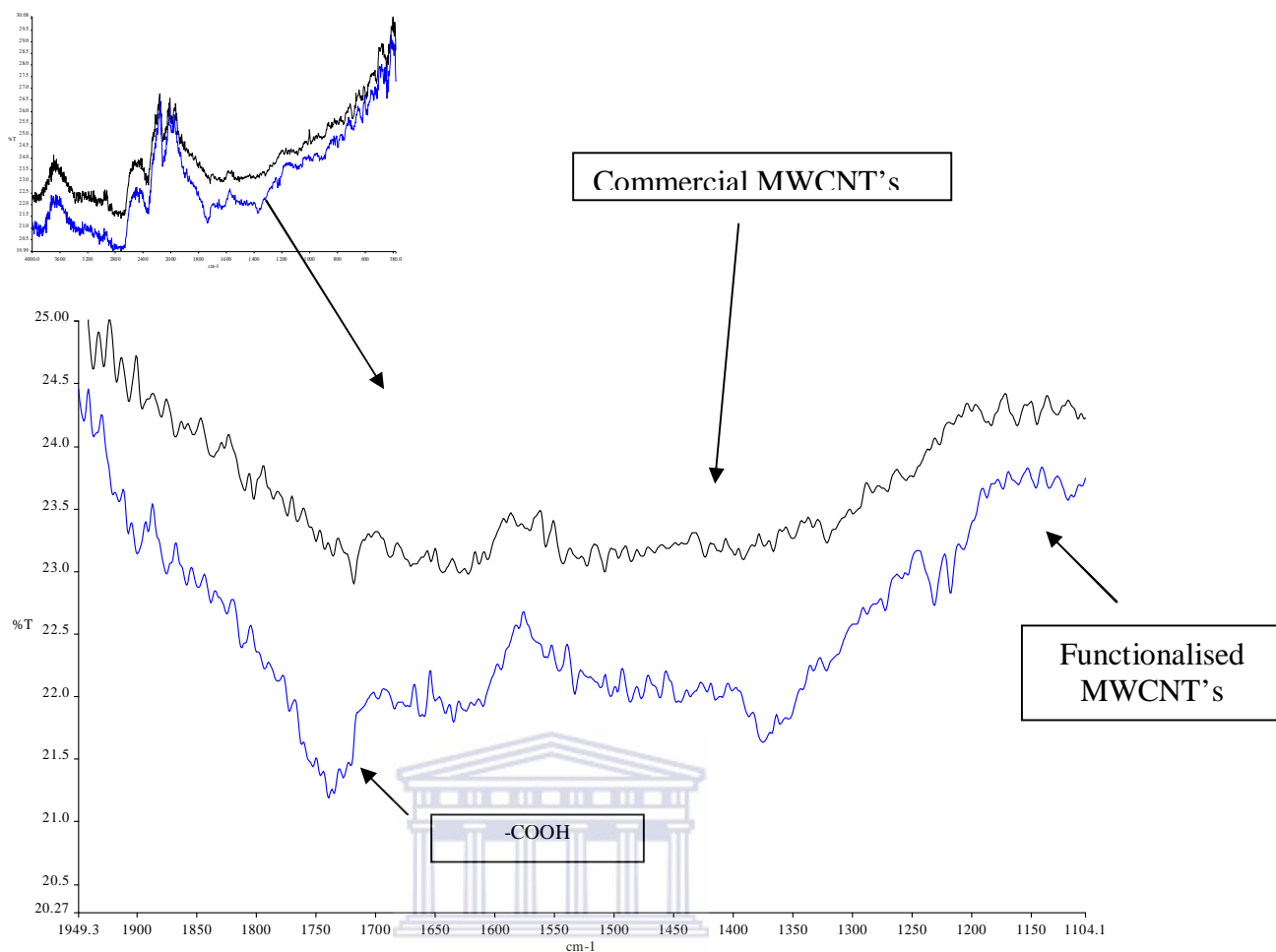
The synthetic protocol employed for the IH catalysts had been essentially optimized as discussed earlier (section's 4.2 and 4.3). Further aims and objectives concerning the proposed work were then addressed viz., usage of different supports, effect of H<sub>2</sub>O on the particle size and distribution and the addition of a stabilizer to control the growth of Pt nanoparticles.

The first of these new parameters investigated was the supports. Different supports were investigated to determine the effect that surface area the structural properties of the supports would have on the electrocatalytic activity of the catalysts and the ORR. Functionalization of the surfaces of the support was used in an attempt to facilitate and improve the adsorption of Pt nanoparticles onto the supports and in this way increase the loading.

In order to do a complete study of the factors which would improve the catalytic activity towards the ORR for DMFC's we decided to look at different supports were used and modified simultaneously. In doing so these parameters could be evaluated simultaneously ensuring that an overall view of what the modifications employed would have on the proposed catalysts.

The supports investigated were namely; XC-72 vulvan carbon, MWCNT's and functionalised MWCNT's (F-MWCNT's). This meant that the MWCNT's had to be functionalised.





#### 4.9: IR spectra of MWCNT's and F-MWCNT's

The functionalization was accomplished through treatment of MWCNT's with a mixture of 4 M  $\text{H}_2\text{SO}_4/\text{HNO}_3$  ratio 3:1. The method has been well documented [124], [125], [126] and [127]. Figure 4.9 displays the FT-IR spectra of MWCNT's and F-MWCNT's. FT-IR was considered the ideal means to allow one to determine whether or not the surface of the MWCNT's was functionalised or not. The small amount of carboxyl groups on the surface of as-received MWCNTs could have been due to the partial oxidation of the surface of MWCNTs during purification by the manufacturer. The relatively strong peak at around  $1750\text{ cm}^{-1}$  is associated with the stretch mode of carboxylic acid groups as observed Fig 4.7 of the acid-treated MWCNTs, suggests that carboxylic groups are formed due to the oxidation of some carbon atoms on the surfaces of the MWCNTs by the strongly oxidizing  $\text{H}_2\text{SO}_4/\text{HNO}_3$  treatment.

#### 4.4 The effect of water on particle size and distribution using the polyol method for the synthesis of IH catalysts:

The polyol method generally uses stabilizers to control the growth of nanoparticles supported on carbon blacks for fuel cell application. In this study we achieved with just the addition of water the ability to effectively control the particle size and distribution on the support without the use of a stabilizer and thus avoid the excessive heating and purification steps to get rid of the stabilizer afterwards.

##### 4.4.1 Physiochemical characterization

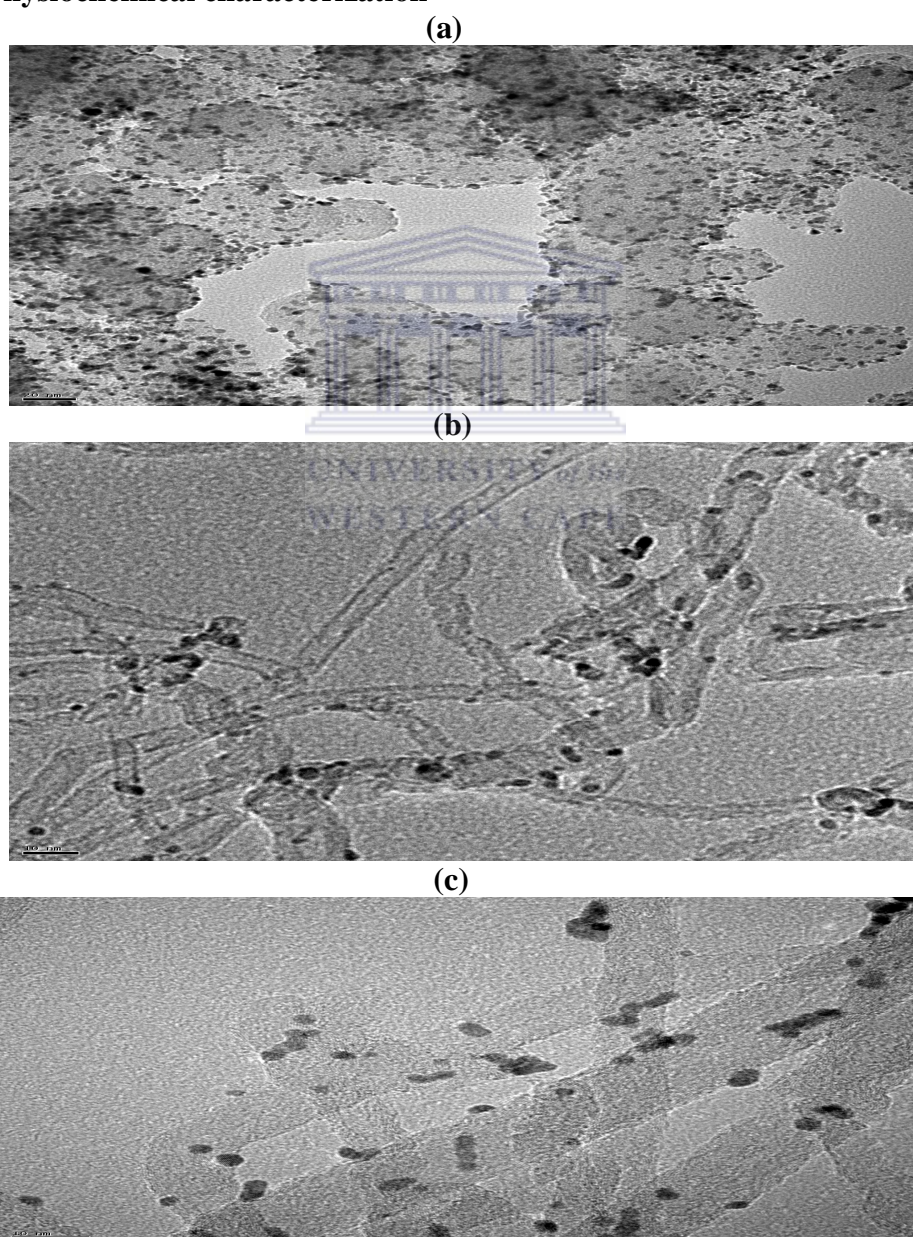


**Figure 4.10:** TEM images of IH catalysts synthesized using the modified polyol method, (a) Pt/C-IH, (b) Pt/MWCNT's-IH and (c) Pt/MWCNT's-F-IH, (scale 20 nm)

Figure 4.10 shows TEM images of IH catalysts synthesized using the modified polyol method, (a) Pt/C-IH, (b) Pt/MWCNT's-IH and (c) Pt/MWCNT's-F-IH. These TEM images indicate that Pt nanoparticles were successfully deposited on the various supports. TEM images figure 4.8 (a, b and c) show that the nanoparticles are spherical and well distributed onto the support with minimal agglomeration observed for the IH catalysts.

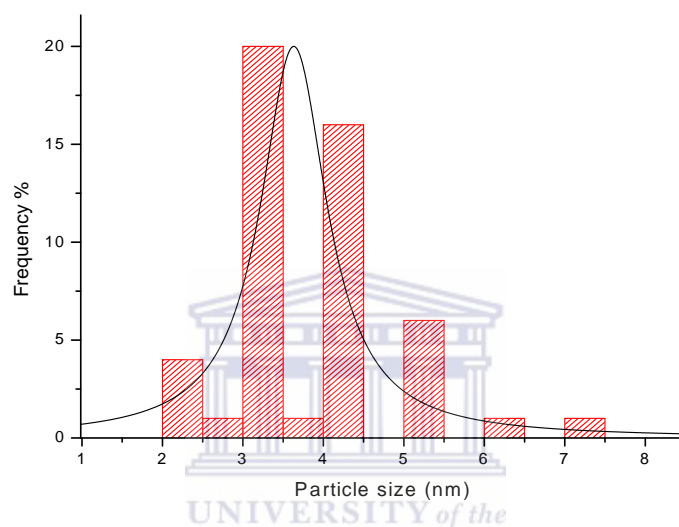


**Figure 4.11:** Histogram of the particle size distribution obtained from the TEM analysis from random particles of IH catalyst (Pt/C-IH) synthesized using the modified polyol method.

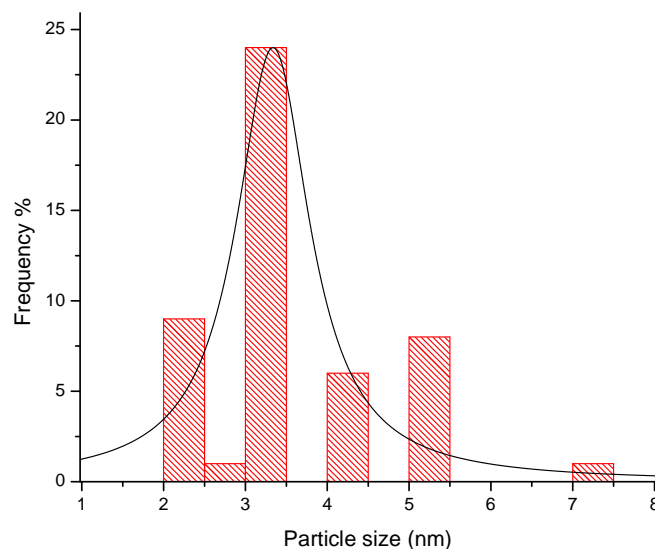


**Figure 4.12:** Histogram of the particle size distribution obtained from the TEM analysis from random particles of IH catalyst (Pt/MWCNT's-IH) synthesized using the modified polyol method.

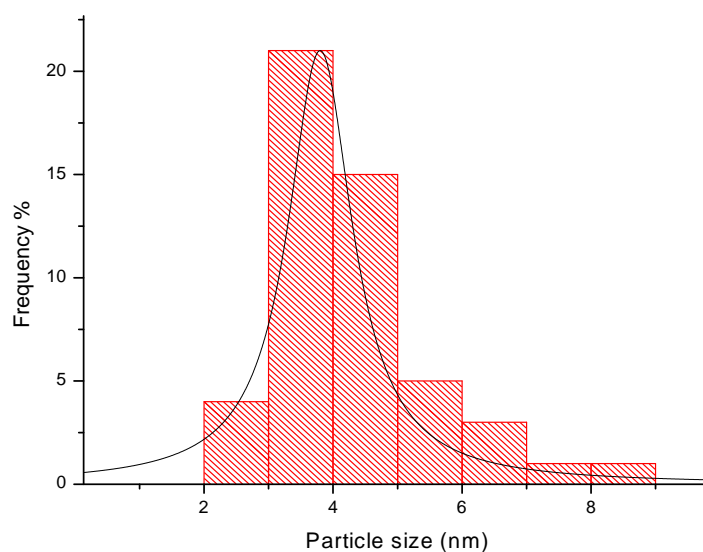


**Figure 4.13:** Histogram of the particle size distribution obtained from the TEM analysis from random particles of IH catalyst (Pt/MWCNT's-F-IH) synthesized using the modified polyol method.

Figure 4.11 displays the histograms of the particle size distributions obtained from the TEM analysis from random particles of IH catalysts (Pt/C-IH) synthesized using the modified polyol method. Figure 4.12 and 4.13 displays the histograms of the particle size distributions obtained from the TEM analysis from random particles of IH catalysts Pt/MWCNT's-IH and Pt/MWCNT's-F-IH respectively. Figure 4.11 indicates the particle size distribution of Pt/C-IH and revealed that the IH catalyst had a broad particle size distribution with a mean particle size of approximately 2- 6 nm. Figure 4.12 also displayed a broad particle size distribution with the majority of the particles 2-6 nm in size. A narrow particle size distribution was displayed by Pt/MWCNT's-F-IH (figure 4.13) and fell in the range of 3-6 nm.

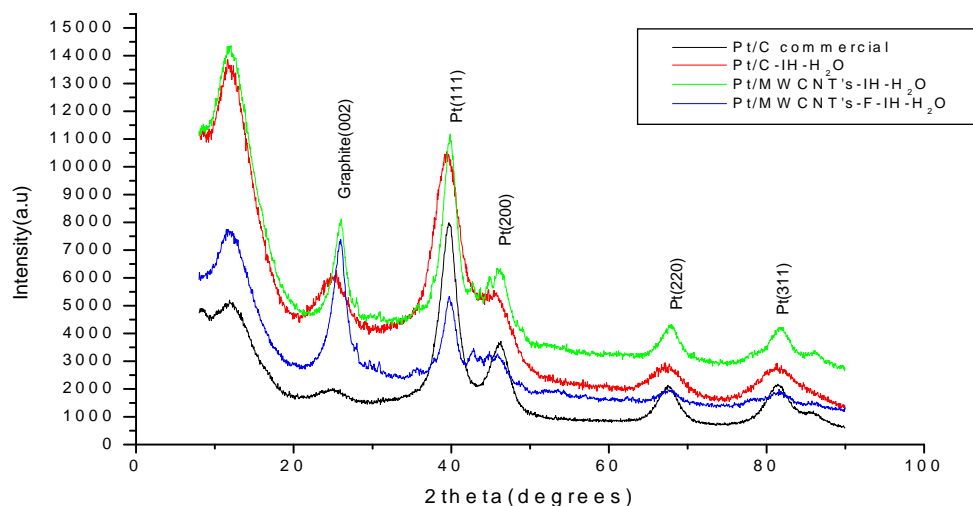


**Figure 4.14:** XRD pattern of commercial catalyst and IH catalysts prepared by modified polyol method.

XRD patterns of the commercial and IH catalysts are shown in figure 4.14. The diffraction peak at  $2\theta = 25.1^\circ$  is attributed to the graphite structure (002) of the carbon supports due to the larger interplanar spacing of XC-72 carbon ( $d_{002} = 0.355$  nm). The broadness of the graphite peak for Pt/C compared to Pt supported on MWCNT's is due to the fact that XC-72 is an amorphous carbon material with small regions of crystallinity whereas the MWCNT's has a more graphite nature [90]. The diffraction peaks at  $2\theta = 39.8^\circ$  (111),  $46.4^\circ$  (200),  $67.8^\circ$  (220) and  $81.2^\circ$  (311) are due to Pt nanoparticles and can be indexed to a face-centered cubic (fcc) platinum, which is consistent with the standard powder diffraction of Pt. The peaks obtained from the XRD appear to be broad suggesting the particle sizes are relatively small. The relative intensities of Pt (111) of Pt/MWCNT-F indicate the abundance of these facets which are required for the ORR due to the facial reaction kinetics [128]. The mean particle sizes of the IH catalysts were calculated from Scherrer's formula based on the Pt (220) peak at  $d = 67.8^\circ$ .

**Table 4.1:** Summary of results obtained form TEM and XRD of the commercial and IH catalysts

Catalyst	Average Particle size (TEM) in nm	Particle size (XRD) in nm
Commercial	3-5 nm	3.6
Pt/C-IH	2-5 nm	2.8
Pt/MWCTN's-IH	2-6 nm	4.2
Pt/MWCNT's-F-IH	3-6 nm	4.5

Table 4.1 shows the summary of results obtained form TEM and XRD of the commercial and IH catalysts. The average particle sizes obtained from the approximation of nanoparticles from the TEM images for the commercial and Pt/C-IH are in good agreement with those obtained from the XRD spectrums based on the Scherrer's formula. The IH catalysts (Pt/C-IH and Pt/MWCNT's-IH) displayed a broad particle size distribution as seen in Figures 4.9 and 4.10. EDX measurements done showed that sufficient metal loading of 32wt% (appendix B1) was obtained for Pt/MWCNT's-F-IH which made it comparable to that of the commercial catalyst.

## 4.3.2 Electrochemical characterization

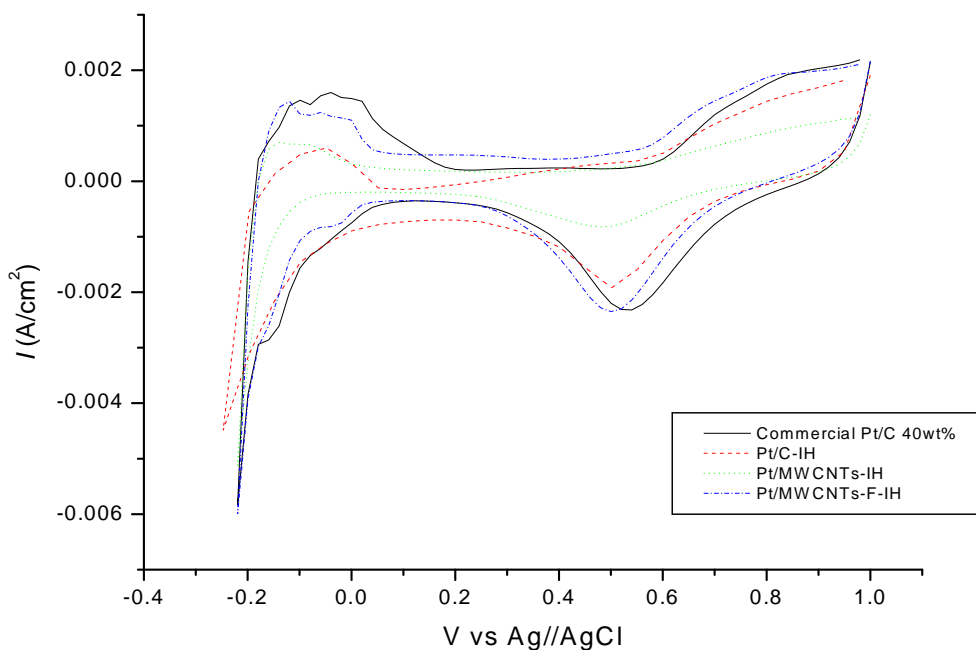


**Figure 4.15** shows the CV's measurements of commercial and IH catalysts in deaerated 0.5M H<sub>2</sub>SO<sub>4</sub> at a scan rate of 20mvs<sup>-1</sup>.

The characteristic peaks associated with Pt supported on carbon catalysts are displayed in figure 4.15. In the anodic scan hydrogen is desorbed (-0.2-0.9 V) vs SCE and upon further scanning Pt oxides are formed beyond 0.6 V. During the cathodic scan Pt oxides were then reduced (0.8-0.5 V) and hydrogen was then adsorbed at more positive potentials between (0.89- -0.2V) vs SCE. It is believed that in acidic media, hydroxyl groups adsorb (OH<sub>ads</sub>) onto the active Pt sites as a result of the oxidation of water at ~ 0.8 V. The OH<sub>ad</sub> then acts to block surface sites for O<sub>2</sub> adsorption thus lowering the ORR activity [129]. The CV displayed that in this region of the IH catalysts had similar onset potentials with the exception of Pt/MWCNT's-IH suggesting OH<sub>ads</sub> occurred to a lesser extent (~ 0.8 V). The characteristic peaks thus indicated that the IH catalysts were indeed electrochemically active.

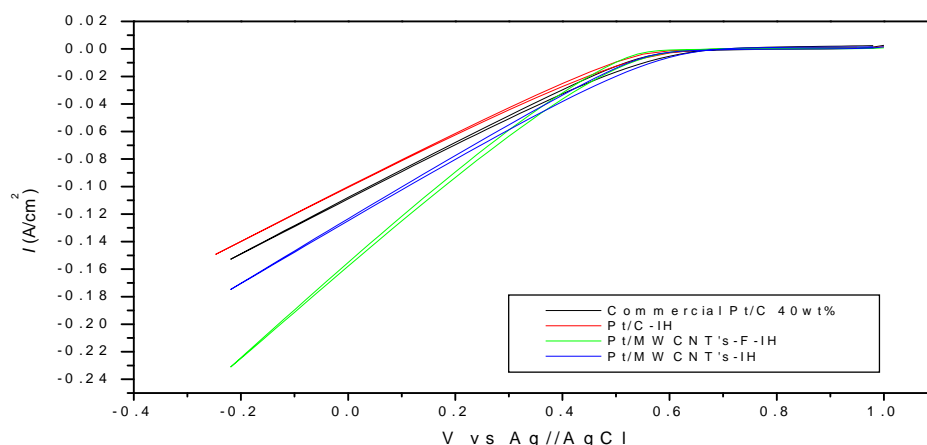


**Figure 4.16:** ORR of the commercial and IH catalysts prepared by the modified polyol method using  $\text{H}_2\text{O}$  without the use of a stabilizer in  $\text{O}_2$  saturated  $0.5\text{M H}_2\text{SO}_4$  at a scan rate of  $20\text{ mv s}^{-1}$

Figure 4.16 shows the ORR of commercial and IH catalysts prepared by the modified polyol method using  $\text{H}_2\text{O}$  without the use of a stabilizer in a  $\text{O}_2$  saturated  $0.5\text{ M H}_2\text{SO}_4$  at a scan rate of  $20\text{ mv s}^{-1}$ . The potential region between  $-0.2\text{-}0.6\text{ V vs Ag/AgCl (SCE)}$  is under mixed diffusion kinetic control. Figure 4.12 also demonstrates that for all the catalysts a single oxygen reduction peak was observed. The major potential region of interest though is between  $-0.2$  and  $0.6\text{V vs SCE}$ . Here the steep increase in current in the potential range between  $-0.2\text{-}0.6\text{V}$  indicates the facile kinetics for the ORR. The optimum operating potential at which the DMFC operates is  $0.3\text{ V}$  and therefore the current values were taken at that point to compare the relative activities of the IH catalysts. In this region Pt/C-IH ORR activity did not compare to that of the commercial, whereas the Pt/MWCNTs and Pt/MWCNT's-F exhibited slightly better activity towards the ORR. This is mainly due to the particle size and distribution ( $2\text{-}6\text{ nm}$ ) onto the supports. It could also be attributed to the extent at which  $\text{OH}_{\text{ads}}$  onto the active Pt sites used for ORR activity. The MWCNT's also provided a greater surface area for the Pt nanoparticles to deposit themselves onto.



**Table 4.2:** ORR current at 0.3 V

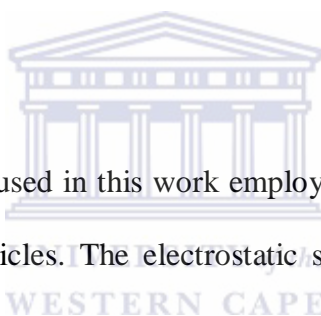
<b>Catalyst</b>	<b>(A/cm<sup>2</sup>)</b>
Commercial	0.047
Pt/C-IH	0.043
Pt/MWCTN's-IH	0.056
Pt/MWCNT's-F-IH	0.058

In conclusion table 4.2 gives a summary of the current obtained at 0.3 V which is the potential at which the ORR occurs in a DMFC during operating conditions. Table 4.2 shows that Pt/C-IH displays ORR activity (0.043 A/cm<sup>2</sup>) close to that of the commercial catalyst (0.047 A/cm<sup>2</sup>), whereas the IH catalyst prepared using MWCNT's as support displayed a slightly superior ORR activity (0.056 A/cm<sup>2</sup> and 0.058 A/cm<sup>2</sup> for Pt/MWCTN's-IH and Pt/MWCTN's-F-IH respectively). The ORR activity obtained by the IH catalysts (Pt/MWCTN's-IH and Pt/MWCTN's-F-IH) was as a result of the modified polyol method. The addition of water (EG/H<sub>2</sub>O) proved to effectively control and stabilize Pt nanoparticle growth. The ORR activity obtained of the IH catalysts (Pt/MWCTN's-IH and Pt/MWCTN's-F-IH) may be attributed to uniform spherical particles (figure 4.8) and narrow particle size distribution (2-6 and 3-6 nm respectively) that meet the requirements of an ORR catalyst.

## CHAPTER 5: RESULTS AND DISCUSSION

### 5.1 Modified polyol method using sodium acetate as a stabilizer

The polyol method generally makes use of polymers or bulky functional groups to create a steric effect to control the growth of the nanoparticles. The purpose of this is to obtain spherical and uniform nanoparticles with narrow particle size distributions [130]. The conventional steric stabilizers that are used tend to adsorb on the active sites of the nanoparticles. In order to remove these stabilizers at the conclusion of the synthetic protocol, excessive heat treatment is usually employed [75] and [131]. This may in turn lead to particle agglomeration and an increased particle size which causes a reduction in electrochemical surface area and hence an overall reduction in electrochemical activity.



The modified polyol method used in this work employed an electrostatic stabilizer in the formation of Pt nanoparticles. The electrostatic stabilizer that was used in the modified polyol method was sodium acetate. It was envisaged that stabilization of Pt nanoparticles would occur for via interaction with the acetate groups of the sodium acetate in its deprotonated form. In this regard acetate anions were found to restrict the agglomeration of ruthenium (Ru) nanoparticles in a polyol synthesis procedure [132]. It was also evident from the literature that Pt and Ru catalysts have been prepared with the addition of sodium acetate as a stabilizer [133]. This would therefore make the use of an acetate ideal for stabilizing the growth of Pt nanoparticles in solution. The advantage of employing electrostatic as apposed to steric stabilization lies in the removal step of the carboxylic anions which act as stabilizers [108]. In this work removal was accomplished through the simple expediency of rinsing the IH catalysts with ultra pure water prior to drying.

## 5.1.1 Physiochemical characterization

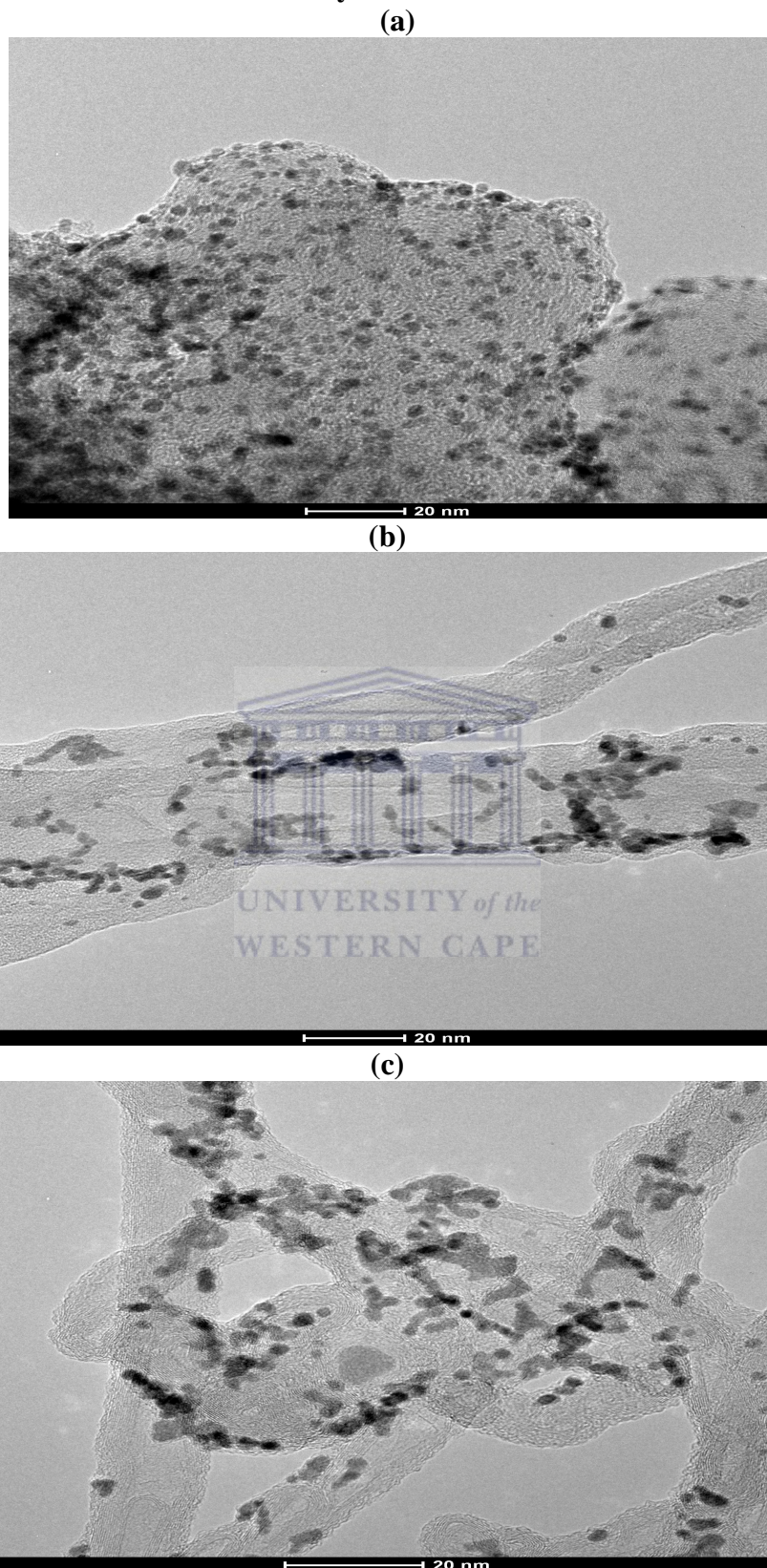


**Figure 5.1:** TEM images of IH catalysts synthesized using the sodium acetate modified polyol method, (a) Pt/C-IH, (b) Pt/MWCNT's-IH and (c) Pt/MWCNT's-F-IH

Figure 5.1 shows the TEM images of IH catalysts synthesized using the sodium acetate modified polyol method, ((a) Pt/C-IH, (b) Pt/MWCNT's-IH and (c) Pt/MWCNT's-F-IH). As seen from the TEM images Figure 4.13(a) NaOAc was effectively used to stabilize the growth of Pt nanoparticles. This was however not the case with the sodium acetate stabilized Pt nanoparticles supported on MWCNT's. Figures 4.13 (b) and (c) show that Pt nanoparticles were not effectively stabilized during synthesis, and particle agglomeration occurred on the support. Even after varying the sodium acetate concentrations during synthesis it was still not possible to effectively stabilize the formation and growth of the Pt nanoparticles. This phenomena is not understood and no literature study was available to explain this occurrence when using NaOAc as a stabilizer for depositing Pt nanoparticles onto MWCNT's

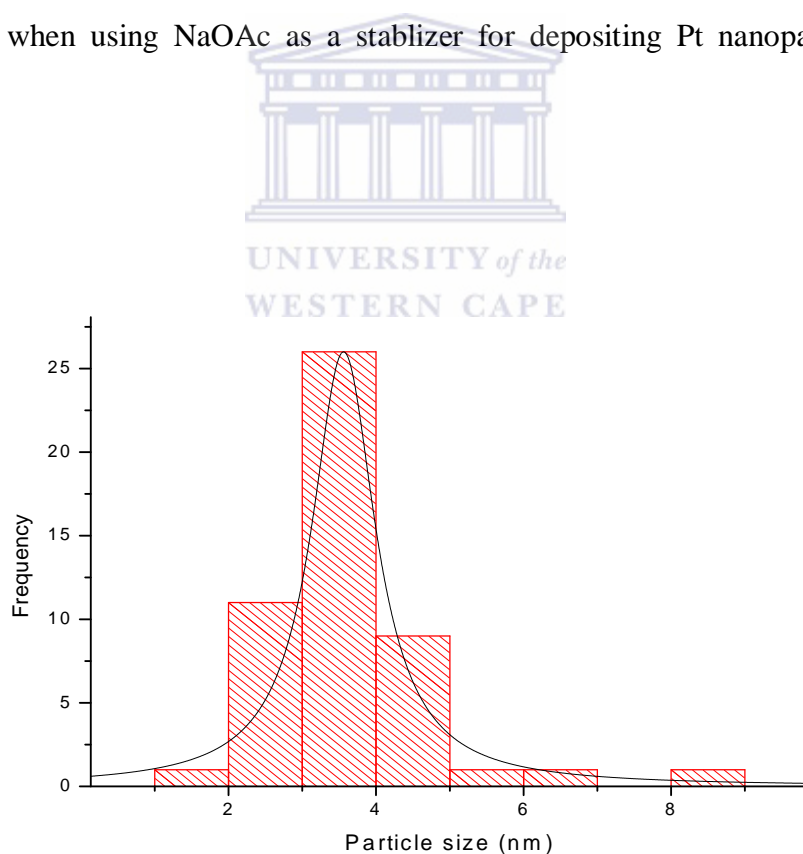


**Figure 5.2:** Histogram of the particle size distribution obtained from the TEM analysis from random particles of IH catalyst (Pt/C-NaOAc-IH) synthesized using the modified polyol method.

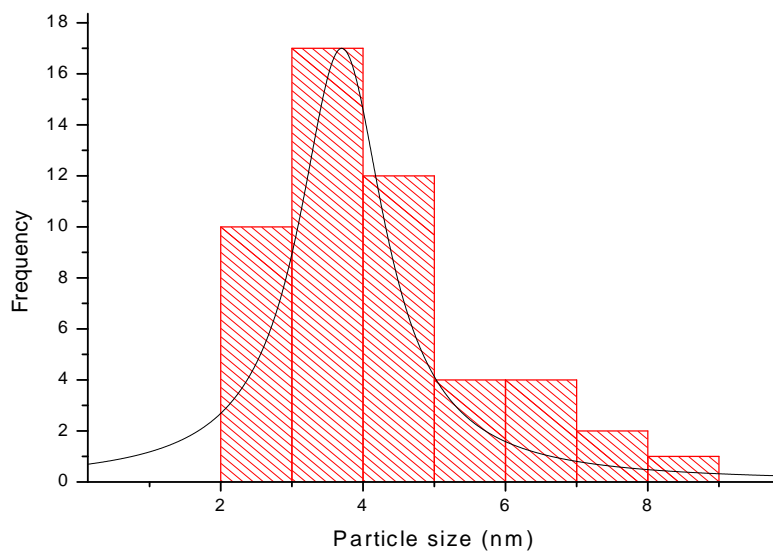


**Figure 5.3:** Histogram of the particle size distribution obtained from the TEM analysis from random particles of IH catalyst (Pt/MWCNT's-NaOAc-IH) synthesized using the modified polyol method.

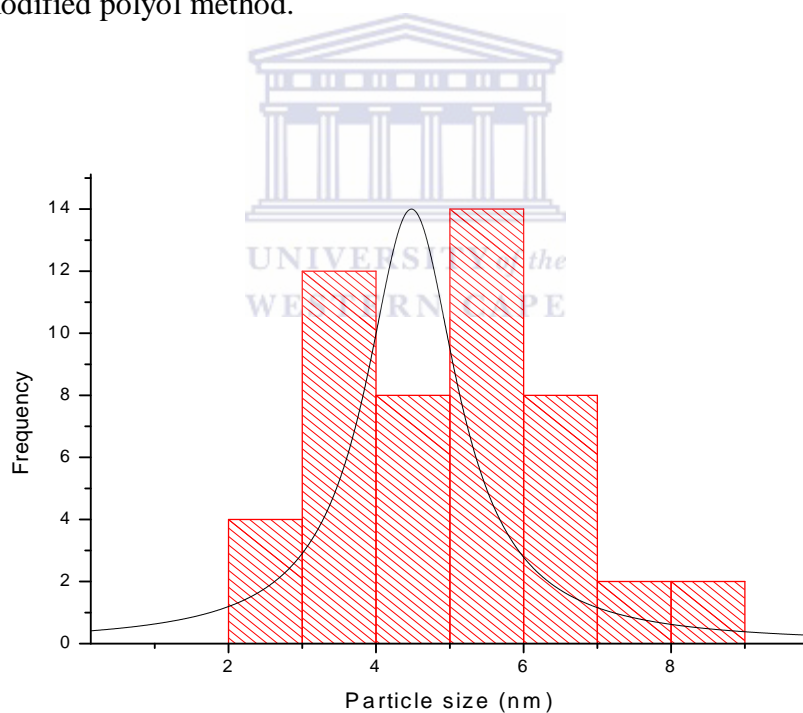


**Figure 5.4:** Histogram of the particle size distribution obtained from the TEM analysis from random particles of IH catalyst (Pt/MWCNT's-F-NaOAc-IH) synthesized using the modified polyol method.

Figure 5.2 display the histograms of the particle size distribution obtained from the TEM analysis from random particles (200 particles) of IH catalyst (Pt/C-NaOAc-IH) synthesized using the modified polyol method. The histogram shows (Figure 5.2) that the particles have a narrow particle size distribution with an average mean particle size of 2-5 nm, implying that NaOAc effectively stabilized the growth of the Pt nanoparticles. The same trend was not observed in Figures 5.3 and 5.4. The histogram (5.3) displayed a broad particle size distribution and an average mean particle size of 2-7 nm. The same trend came to the for in figure 5.4 with an even broader particle size distribution and an average mean particle size of 2-8 nm. The Pt nanoparticles could not effectively be stabilized and deposited onto the MWCNT's. This could have been due to a number of reasons namely; pH which affects the growth of nanoparticles in the polyol method, solubility of surface oxidized MWCNT's in the solvent used and the functional groups on the surface of the MWCNT's acting as anchorage sites for Pt nanoparticles competing with the electrostatic stabilizers. This was evident in the broad particle size distribution obtained (figures 5.3 and 5.4). The TEM images confirmed this by considerable particle agglomeration (figure 5.1 b and c).

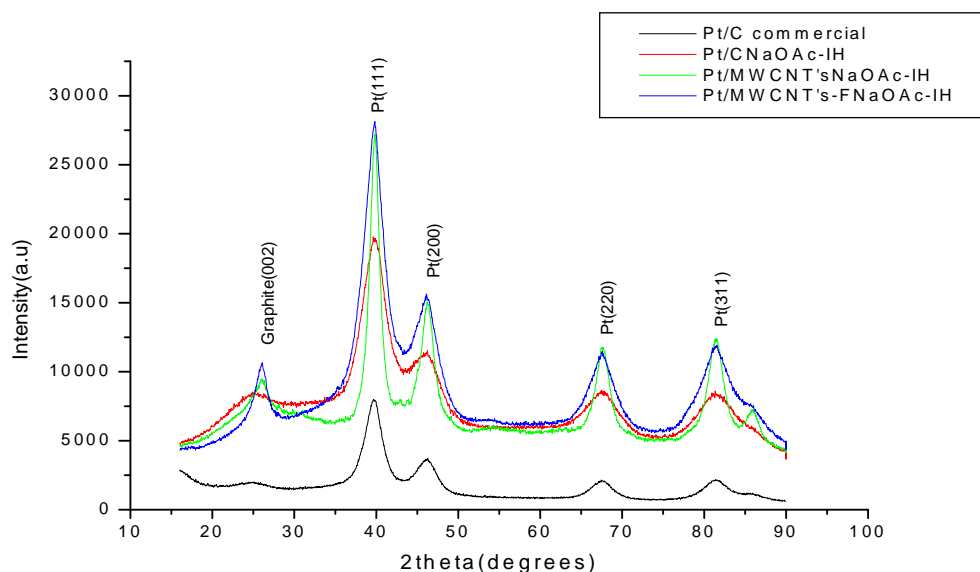


**Figure 5.5:** XRD patterns of commercial and IH catalysts prepared using NaOAc as a stabilizer.

Figure 5.5 shows the XRD spectrum of commercial and IH catalysts prepared by using NaOAc as a stabilizer. The broad diffraction peak at  $2\theta = 25.1^\circ$  (002) may be attributed to carbon graphite from the supports. Once again the broadness displayed by the graphite peaks of XC-72 compared to Pt supported on MWCNT's is due to the fact that XC-72 is an amorphous carbon material with small regions of crystallinity whereas MWCNT's is in a graphite form. The sharp peaks of Pt/MWCNT's-NaOAc and Pt/MWCNT's-F-NaOAc suggests relatively larger particles in comparison to that of Pt/C-NaOAc. The diffraction peaks with  $2\theta$  values of  $39.8^\circ$  (111),  $46.4^\circ$  (200),  $67.8^\circ$  (220) and  $81.2^\circ$  (311) are due to Pt nanoparticles that can be indexed to fcc phase of Pt, which is consistent with the standard powder diffraction of Pt. The sharpness of the peak can be related to particle size, and this is explained by the Scherrer equation in terms of incident beam divergence. The broadness of the peaks suggests that the Pt particle sizes are relatively small. The particle sizes of the commercial and IH catalysts were calculated from Scherrer's formula based on Pt (200) peak.

**Table 5.1:** Summary of results obtained from TEM and XRD of the commercial and IH catalysts synthesized using NaOAc as a stabilizer.

Catalyst	Average Particle size (TEM)	Particle size (XRD)
Commercial	3	3.6
Pt/C-NaAc-IH	2-5 nm	3.2
Pt/MWCTN's-NaAc-IH	2-7 nm	4.3
Pt/MWCNT's- NaAc -F-IH	2-8nm	4.2

Table 5.1 shows a summary of the results obtained from TEM and XRD studies of the commercial and IH catalysts synthesized using NaOAc as a stabilizer. The average particle sizes obtained from the TEM images are in good agreement with those obtained from XRD spectra using the Scherrer formula. The trend was consistent for all the IH catalysts. Pt/C-NaOAc-IH displayed relatively good particle size and distribution (2-5 nm) onto the carbon support. This was not observed for Pt/MWCTN's-NaOAc-IH and Pt/MWCTN's-F-NaOAc-IH with particle size distributions of 2-7 and 2-8 nm respectively. Compositional analysis (EDX) of Pt/C-NaOAc-IH was done (Appendix B2) and by integrating the area under the Pt peak relative to the carbon peak and a nominal loading of 36wt % was obtained. The EDX spectrum of Pt/C-NaOAc-IH revealed that sufficient Pt loading was obtained which made it comparable to that of the commercial catalyst.



### 5.1.2 Electrochemical characterization

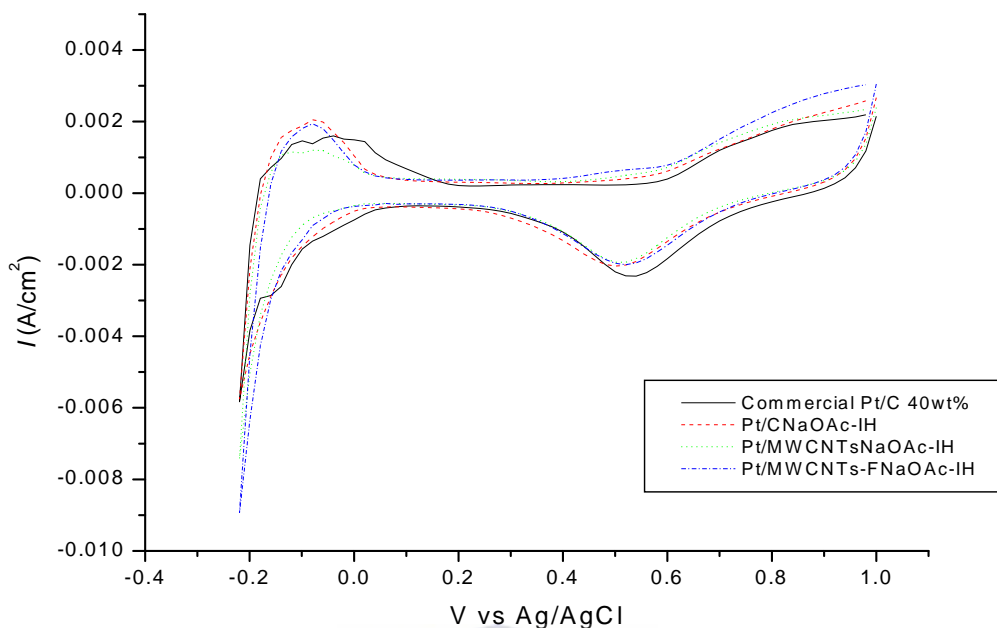


**Figure 5.6:** CV of commercial and IH catalysts prepared by the modified polyol method using NaOAc as a stabilizer in 0.5 M  $\text{H}_2\text{SO}_4$  at a scan rate of  $20 \text{ mV s}^{-1}$

Figure 5.6 shows the CV's of commercial and IH catalysts prepared by the modified polyol method using NaOAc as a stabilizer in 0.5 M  $\text{H}_2\text{SO}_4$  at a scan rate of  $20 \text{ mV s}^{-1}$ .

The CV's obtained all display the characteristic peaks associated with Pt on carbon supported catalysts. The quasi reversible hydrogen desorption/adsorption peaks (-0.2 to 0.9V), the double layer region (0.1 to 0.6V) which arises from an interfacial boundary formed between an electrical field and the electrode surface, Pt oxide formation (0.65-1.2V) and Pt-oxide reduction (0.9 to 0.55V) are all observed. Pt  $\text{OH}_{\text{ad}}$  occurred to a greater extent with Pt/MWCNT's-F-NaOAc than the commercial, Pt/C-NaOAc-IH and Pt/MWCNT's-NaOAc suggesting it would have a lower ORR activity due to OH groups adsorbed onto the active Pt sites.

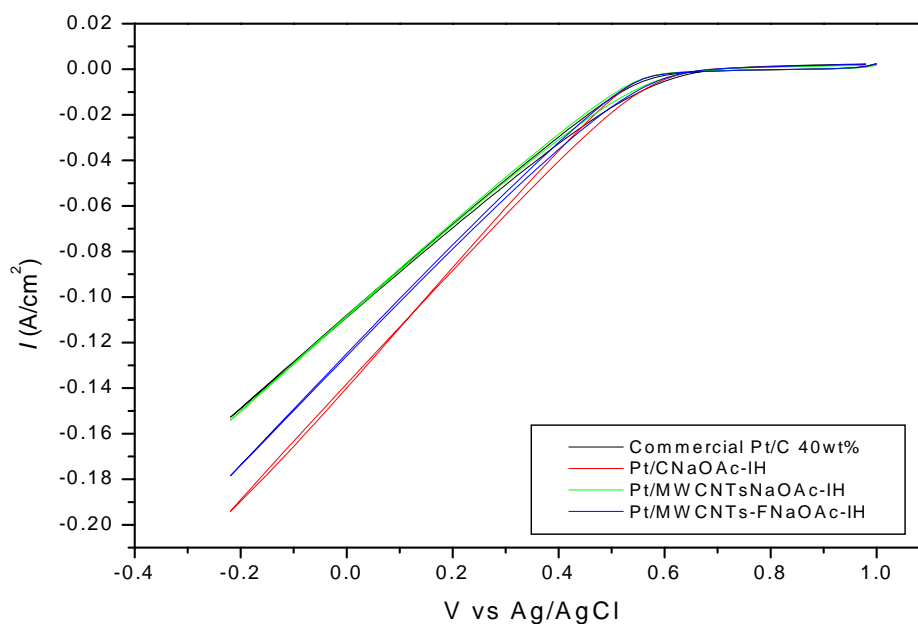


**Figure 5.7:** ORR of commercial and IH catalysts prepared by the modified polyol method using NaOAc as a stabilizer in a  $O_2$  saturated 0.5 M  $H_2SO_4$  at a scan rate of  $20 \text{ mv s}^{-1}$

Figure 5.7 shows the ORR of commercial and IH catalysts prepared by the modified polyol method using NaOAc as a stabilizer in a  $O_2$  saturated 0.5 M  $H_2SO_4$  at a scan rate of  $20 \text{ mv s}^{-1}$ . The commercial and IH catalysts all displayed a single oxygen reduction peak in the potential range between -0.2-1V vs SCE. The ORR is diffusion controlled in the potential region 1-0.7V vs SCE. A steep increase in current (-0.2 to 0.6V vs SCE) was observed for the ORR of all the catalysts. The region suggests facial kinetics of the ORR. The current densities of the commercial and IH catalysts were compared at 0.3 V and Pt/C-NaOAc proved to have the slightly superior activity (0.064 amps) towards the ORR. The observed result confirmed that particle size and dispersion (Table 5.1) on supports contribute to the electrochemical catalytic activity of FC catalysts, and in this case cathode catalysts for the ORR in DMFC's

**Table 5.2:** ORR current at 0.3 V

Catalyst	(A/cm <sup>2</sup> )
Commercial	0.047
Pt/C-IH	0.043
Pt/MWCTN's-IH	0.058
Pt/MWCNT's-F-IH	0.056
Pt/C-NaOAc-IH	0.064
Pt/MWCNT's-NaOAc-IH	0.048
Pt/MWCNT's-F-NaOAc-IH	0.056

In conclusion table 5.2 shows all the ORR currents obtained for the commercial and IH catalysts. All the IH catalysts synthesized with the exception of Pt/C-IH has slightly higher currents at 0.3 V implying that they have a better ORR activity than compared to the commercial catalyst. In comparing the ORR activity of all the IH catalysts table 5.2 shows that Pt/C-NaOAc-IH exhibited the highest ORR current, which is attributed to the fact that NaOAc effectively stabilized and controlled the growth of Pt nanoparticles. Figure 5.1 a displayed small and spherical particles which is evenly distributed onto the support, and figure 5.2 further justified this by displaying a narrow particle size distribution (2-5 nm).

The modified polyol method using NaOAc as a stabilizer for the synthesis of cathode catalysts for a DMFC yielded the best IH catalysts of all the IH catalysts synthesized.

## CHAPTER 6: CONCLUSIONS AND RECOMMENDATIONS

### 6.1 Conclusions

A number of IH FC catalysts were successfully synthesized using the polyol method which proved to be a cheap, simple and efficient way to prepare cathodic FC catalysts. In relation to the completed work, the colloidal method was seen to be the most effective way to control particle size growth and distribution of Pt nanoparticle supported catalysts.

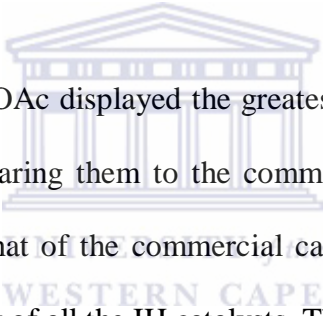
Modification of the initial synthetic protocol proved to have a considerable impact on the end result of the IH catalysts obtained. This was evident when the pH of the reaction mixture was lowered after the reduction step the pH greatly facilitated the deposition of uniformly formed Pt nanoparticles onto the support entities. In lowering the pH after complete reduction the glycolate anion concentration was effectively decreased, freeing up nanoparticles that underwent stabilization through chelate type complexes via the acetyl groups. This meant that more Pt nanoparticles could then deposit themselves onto the supports. It was found that the pH had to be lowered to approximately 9 to obtain the desired results. TEM images obtained revealed the fact that the sedimentation promoter employed was most effective by yielding a particle size distribution of 2-6 nm with a narrow particle distribution. Functionalization of MWCNT's was also accomplished through oxidative acid treatment. The relative intensities of the functional groups on the surfaces of the modified supports appeared to be relatively greater than compared to MWCNT's that did not undergo acid treatment. FT-IR spectra supported the fact that functionalization viz., the process of oxidising a proportion of the surface C to COOH ( $1750\text{ cm}^{-1}$ ) groups had occurred.

Other variables were investigated proved to observe their effect on the overall electro catalytic activity of the IH catalysts. For instance, use of XC-72 carbon, MWCNT's

and MWCNT's-F proved to influence the activity of the IH catalysts compared to XC-72 carbon and MWCNT's by providing not only chemical stability and conductivity but also by acting as effective anchorage sites through the various functional groups on the surface for Pt nanoparticles. This was evident using the modified polyol method with the addition of water. Pt/MWCNT's-F had spherical and well dispersed (3-6 nm) Pt nanoparticles with a narrow particle size distribution. This was due to the water content in the reaction mixture controlling particle growth, and various functional groups on the functionalized MWCNT's surface (hydroxyl, carboxylic acid) which served as anchorage sites for the Pt nanoparticles. The CV's of the IH catalysts were comparable to those of the commercial catalyst. Pt/MWCNT's-F showing a slightly better activity ( $0.058 \text{ A/cm}^2$ ) than the commercial ( $0.047 \text{ A/cm}^2$ ), Pt/C-IH ( $0.043 \text{ A/cm}^2$ ) and Pt/MWCNT's ( $0.056 \text{ A/cm}^2$ ) towards the ORR.

Addition of an electrostatic stabilizer in place of a steric stabilizer proved to be beneficial in terms of the modified polyol method. Sodium acetate effectively stabilized the growth of spherical Pt nanoparticles onto XC-72. This was evident by the TEM images obtained for Pt/C-IH-NaOAc which revealed a narrow particle size distribution with a mean particle size of approximately 2-5 nm. The advantage of using electrostatic stabilizers over steric stabilisers revolves around the removal step. Steric stabilizers tend to adsorb onto the active sites of the Pt particles so much so that excessive temperatures are required to remove them, resulting in an artifactual particle agglomeration and a lower electro catalytic activity due to a decrease in the surface area. The beauty of the electrostatic stabilizer used in the modified polyol method lies in their relatively easy removal of the stabilizer by continuous rinsing of the samples with ultra pure water. This essentially ensures that the electro catalytic integrity of the IH catalysts were not compromised during the removal step.

Sodium acetate could not effectively stabilize the growth of Pt nanoparticles on Pt/MWCNT's-NaOAc and Pt/MWCNT's-F-NaOAc. Pt/C-NaOAc, Pt/MWCNT's-NaOAc and Pt/MWCNT's-F-NaOAc displayed similar electrocatalytic activity which was comparable to the commercial catalysts during CV studies in acidic media. Pt/C-NaOAc proved to have the superior ORR activity ( $0.064 \text{ A/cm}^2$ ) when comparing the IH to the commercial catalysts ( $0.047 \text{ A/cm}^2$ ). This was mainly attributed to the fact that Pt nanoparticles were evenly distributed onto the support with a narrow particle size distribution. This meant that a larger surface area was made available and Pt utilization was optimized and was evident in the ORR activity obtained. Pt/C-NaOAc therefore meets the requirements needed for an ideal cathode FC catalyst of a DMFC



Pt/MWCNT's-F and Pt/C-NaOAc displayed the greatest activity towards the ORR of the IH catalysts and in comparing them to the commercial catalyst; they displayed slightly superior activity to that of the commercial catalyst. Pt/C-NaOAc proved to have the greatest ORR activity of all the IH catalysts. This was as a direct result of the various modifications employed in the polyol method.

## 6.2 Recommendations for future work

This first issue that would need addressing is the deposition of the Pt nanoparticles onto MWCNT's using NaOAc. This would have to be accomplished by evaluating the factors affecting the control and deposition of Pt particles. The MWCNTs offer a larger surface area than XC-72 which would allow for a greater area for Pt deposition and increase the overall electro catalytic activity of the catalysts.

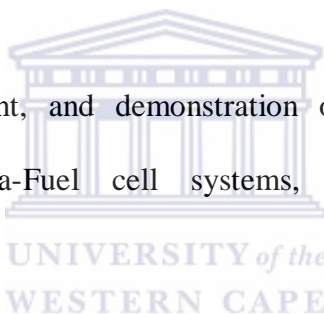
### Future work would involve:

- The use of various polymers and dendrimers to stabilize the growth of Pt nanoparticles [134].
- Employing a second, third or even fourth metal to reduce Pt usage which is very expensive and thereby lowering the overall costs of catalyst. The metals employed would also serve to facilitate the ORR increasing the electro catalytic activity of the catalysts.
- Testing the activity of the IH catalysts by actually putting the IH catalysts in MEA's in a DMFC, where the single cell performance of the IH catalysts may be evaluated.

In conclusion the polyol method may be viewed as an effective synthetic route for the synthesis of nanoparticles for FC applications. The strength of the method lies in its ability to effectively control the size and distribution of nanoparticles without complicated procedures. The fact that the catalysts are made in a so-called 'one pot synthesis' makes it ideal for up scaling and eventually commercialisation.

**CHAPTER 7: BIBLIOGRAPHY****7.1. Bibliography**

1. Thomas Thielemann, Sandro Schmidt , J. Peter Gerling, International Journal of Coal Geology 72 (2007) 1–14
2. Ali Osman Yilmaz\_, Tuncay Uslu, Energy Policy 35 (2007) 1117–1128
3. Shahriar Shafiee, Erkan Topal, Energy Policy 37 (2009) 181–189.
4. [Online], Available: [www.world-agriculture.com](http://www.world-agriculture.com)
5. Fuel cell diagram, [Online], Available: [people.clarkson.edu](http://people.clarkson.edu)
6. Fuel cells, [Online], Available: [www.eere.energy.gov/hydrogenandfuelcells](http://www.eere.energy.gov/hydrogenandfuelcells)
7. Different types of fuel cells, by Sandra Curtin, [Online], Available: [www.fuelcells.org](http://www.fuelcells.org)
8. Research, development, and demonstration of phosphoric acid fuel cell systems, R Anahara-Fuel cell systems, 1993, [Online], Available: [books.google.com](http://books.google.com)
9. Alkaline fuel cell, [Online], Available: [fuelcells.si.edu/basics.htm](http://fuelcells.si.edu/basics.htm)
10. [Online], Available: <http://www.prototech.no/index.cfm?id=223469>
11. James D. Maclay, Jacob Brouwer, G. Scott Samuelsen, International Journal of Hydrogen Energy 31 (2006) 994 – 1009
12. Mitlitsky F, Myers B, Weisberg AH. Regenerative fuel cell, systems. Energ Fuels 1998; 12(1):56–71
13. Burke KA. Unitized regenerative fuel cell system development. In: First international energy conversion engineering conference, August 17–21 2003
14. [Online], Available: [zincenergystorage.org](http://zincenergystorage.org)
15. Prabal Sapkota and Honggon Kim, Journal of Industrial and Engineering Chemistry, Volume 15, issue 4, 25 July 2009, 445-450





16. K. Kordesch G. Simader, Fuel Cells and their Applications, Wiley-VCH, Weinheim, 1996.
17. Dillion. R, Srinivasan. S, Arico`. A.S. Antonucci. V, J Power Sources, 2004.127, 1-2, 112-126
18. Casalengo, Andrea, Grassini, Paolo; Marchesi, Renzo, Appl. Therm Eng., 2007, 27, 4, 748-754
19. Aricò, S. Srinivasan and V. Antonucci, DMFCs: From fundamental aspects to technology development, Fuel Cells, 1 (2001) (2), pp. 133–161.
20. Hansan Liu, Chaojie Song, Lei Zhang, JiuJun Zhang, Haijiang Wang, David P. Wilkinson, Journal of Power Sources 155 (2006) 95–110
21. C. Lamy, J.M. Leger and S. Srinivasan In: J.O'M. Bockris, B.E. Conway and R.E. White, Editors, Modern Aspects of Electrochemistry vol. 34 (2001), pp. 53–118
22. PEM fuel cell electrocatalysts and catalyst layers: Fundamentals and Applications, JiuJun Zhang, JiuJun Zhang - 2008 - Science - 1137 pages, [Online], Available: [books.google.co.za](http://books.google.co.za)
23. A.K. Shukla and R.K. Raman, Annu. Rev. Mater. Res. 2003. 33:155–68
24. Carbon blacks, [Online], Available; <http://www.carbon-black.org>
25. Carbon blacks, [Online], Available; <http://www.carbonblack.jp/en/cb/seizou>.
26. Daniele Mirabile Gattiaa, Marco Vittori Antisaria, Leonardo Giorgia, Renzo Marazzia, Emanuela Piscopiello, Amelia Montonea, Serafina Bellittoc, Silvia Licoccia and Enrico Traversac, Journal of Power Sources Volume 194, Issue 1, 20 October 2009, Pages 243-251
27. R.J. Madix, J. Benziger, Ann. Rev. Phys. Chem. 29 (1978) 285–306
28. Norton Haner, P.N. Ross, J. Phys. Chem. 95 (1991) 3740–3746

29. E. Herrero, K. Franaszczuk, A. Wieckowski, *J. Phys. Chem.* 98 (1994) 5074–5083
30. E. Herrero, W. Chrzanowski, A. Wieckowski, *J. Phys. Chem.* 99 (1995) 10423–10424
31. Carbon Nanotubes--the Route Toward Applications Ray H. Baughman, Anvar A. Zakhidov, Walt A. de Heer ,*Science* 2 August 2002:, Vol. 297. no. 5582, pp. 787 – 792.
32. R. G. Ding, G. Q. Lu, Z. F. Yan, M. A. Wilson, *J. Nanosci. Nanotechnol.* 1, 7 (2001)
33. N. M. Rodriguez, M.-S. Kim and R.T.K. Baker, *J. Phys. Chem.* 98 (1994), pp. 13108–13111
34. Chambers, T. Nemes, N.M. Rodriguez and R.T.K. Baker, *J. Phys. Chem. B* 102 (1998), pp. 2251–2258
35. F. Salman, C. Park and R.T.K. Baker, *Catal. Today* 53 (1999), pp. 385–394
36. Bing Liu, Stephen Creager, *Journal of Power Sources*, Volume 195, Issue 7, 2 April 2010, Pages 1812-1820
37. L. GenieÁ s, R. Faure, R. Durand LEPMI (U.M.R. 5631 CNRS-INP. Grenoble associated to UJF), ENSEEG, BP 75, 38402 Saint Martin D'Herès Cedex, France Received 1 October 1997.
38. Bard AJ. Faulkner LR. *Electrochemical methods: Fundamentals and applications*. New York: Wiley. 1980
39. Blurton KF, Greenburn P, Oswin HG, Rutt DR. The electrochemical activity of dispersed platinum. *J Electrochem Soc* 1972;119:559–64

40. Bett J, Lundquist J, Washington W, Stonehart P. Platinum crystallite size considerations for electrocatalytic oxygen reduction. *Electrochim Acta* 1973; 18:3438
41. Kinoshita K. Particle size effects for oxygen reduction on highly dispersed platinum in acid electrolytes. *J Electrochem, Soc* 1990;137: 845–848.
42. Chitturi Venkateswara Rao, April 2008, On the search for efficient catalysts for the oxygen reduction reaction.
43. Geins, L., R. Faure and R Durand (1998) Electrochemical reduction of oxygen on platinum nanoparticles in alkaline media, *Electrochim. Acta.*, 44, 1317-1327.
44. Gamez, D. Richard, P. Gallezot, F. Gloaguen, R. Faure and, R. Durand, *Electrochimica Acta*, Volume 41, Issue 2, February 1996, Pages 307-314.
45. G. Tamizhmani, J.P. Dodelet and D. Guay. *J. Electrochem. Soc.* 143 (1996), p. 18.
46. Review: Formation, microstructural characteristics and stability of carbon supported platinum catalysts for low temperature fuel cells, *Journal of materials science* 38 (2003) 2995 – 3005.
47. Masahiro Watanabe, Makoto Uchida and Satoshi, *J. Electroanal. Chem.* 229 (1987) 395-406
48. Bönemann H, Brijoux W. 1991. *Angew.Chem. Int. Ed. Engl.* 30:1312–14
49. Bönemann H, Britz P, Endruschat U, Mörstel R, et al. 2000. *J. New Mater. Electrochem. Syst.* 3:199–206
50. Xingwen Yu , Siyu Ye, *Journal of Power Sources* 172 (2007) 133–144
51. Kwong-Yu Chan, Jie Ding, Jiawen Ren, Shaoan Cheng and Kwok Ying Tsang, *J. Mater. Chem.*, 2004, 14, 505 – 516.

52. M.S. Nashner, A.I. Frenkel, D.L. Adler, J.R. Shapley, R.G. Nuzzo, *J. Am. Chem. Soc.* 119 (1997) 7760.
53. Fujiwara, Y. Murakami, K. Sasaki, M. Oguri, T. Asaki, W. Sugimoto, *J. Electrochem. Soc.* 147 (2000) 4421.
54. MacDougall, Y. LePage, *J. Electrochem. Soc.* 151 (2004) A 1269 .
55. A. Marshall, B. Børresen, G. Hagenm, M. Tsytkin, R. Tunold, *Materials Chemistry and Physics* 94 (2005) 226–232
56. Hu, Z.S., Chen, S.Y., Peng, S.Y., *Prep. Cat. VI*, 6: 197-206 (1995)
57. Barnickel, P., Wokaun, A., Sager, W., Eicke, H.F., *J. Coll. Inter. Sci.*, 148(1): 80-90 (1992)
58. Barnickel, P., Wokaun, A., *Molec. Phys.*, 67: 1355-1359 (1989)
59. Mark T. Swihart, *Current Opinion in Colloid and Interface Science* 8 (2003) 127-133.
60. Sol gel method, [Online] Available: [www.techbriefs.com/component](http://www.techbriefs.com/component)
61. H.B. Suffredini, V. Tricoli, L.A. Avaca, N. Vatistas, *Electrochemistry Communications*, Volume 6, Issue 10, October 2004, Pages 1025-1028
62. Linjie Hu, Kenneth A. Boateng, Josephine M. Hill, *Journal of Molecular Catalysis A: Chemical*, Volume 259, Issues 1-2, 15 November 2006, Pages 51-60
63. M.L. Calegaro, H.B. Suffredini, S.A.S. Machado, L.A. Avaca, *Journal of Power Sources* 156 (2006) 300–305
64. Fievet, F.; Lagier, J. P.; Figlarz, M. *MRS Bull.* 1989, 14, 29
65. Elisabete I. Santiago, Laudemir C. Varanda, and H. Mercedes Villullas, *J. Phys. Chem. C* 2007, 111, 3146-3151
66. B. He, Y. Chen, H. Liu and Y. Liu. *J. Nanosci. Nanotechno.*, 5 (2005) 266

67. [Online], Available: <http://www.strem.com/uploads/>
68. CRC Handbook of Chemistry and Physics, 71st ed.; Lide, D. R., Ed.; CRC Press: Boston, 1990
69. Christina Bock, Chantal Paquet,, Martin Couillard, Gianluigi A. Botton and Barry R. McDougall, J. AM. CHEM. SOC2004, 126, 8028-8037.
70. [Online], Available: [www.nacatsoc.org/20nam/abstracts/P-S14-03A.pdf](http://www.nacatsoc.org/20nam/abstracts/P-S14-03A.pdf)
71. Y. Wang, J. Ren, K. Deng, L. Gui and Y. Tang, Chem Mater. 14 (2002) 3953.
72. W. Li, W. Zhou, Li. H, Z. Zhou, B. Zhou, G. Sun, Q. Xin, Electrochim. Acta 2004, 49.
73. C. Lim and C.Y. Wang, J. Power Sources 113 (2003), p. 145
74. B. Legratiet, H. Remita, G. Picq, M.O. Delcourt, J. Catal. 164 (1996) 36
75. Guiyan Yu, Weixiang, Jie Zhao and Qiulin, Journal of Applied Electrochemistry (2006) 36:1021–1025
76. Jie Zhao, Weixiang Chen, Yifan Zheng, Xiang Li, Zhude Xu, J Mater Sci (2006) 41:5514–5518
77. Zhenhua Zhou, Weijiang Zhou, Suli Wang, Guoxiong Wang, Luhua Jiang, Huanqiao Li, Gongquan Sun, Qin Xin, Catalysis Today 93–95 (2004) 523–528
78. Zhaolin Liu, Leong Ming Gan, Liang Hong, Weixiang Chen, Jim Yang Lee, Journal of Power Sources 139 (2005) 73–78
79. Hyung-Suk Oh, Jong-Gil Oh, Hansung Kim, Journal of Power Sources 183 (2008) 600-603
80. S. Iijima, Nature 354 (1991) 56–58
81. K. Lee, J. Zhang, H. Wang, D. Wilkinson, J. Appl. Electrochem, 60 (2006) 507-522

82. W. Li, C. Liang, W. Zhou, J. Qiu, Z. Zhou, G. Sun and Q. Xin, *J. Phys. Chem. B* 107 (2003) 6292-6299
83. Perica Paunović, Aleksandar T. Dimitrov, Orce Popovski, Dragan Slavkov, Svetomir Hadži Jordanov, *Macedonian Journal of Chemistry and Chemical Engineering*, Vol. 26, No. 2, pp. 87–93 (2007)
84. A. Rinzler, D.T. Colbert, G. Scuseria, D. Tomanek, J.E. Fischer, R. Smalley, *Science* 273 (1996) 483–487
85. D. Pantea, H. Darmstadt, S. Kaliaguine, L. Summchen, C. Roy, *Carbon* 39 (2001) 1147–1158
86. Che GL, Lakshmi BB, Fisher ER, Martin R. Carbon nanotubule membranes for electrochemical energy storage and production. *Nature* 1998;393:346–9
87. Bessel CA, Laubernds K, Rodriguez NM, Baker RTK. Graphite nanofibers as an electrode for fuel cell applications. *J Phys Chem B* 2001;105:1115–8
88. Seth L. Knupp, Wenzhen Li, Odysseas Paschos, Thomas M. Murray, Jeremy Snyder, Pradeep Haldar, *CARBON* 46 (2008) 1276–1284
89. Joo SH, Choi SJ, Oh I, Kwak J, Liu Z, Terasaki O, et al. Ordered nanoporous arrays of carbon supporting high dispersion of platinum nanoparticles. *Nature* 2001; 412:169–73
90. Kunchan Lee, JiuJun Zhang, Haijiang Wang and David P. Wilkinson, *Journal of Applied Electrochemistry* (2006) 36:507–522.
91. Wenzhen Li, Changhai Liang, Weijiang Zhou, Jieshan Qiu, Huanqiao Li, Gongquan Sun, Qin Xin, *Letters to the Editor / Carbon* 42 (2004) 423–460
92. Shuihua Tang, Gongquan Sun, Shiguo Sun, Jing Qi, Qin Xin and Gein Martin Haarberg, *J. Electrochem. Soc.*, Volume 157, Issue 9, pp. B1321-B1325 (2010)

93. H. Bonnemann and K.S Nagabhushana, *Journal of New Materials for Electrochemical Systems* 7, 93-108 (2004)
94. Overbeek, J. T. G. In *Colloidal Dispersions*; Goodwin, J. W., Ed.; Royal Society of Chemistry: London, 1981; pp 1-23
95. R. Franke, J. Rothe, J. Pollmann, J. Hormes, H. Bonnemann, W. Brijououx, Th. Hindenburg, *J. Am. Chem. Soc.*, 118, 12090 (1996)
96. Hirai, H.; Nakao, Y.; Toshima, N. *J. Macromol. Sci., Chem.* 1978, A12, 1117
97. Hirai, H.; Nakao, Y.; Toshima, N. *J. Macromol. Sci., Chem.* 1979, A13, 727
98. Borsla, A.; Wilhelm, A. M.; Delmas, H. *Catal. Today* 2001, 66, 389
99. Hirai, H. *J. Macromol. Sci., Chem.* 1979, A13, 633
100. Hirai, H. *Makromol. Chem., Suppl.* 1985, 14, 55
101. Hirai, H.; Nakao, Y.; Toshima, N. *Chem. Lett.* 1978, 545
102. Ahmadi TS, Wang ZL, Green TC, Henglein A, El-Sayed MA (1996) *Science* 272:1924
103. Komiyama, M.; Hirai, H. *Bull. Chem. Soc. Jpn.* 1983, 56, 2833.
104. Min Chen and Yangchuan Xing, *Langmuir* 2005, 21, 9334-9338.
105. Alain Roucoux, Ju'rgen Schulz, and Henri Patin, *Chem. Rev.* 2002, 102, 3757-3778.
106. J.W. Guo, T.S. Zhao, J. Prabhuram, C.W. Wong, *Electrochimica Acta* 50 (2005) 1973–1983
107. Chia-Shiang Lin, Maksudur R. Khan, Shawn D. Lin, *Journal of Colloid and Interface Science* 299 (2006) 678–685
108. Jie Zhao, Peng Wang, Weixiang Chen, Run Liu, Xiang Li, Qiulin Nie, *Journal of Power Sources* 160 (2006) 563–569
109. [Online], Available: <http://nobelprize.org/educational/physics>

110. [Online], Available: [bullenh1@nku.edu](mailto:bullenh1@nku.edu)
111. Patterson, A.L., (1939) The Scherrer formula for X-ray particle size determination. *Phys. Rev.* 56, 978-982
112. [Online], Available: [\\_assay.nih.gov](http://assay.nih.gov)
113. Book : Modern Infrared spectroscopy, Stuart, George and McIntyre
114. PDF: Cyclic Voltammetry, Prof. S. Shippy and M-J Lu, March/2007 [Online], Available: [www.chem.uic.edu/chem421/cv.PDF](http://www.chem.uic.edu/chem421/cv.PDF)
115. [Online], Available: [www.absoluteastronomy.com](http://www.absoluteastronomy.com)
116. Zhenhua Zhou,<sup>a</sup> Suli Wang,<sup>a</sup> Weijiang Zhou,<sup>a</sup> Guoxiong Wang,<sup>a</sup> Luhua Jiang,<sup>a</sup> Wenzhen Li,<sup>a</sup> Shuqin, Song,<sup>a</sup> Jianguo Liu,<sup>a</sup> Gongquan Suna and Qin Xin, *CHEM. COMMUN.*, 2003, 394–395
117. Seth L. Knupp, Wenzhen Li, Odysseas Paschos, Thomas M. Murray, Jeremy Snyder, Pradeep Haldar, *CARBON* 46 (2008) 1276–1284
118. GAN Lin, DU Hong-da, LI Bao-hua, KANG Fei-yu, *New Carbon Materials*, 2010, 25(1): 53–59
119. J.A. Creighton, D.G. Eadon, *J. Chem. Soc. Faraday Trans.* 87 (1991) 3881.
120. Duff DG, Edwards PP, Johnson BFG (1995) *J Phys Chem* 99:15934
121. Henglein A, Ershov BG, Malow M (1995) *J Phys Chem* 99:14129
122. Joelma Perez, E.R. Gonzalez, E.A. Ticianelli, *Electrochimica Acta* 44 (1998) 1329±1339
123. R.J Hunter, *Zeta potential in Colloid Science*, Academic Press, UK, 1981
124. Yu-Chun Chiang, Wei-Hsiang Lin and Yung-Chia Chang, Article in Press
125. Y. Xing, L. Li, C.C. Chusuei and R.V. Hull, *Langmuir* 21 (2005), pp. 4185–4190.



- 126.** A.G. Osorio, I.C.L. Silveira, V.L. Bueno and C.P. Bergmann, *Appl. Surf. Sci.* 255 (2008), pp. 2485–2489.
- 127.** B.I. Rosario-Castro, E.J. Contés, M. Lebrón-Colón, M.A. Meador, G. Sánchez-Pomales and C.R. Cabrera, *Mater. Charact.* 60 (2009), pp. 1442–1453.
- 128.** Panchenko, A., M.T.M. Koper, T.E. Shubina, S.J. Mitchell, and E. Roduner (2004) Ab-initio calculations of intermediates of oxygen reduction on low-index platinum surfaces. *J. Electrochem. Soc.*, 151, A2016-A2027
- 129.** Vladimir Komanicky, Andreas Menzel, and Hoydoo You, *J. Phys. Chem. B* 2005, 109, 23550-23557.
- 130.** L. Dubeau, C. Coutanceau, E. Garnier, J.M. Leger and C.J. Lamy, *Appl. Electrochem.* 33 (2003) 419.
- 131.** N. Chakroune, G. Viau, S. Ammar, L. Poul, D. Veautier, M.M. Chehimi, C. Mangeney, F. Villain, F. Fievet, *Langmuir* 21 (2005) 6788.
- 132.** J. Yang, T.C. Deivaraj, H.P. Too and J.Y. Lee, *Langmuir* 20 (2004) 4241.
- 133.** F. Rodriguez-Reinoso, in: J.W. Patrick (Ed), *Porosity in Carbon, Characterization and Applications*, John Wiley & Sons, New York, 1995, p.253.
- 134.** Mari´a Bernechea, Sergio Garc´ıa-Rodr´ıguez, Pilar Terreros, Ernesto de Jesu´s, Jose´ L. G. Fierro and Sergio Rojas, *J. Phys. Chem. C* 2011, 115, 1287–1294

## Appendices

### APPENDIX

#### Appendix A: Theoretical Pt loading calculations of the IH catalysts

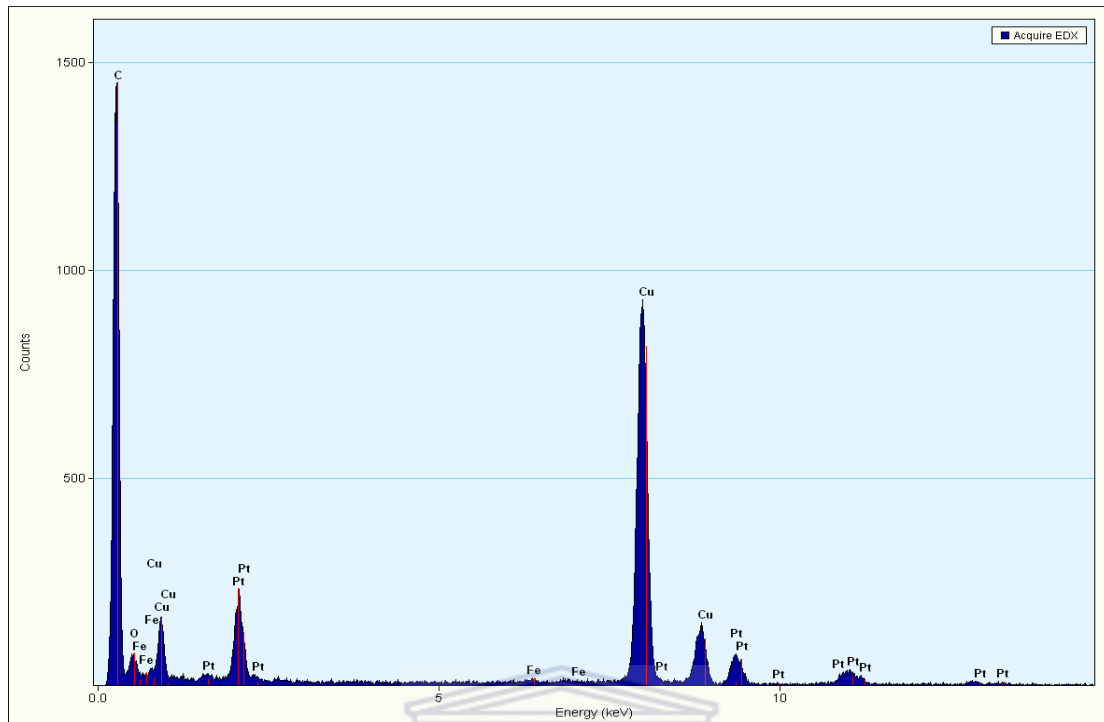
$$\begin{aligned}\text{Mole of Pt} &= \text{mole of H}_2\text{PtCl}_6 \cdot 6\text{H}_2\text{O} \\ &= \frac{(\text{mass of H}_2\text{PtCl}_6 \cdot 6\text{H}_2\text{O})}{(\text{molecular weight of H}_2\text{PtCl}_6 \cdot 6\text{H}_2\text{O})} \\ &= \frac{0.1\text{g}}{409.18 \text{ g/mol}} \\ &= 2.44 \times 10^{-4}\end{aligned}$$

$$\begin{aligned}\text{Therefore the mass of Pt} &= (\text{molecular weight of Pt}) \times (\text{mole of Pt}) \\ &= 195 \times (2.44 \times 10^{-4}) \\ &= 0.048\text{g}\end{aligned}$$

$$\begin{aligned}\text{Therefore Pt loading (wt \%)} &= \frac{(\text{mass of Pt})}{[(\text{mass of Pt}) + (\text{mass of C})]} \times 100\% \\ &= \frac{0.048}{(0.015 + 0.07)} \times 100\% \\ &= 40.7 \text{ wt \%}\end{aligned}$$

## Appendices

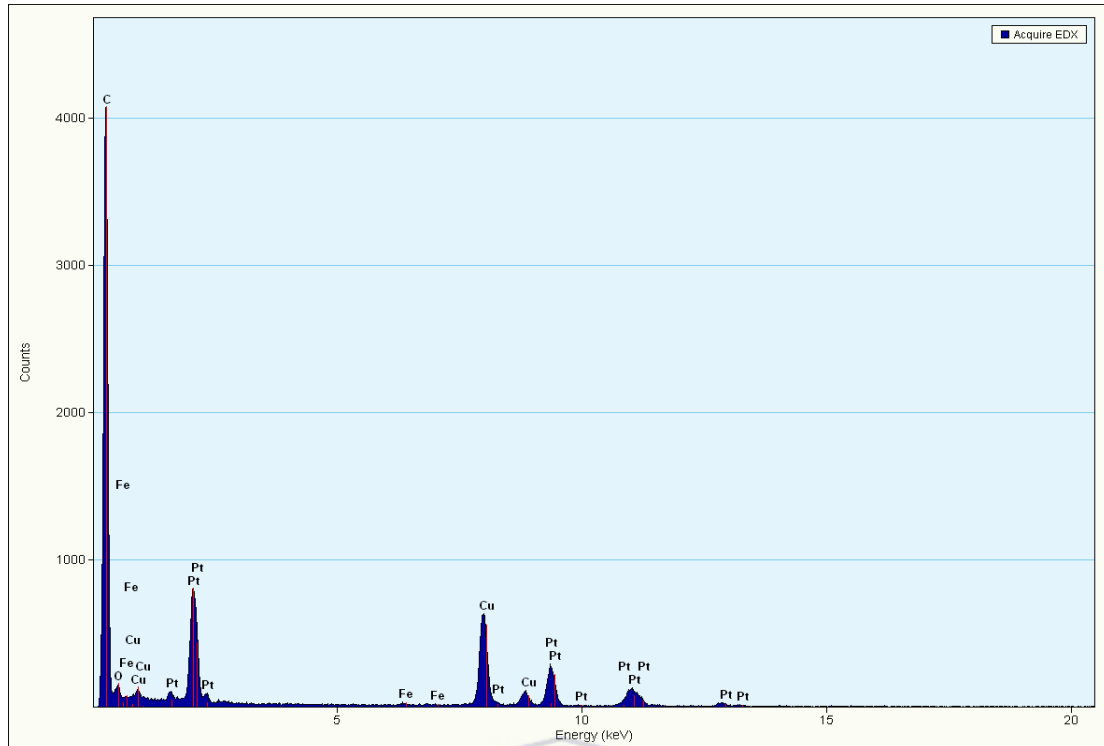
### Appendix B: EDX graphs and data obtained from the IH catalysts



### Appendix B1: EDX of Pt/MWCNT's-F-IH

Element	Weight %	Atomic %	Uncert. %	Correction	k-Factor
C(K)	61.45	96.28	2.03	0.26	3.940
Pt(L)	31.55	3.71	1.16	0.75	5.547

## Appendices



**Appendix B2: EDX data of Pt/NaAOC-IH**

Element	Weight %	Atomic %	Uncert. %	Correction	k-Factor
C(K)	58.91	94.23	0.60	0.26	3.940
Pt(L)	35.55	3.30	0.43	0.75	5.547

## Appendices



## Appendices

